Bridges with Premature Concrete Deterioration: Fatigue Testing of Full-Scale, Prestressed Concrete Box Girders Failing in Shear

by

Joseph M. Roche, B.S.C.E.

Thesis

Presented to the Faculty of the Graduate School of

The University of Texas at Austin

in Partial Fulfillment

of the Requirements

for the Degree of

Master of Science in Engineering

The University of Texas at Austin

May 2001

Bridges with Premature Concrete Deterioration:
Fatigue Testing of Full-Scale, Prestressed Concrete Box Girders Failing in Shear

Approved by
Supervising Committee:

_____

_____

Dedication

To my loving wife, Laura, and our three beautiful children; Michael, Kathleen, and Mary Kate.

To my parents for their love and support throughout my life.

Acknowledgements

I would like to express my appreciation to Dr. Richard E. Klingner for his direction throughout this investigation, and for his advice while writing my thesis. Thank you, also, to Dr. Timothy J. Fowler and Dr. Michael E. Kreger, who provided assistance and expertise during this research. I am grateful to the staff at the Phil M. Ferguson Structural Engineering Laboratory – especially Blake Stasney, Mike Bell, Ray Madonna, Dennis Fillip, Regina Forward, Ruth Goodson, Dijaira Smith, and Wanda Kitts.

This research was funded by the Texas Department of Transportation (TxDOT) under Study 1857, and I would like to thank Brian Merrill for his assistance as the TxDOT contact.

I greatly appreciate the hard work and encouragement of fellow research team members: Piya Chotickai, Yong-Mook Kim, Anna Boenig, Brian Tinkey, Luz Marina Fúnez, Amy Eskridge, and Larry Memberg.

May 2001

Abstract

Bridges with Premature Concrete Deterioration: Fatigue Testing of Full-Scale, Prestressed Concrete Box Girders Failing in Shear

Joseph M. Roche, M.S.E.

The University of Texas at Austin, 2001

Supervisor: Richard E. Klingner

This thesis describes part of the work associated with TxDOT Study 1857, "Structural Assessment of In-Service Bridges with Premature Concrete Deterioration." The theoretical background of premature concrete deterioration, while not the focus of this thesis, is reviewed. The focus of this thesis is to determine the effects of premature concrete deterioration on shear-fatigue strength of pre-cracked, prestressed concrete girders; to predict the service life of pre-cracked girders in shear-critical loading configurations using S-N curves established from data collected during two full-scale fatigue tests; and to determine the possible shear-fatigue failure modes. Also, to determine the overall level of concrete damage, S-N data from the two shear-dominated fatigue tests are related to measured beam stiffness, crack widths, and visual damage indices.

Table of Contents

List of Tables

List of Figures

Chapter 1: Introduction

1.1 INFORMATION ON TXDOT STUDY 1857

In late 1995 the Texas Department of Transportation (TxDOT) became aware of premature concrete deterioration in several in-service structures around the state. Most of the affected structural elements are prestressed girders, though substructures (abutments, columns and bents) are also damaged at some bridge sites. Typical damage to prestressed girders is described as horizontal cracking in the bottom flanges, longitudinal cracks in the underside of the bottom flange, and distributed "map cracking," concentrated at but not limited to the end regions. This premature concrete deterioration has been attributed to two expansive distress mechanisms: Alkali-Silica Reaction (ASR) and Delayed Ettringite Formation (DEF). TxDOT is now deciding how to address this damage. In past instances, structures have been removed from service or repaired after only several years of service (TxDOT 1998). As statewide inspection of in-service concrete structures progresses, more structures with this problem are being identified. The cost for replacing and repairing these structures is already significant, and will continue to increase. This situation was the motivation for TxDOT Study 1857, "Structural Assessment of In-Service Bridges with Premature Concrete Deterioration." In this thesis, specific portions of study 1857 are reviewed and reported. Section 1.1 is taken almost verbatim from a previous thesis (Boenig 2000).

1.2 SCOPE AND OBJECTIVES OF STUDY 1857

TxDOT Study 1857, "Structural Assessment of In-service Bridges with Premature Concrete Deterioration," focuses on seven specific tasks that were outlined in the project proposal (Klingner 1998):

1) Conduct field investigation to confirm and monitor existing premature concrete deterioration and the rate of increase of such deterioration, where numerical measures of this increase include crack width and crack density. Also, determine typical development of damage in laboratory specimens and correlate these results with field observations, with the objective of predicting the distribution of crack widths in a field girder over time.

2) Conduct laboratory investigations of local effects of premature concrete deterioration. Perform tests on cores and slices removed from several girders with varying degrees of deterioration, to acquire data on the compressive strength and modulus of elasticity. Conduct prestressing strand pull-out tests to determine the bond strength between concrete and strand. In addition to tests on cores and slices, perform full-scale tests to failure on prestressed concrete girders, using various loading setups to produce different girder failure modes.

3) Develop nondestructive evaluation (NDE) techniques for determining degree and type of concrete deterioration. Specifically, investigate three groups of NDE techniques: global methods that test the entire structure (acoustic emission as the primary method), local methods that cover an

area or volume of the structure, and methods that characterize material deviations or suspected defects.

4) Develop petrographic techniques for assessing the severity of concrete deterioration, and establish the relationship between various types of deterioration in structural effectiveness, and various changes in internal structure. TxDOT personnel will perform this task, using cores extracted from the laboratory specimens. No work has been completed on this task by The University of Texas at Austin.

5) Develop engineering models for evaluating the global reduction in capacity of a structural element due to local premature concrete deterioration. Using the results from experimental studies and NDE techniques developed in Tasks 2 and 3 respectively, develop engineering models for the behavior of elements showing various degrees and types of premature concrete deterioration.

6) Develop an overall methodology for predicting the probable loss in capacity over time of a deteriorated structural element, based on external evidence, NDE, and engineering models; and to estimate the remaining service life of structures with premature concrete deterioration.

7) Develop recommended actions for TxDOT to handle any given case of premature concrete deterioration. Using the results of Tasks 1-6, provide specific guidelines for assessing the probable capacity of a structure as a function of time.

1.3 SCOPE OF THIS THESIS

The part of Study 1857 reported here concerns Task (2); the testing program for this part of the study was developed to determine the effects of premature concrete deterioration on shear-fatigue strength of pre-cracked, prestressed concrete girders. Two shear-dominated fatigue tests were conducted in the laboratory on separate halves of one prestressed concrete box girder that exhibited extensive premature concrete deterioration in the end regions. Each fatigue test subjected a specimen to a particular load range and loading frequency. At pre-determined numbers of cycles, the specimen was loaded quasi-statically to a load 5 percent higher than the maximum cyclic load (to acquire acoustic-emission data), and complete load-displacement data were taken. Crack width and length, web deformation, and vertical deflection were measured, and visual damage indices were calculated.

1.4 OBJECTIVES OF THIS THESIS

The primary objective of this thesis is to predict the service life of pre-cracked prestressed concrete girders with premature concrete deterioration, in shear-critical loading configurations. Results from the shear-dominated fatigue tests are used to relate the range and number of cyclic loads to crack widths and visual damage indices, and to girder stiffness as measured by vertical deflection and web deformation. These measured parameters are used to further aid in determining the overall level of damage. In conjunction with S-N curves (shear force range plotted against number of cycles to failure) created from data

collected during full-scale tests, techniques are developed for predicting the life of girders in service.

1.5 COMPLEMENTARY WORK

The research conducted for this thesis is complemented by research of several other students on laboratory specimens and field structures. Luz Marina Fúnez presented the background and fieldwork in a report in December 1999, that included monitoring crack patterns and crack widths for prestressed I-beams in four TxDOT bridge structures, and for prestressed concrete box girders in the laboratory (Task 1) (Fúnez 1999). Anna Boenig expanded upon that field work, and correlated the damage in prestressed girders over time with their structural capacity (Tasks 1 and 2) (Boenig 2000). To determine these correlations, Boenig performed a series of laboratory tests on prestressed concrete box girders, each of which displayed a different level of premature concrete deterioration. She performed both static flexural tests and static shear tests to determine the ultimate capacity of each specimen, which was then compared to the calculated capacity using current code equations. She also performed compressive strength tests and modulus of elasticity tests on cores taken from the same girders. Yong-Mook Kim conducted similar laboratory tests as those described above on prestressed concrete I-beams, and is developing finite-element models to predict structural capacities of similar I-beams, given a level of deterioration (Task 5).

Brian Tinkey investigated the use of nondestructive test methods (Task 3), including acoustic emission, impact echo, and short pulse radar, to assess the degree of distributed damage in the laboratory specimens tested by Boenig and Kim (Tinkey 2000). Piya Chotickai is developing nondestructive testing procedures for use in the field (Task 3), as well as using acoustic emission to monitor damage in the shear-dominated fatigue specimens discussed in this thesis. Larry Memberg will perform strand pull-out tests on slices removed from the laboratory specimens (Task 2).

In addition to the laboratory testing, members of the project also continue the ongoing monitoring of in-service bridges in Texas with premature concrete deterioration.

Chapter 2: Premature Concrete Deterioration – A Literature Overview of Damage from Delayed Ettringite Formation (DEF) and Alkali-Silica Reaction (ASR)

In this chapter, background information on ASR and DEF, from a previous Project 1857 thesis by Boenig (2000), is presented in Sections 2.1 through 2.5. Section 2.6 is a summary of the full-scale static load testing previously performed for Project 1857, and Section 2.7 is a brief review of previous studies that involved fatigue testing of prestressed concrete members.

The following is from Boenig (2000).

> This chapter presents background information on ASR and DEF, as well as their role in premature concrete deterioration. Pertinent information from a literature search performed by contributors to Project 1857 is included (Fúnez 1999, Klingner 2000). The presently known impact of premature deterioration on concrete structures in Texas is discussed. Gaps in knowledge of the influence of premature deterioration on concrete structures are introduced, as well as how this research has attempted to fill those gaps.

2.1 INTRODUCTION

> Premature concrete deterioration can result from a number of mechanisms. A previous TxDOT investigation of damage to 56 precast, prestressed concrete box girders (Lawrence et al. 1998), identified two possible expansive mechanisms, Alkali-Silica Reaction (ASR) and Delayed Ettringite Formation (DEF).
>
> Premature concrete damage from ASR and DEF, either alone or in combination, typically shows itself through distributed internal and external cracking of the concrete, and a progressive loss of member function with time. This distributed damage also increases a concrete element's susceptibility to corrosion of reinforcement and other types of deterioration due to environmental exposure.

2.2 ALKALI-SILICA REACTION (ASR)

ASR, discussed at length in ACI 221.1 (1998), is caused by a chemical reaction between hydroxyl (OH^-) ions present in the pore-water solution, and various forms of silica present in many aggregates. The silica enters into solution and forms an alkali-silica gel, which absorbs water and increases in volume. This increase in volume produces expansive forces within the concrete, leading to distributed cracking. When the alkalis are present in the fresh concrete, ASR begins at the interface between the aggregate and the paste. It requires three conditions: highly alkaline pore water; high humidity; and reactive silica.

ASR in new structures can be controlled by limiting the total alkalinity in the concrete, by controlling the composition of the cement, and by eliminating combinations of cement and aggregates that are known to be reactive. These measures can be applied alone or in combination. ASR in existing structures can be mitigated only by controlling the humidity of the concrete: below about 80 percent relative humidity, ASR stops. In hardened concrete, relative humidity is controlled by the hydration of the cement, and by controlling the ingress of water from external sources.

2.3 DELAYED ETTRINGITE FORMATION (DEF)

2.3.1 Background of Normal Ettringite Formation

Ettringite is calcium aluminum sulfate ($3CaO{\cdot}Al_2O_3{\cdot}3CaSO_4{\cdot}32H_2O$). It is a normal hydration product of the tricalcium aluminate (C_3A) component of portland cement. Upon contact with water, the C_3A reacts immediately, forming crystalline hydrates such as C_3AH_6, C_4AH_{19} and C_2AH_8, and liberating substantial heat. To reduce the rate of this reaction and the associated heat and loss of workability, small quantities of gypsum (calcium sulfate, $CaSO_4{\cdot}2H_2O$) are added to the cement. The sulfate in the gypsum reacts with C_3A and water to form crystals of "primary ettringite," which bind to the C_3A, impeding the access of water to the C_3A particles. Later in the hydration process, when the pore water is depleted of sulfate and richer in aluminate, this primary ettringite becomes unstable, and is gradually converted to monosulfate ($3CaO_4{\cdot}A_{12}O_3{\cdot}SO_3{\cdot}18H_2O$), a stable hydration product.

2.3.2 Historical Background of DEF

DEF was first noticed in the early 1980's in Germany, and later in the United States, when prestressed concrete railway ties on the east coast

began to show distress just a few years after installation. Studies, made using petrographic microscopy, scanning electron microscopy (SEM) and energy-dispersive x-ray elemental analysis, led to the conclusion that although some alkali-silica reaction (ASR) had occurred, the distress was largely or completely due to DEF (Mielenz et al. 1995).

DEF has also been encountered in Canada, South Africa, Australia and Europe. Distress, found mainly in prestressed elements, begins to appear after several years of exterior exposure. The deterioration is often reported because of the appearance of map cracking on the surface of the element (Kesner 1997).

A major question has arisen: was DEF not noticed before 1980? Researchers have identified two possible answers:

1) it did occur, but was not recognized; and
2) composition of portland cements has changed radically during the last few decades.

The first answer relates to the fact that the ettringite present from DEF is often hard to detect. Ettringite crystals normally have a needle-shaped structure that allows easy recognition under microscopy. In DEF, however, the crystals may be so fine as to be resolvable only using SEM at magnifications of 5,000 to 25,000. In several such cases, DEF has been misdiagnosed as ASR.

The second answer relates to the fact that maximum SO_3 levels in portland cement clinker have increased from about 2% in the 1940's to more than 4% now (Hime 1996).

2.3.3 Latest Theories on DEF

The most recent research on DEF and its causes have been compiled and interpreted by Hime (1996) and Collepardi (1999). According to Hime,

1) DEF almost certainly will occur only if the concrete is frequently exposed to substantial amounts of water.
2) Destructive DEF will probably not occur, or its effect will be lessened, if the concrete is well air-entrained.
3) If precast concrete is not air-entrained, and exposure to water is frequent, then DEF may occur if either:
   - the concrete temperature during curing or in service becomes high enough to decompose primary ettringite. Depending on cement composition, this temperature may be as low as 140 F (60 C).

- the clinker contains a substantial amount of slowly soluble sulfate. Sulfate levels as low as 1.5% in normal cement, and 2% in high-alkali cements have caused DEF.

4) Tests of cement by ASTM C 265 or of concrete by the Dugan procedure (1989) may reveal a potential DEF problem for non-air-entrained concrete that will be exposed to substantial amounts of water.

According to Collepardi (1999), the following factors cause DEF:

1) Microcracks formed during manufacturing, either from Alkali-Silica Reactivity (ASR) or from other causes including those related to steam curing;
2) Exposure to cycles of wetting and drying;
3) Late release of sulfate from the cement clinker or other sources;
4) Migration of reactant ions (SO_4^{-2}, Al^{+3}, Ca^{+2}) through the pore-water solution of concrete exposed to water or saturated air; and
5) Ettringite deposits inside existing microcracks, and subsequent crack opening by ettringite swelling or crystal growth.

Collepardi proposes a holistic approach to understanding DEF-induced damage, based on the interaction of three essential elements (Figure 2.1):

1) microcracking,
2) exposure to water or saturated air, and
3) late sulfate release.

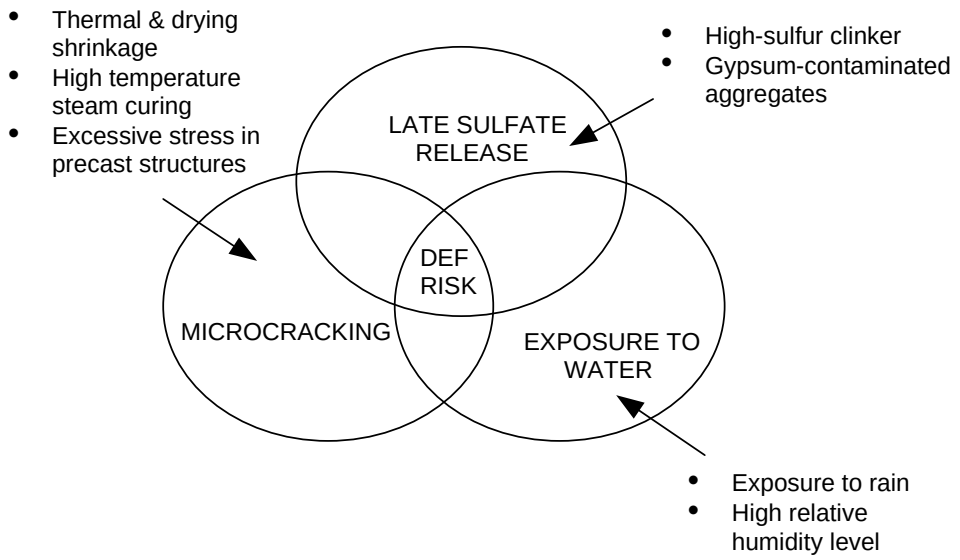

Figure 2.1 A holistic model showing DEF-damage as a function of late sulfate release, microcracking, and exposure to water (Collepardi 1999)

In the absence of any one of these elements, Collepardi states, DEF-related deterioration cannot occur.

2.4 GAPS IN KNOWLEDGE REGARDING DEF

Previous research on DEF damage has concentrated on its chemistry, possible causes, and prevention. As noted in the previous section, however, there is no consensus regarding its causes. Measures to prevent it must be taken before fabricating the concrete elements (for example, reducing the sulfate in the clinker, or using low-temperature steam curing).

Four important areas of research on premature concrete deterioration are as yet unexplored:

1) the long-term growth or shrinkage of DEF-induced cracking;
2) whether ASR/DEF-related deterioration can be stopped;
3) the effect of ASR/DEF on structural integrity; and
4) the effectiveness of repair techniques for structures damaged by ASR, DEF, or both.

2.5 HOW TXDOT STUDY 1857 WILL FILL THOSE GAPS

The objectives of TxDOT Study 1857 have been to assess the structural adequacy of in-service structures that are prematurely deteriorated, and to determine the degree to which that deterioration will continue. Information on how DEF affects a structure through time will be used to predict the remaining service life of a concrete element with DEF. Researchers trying to find the causes of DEF may use this information to develop better models of the problem. Researchers trying to find methods of repairing in-service structures might use this information to tell them at which moment in time their solution could be applicable.

2.6 SUMMARY OF PREVIOUS STATIC TESTS PERFORMED FOR PROJECT 1857

Full-scale static testing of prestressed concrete box girders with premature concrete deterioration was performed by Boenig on specimens similar to those reviewed in this thesis. For details of both the static test specimens, and the shear-dominated fatigue specimens tested for this thesis, see Section 3.3 and Appendix A. Three prestressed concrete box girders with various degrees of premature deterioration were statically tested. Tests to failure were performed on three flexure-dominated and three shear-dominated specimens.

2.6.1 Results of Previous Flexure-dominated Static Tests

Test results for the three flexure-dominated specimens are reported below. Specimen BG1F, the least deteriorated girder, failed under an externally applied quasi-static load of 119 kips (529 kN). Specimens BG2F and BG4F exhibited significantly more deterioration than BG1F, and failed under externally applied loads of 116 kips (516 kN) and 119 kips (529 kN) respectively. From these results, it appears that the level of concrete deterioration in these specimens,

which was worst near the girder ends, did not significantly affect the flexural capacity. This is not unexpected, because nearly all of the pre-existing damage was concentrated near the girder ends, and only minimal pre-existing damage was in the flexure-critical regions near mid-span.

2.6.2 Results of Previous Shear-dominated Static Tests

Test results for the three shear-dominated specimens are reported below. Specimen BG1S, the least deteriorated girder, failed under an externally applied quasi-static load of 423 kips (1880 kN); a shear force of 302 kips (1340 kN). Specimens BG2S and BG4S exhibited significantly more deterioration near the girder ends than did BG1S, and subsequently failed under lower externally applied loads of 378 kips (1680 kN) and 377 kips (1680 kN) respectively; shear forces of approximately 269 kips (1200 kN). From these results, it appears that an increased level of concrete deterioration near the girder ends adversely affects the shear capacity. Again, this is not unexpected, because the concrete compressive strength and the bond between concrete and prestressing strands is most crucial to shear capacity in the shear-critical regions near the girder ends.

2.6.3 Recommended Fatigue Testing

Based upon the experimental results from the flexure-dominated and shear-dominated static tests, as well as the visually observed locations of concrete deterioration in typical in-service girders, it was determined that fatigue testing would be most critical for shear-dominated specimens. Therefore, this thesis concentrates on shear-dominated fatigue testing to more fully determine the

effects of premature concrete deterioration on the structural capacity and service life of prestressed concrete girders.

2.7 REVIEW OF PREVIOUS STUDIES THAT INVOLVED FATIGUE TESTING OF PRESTRESSED CONCRETE MEMBERS

Many studies were reviewed, however, only three of the most relevant reports are briefly discussed here. One study was by Graddy (2000), "Factors Affecting the Design Thickness of Bridge Slabs." Another study was by Bachman (1987), "Exploratory Investigation of Shear Fatigue Behavior of Prestressed Concrete Girders." The final study discussed here was by Matsumoto (1985), "A Fatigue Study of Deformed Reinforcing Bars." The most applicable findings of these studies, to the research performed for this thesis, are: the basic principle of using S-N curves to predict fatigue life of prestressed concrete members, and the basic understanding of fatigue life for shear reinforcement (stirrups) in the webs of prestressed concrete girders.

Full-scale fatigue testing of precast prestressed concrete panels (PCP) was performed by Graddy, and S-N curves for punching shear fatigue were developed from the experimental results. Although these specimens are different than the box girder specimens, and the failure modes are not quite the same, it appears that the idea of using S-N curves to predict fatigue life of prestressed concrete members is feasible.

Full-scale fatigue testing of Texas Type C prestressed concrete girders was performed by Bachman to gain a better understanding of fatigue behavior of

girders and component materials. This research, together with the companion study performed by Matsumoto, concluded that the fatigue life of shear reinforcement in the web of a prestressed concrete girder is less than the fatigue life of similar reinforcing steel tested in air. These results are also important to understanding the fatigue life of the box girder specimens tested in the research for this thesis.

Chapter 3: Development of Testing Program

3.1 OBJECTIVES AND PLAN

The testing program was designed to investigate structural performance and service life of a prestressed concrete box girder with premature deterioration, subjected to shear-dominated fatigue loading. The testing program relates the level and number of cyclic loads to failure modes and the amount of apparent concrete damage.

3.2 TEST NOMENCLATURE

Individual test specimens are categorized by the box girder and the location within that box girder from which they were taken. The box girders were designated BG1, BG2, BG3, and BG4 ("Box Girder 1," etc.). The suffixes "S" and "N" respectively denote south and north ends of a box girder, as pre-determined by Boenig during crack monitoring of girders in the Ferguson Structural Engineering Laboratory (FSEL) storage yard. For example, the shear-dominated fatigue test performed on the south end of Box Girder 3 is denoted as BG3S. The suffixes "S" and "N" are not related to the girder orientation as tested in the laboratory.

3.3 TEST SPECIMENS

Fifty-six prestressed concrete box girders, fabricated at Heldenfels Brothers, Inc. plant in San Marcos, TX, in June through September 1991, displayed premature concrete deterioration while still in the storage yard, and were never installed in TxDOT bridges. Four of those girders, representing typical ranges of damage, were brought to Ferguson Structural Engineering Laboratory (FSEL) at the University of Texas at Austin (UT Austin) for examination. Laboratory tests were previously performed on three of these girders (BG1, BG2, BG4), and the results were reviewed in an earlier thesis (Boenig 2000), and in Section 2.6 of this thesis. One girder, BG3, remained for the shear-dominated fatigue tests described in this thesis.

The box girders had a nominal length of 69.83 ft (21.28 m), with solid end blocks 2.17 ft (0.66 m) long, and 1 ft (0.30 m) thick intermediate stiffeners were cast at 23.33 ft (7.11 m) from each end. Expanded polystyrene was used to form interior voids. Thirty ½-inch (13 mm) diameter, 270 ksi (1860 MPa) prestressing strands were distributed in the bottom of the girder (Figure 3.1). Reinforcing steel was ASTM A615 Grade 60 (420 MPa), and the design compressive strength of the concrete was 6000 lb/in.^{2} (41.4 MPa). Figure 3.1 shows the cross-sectional dimensions of these girders, and fabrication details are included in Appendix A.

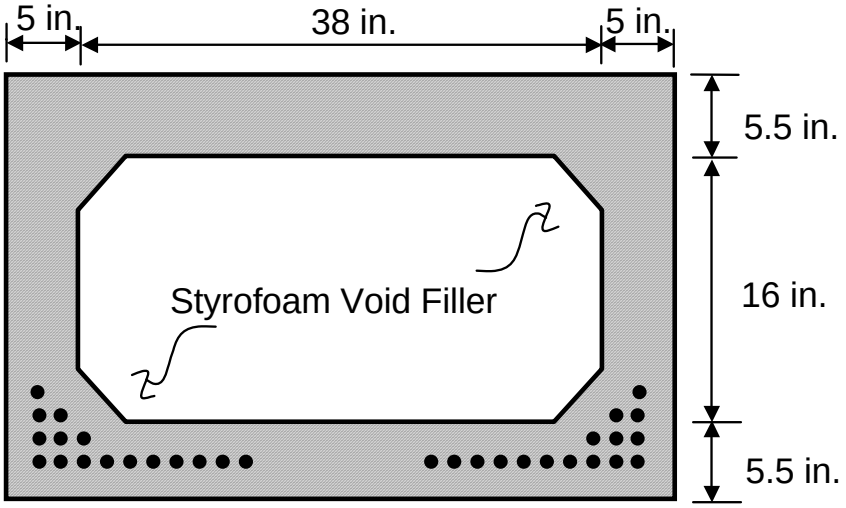

Figure 3.1 Cross-section of box girders from Heldenfels Brothers, Inc. - San Marcos (Boenig 2000)

BG1 and BG2 were immediately moved inside the laboratory, while BG3 (the specimen used for shear-dominated fatigue tests in this thesis) and BG4 were left outside and uncovered. BG4 was subjected to random periods of wetting and drying in order to accelerate damage.

The condition of each girder was documented, and Table 3.1 outlines their general appearance. Following the table is a detailed description of BG3, the specimen used for the shear-dominated fatigue tests described in this thesis.

Table 3.1 Condition of box girders (Boenig 2000)

Girder	Condition
BG1	Good
BG2	Severe end damage
BG3	Less severe end damage
BG4	Extensive damage over entire length

BG3 was cast on September 11, 1991, with TxDOT identification number A3-F37. The materials used are presented in Table 3.2, and the 7-day compressive strength cylinder average was 8180 lb/in.^{2} (56.4 MPa).

Table 3.2 Materials used for BG3

Material	Description	Producer
Cement	Type III	Alamo Cement Co., San Antonio, TX
Fine Aggregate	Siliceous sand	Heldenfels Brothers, Inc., Victoria Pit
Coarse Aggregate	Limestone	Gifford-Hill, Yelverton Pit

The ends of BG3 were more damaged than those of BG1 and BG4, but slightly less damaged than those of BG2. Cracks 0.125 to 0.313 in. (3.2 to 7.9 mm) wide had developed in the end faces, and in the sides over the end 1.5 ft (0.46 m) of the girder. Two horizontal cracks in each side extended the entire length of the girder; one of these cracks was 5.5 in. (0.14 m) from the bottom and 0.007 to 0.03 in. (0.18 to 0.76 mm) wide; the other was 17 in. (0.43 m) from the

bottom and 0.01 to 0.013 in. (0.25 to 0.33 mm) wide. BG3S, the south half of the girder used for Shear Fatigue Test Number 2, was slightly more damaged than BG3N, the north half of the girder used for Shear Fatigue Test Number 1.

3.4 TEST SETUP

Two shear-dominated fatigue tests were conducted in the laboratory, one test on each separate half of BG3. The north half of BG3 was designated BG3N (Test 1), and the south half of BG3 was designated BG3S (Test 2).

The shear-dominated fatigue tests were conducted at FSEL in a loading frame assembled around four wide-flange steel columns, each anchored to the floor slab with four 1-inch (25 mm) diameter, high-strength anchor bolts. Two 35 gpm (0.132 m^3/min) electric pumps, running in parallel, supplied hydraulic fluid to two hydraulic rams. These two rams applied load to two respective transverse spreader beams, which together applied vertical load to the webs of the box girder in four locations to prevent punching shear failure of the top flange (Figures 3.2 and 3.3). The transverse spreader beams were simply supported on 2-inch (51 mm) diameter steel rods welded to steel plates. A layer of gypsum plaster (Hydrostone) provided a smooth, level bearing surface on top of the box girder, and 1/8-inch (3.2 mm) thick neoprene pads were placed between the Hydrostone and the steel plates. These thin neoprene pads were used to isolate noise and vibrations from the test frame and hydraulics that might have introduced undesirable noise in the acoustic emission (AE) data being collected from the concrete girder.

The load applied to the girder was measured by placing one 200 kip (890 kN) load cell between the hydraulic ram nearest to the end of the girder and the respective transverse spreader beam. The two rams were hydraulically connected so that the total load applied to the girder was twice that of the load recorded by the load cell placed under one ram.

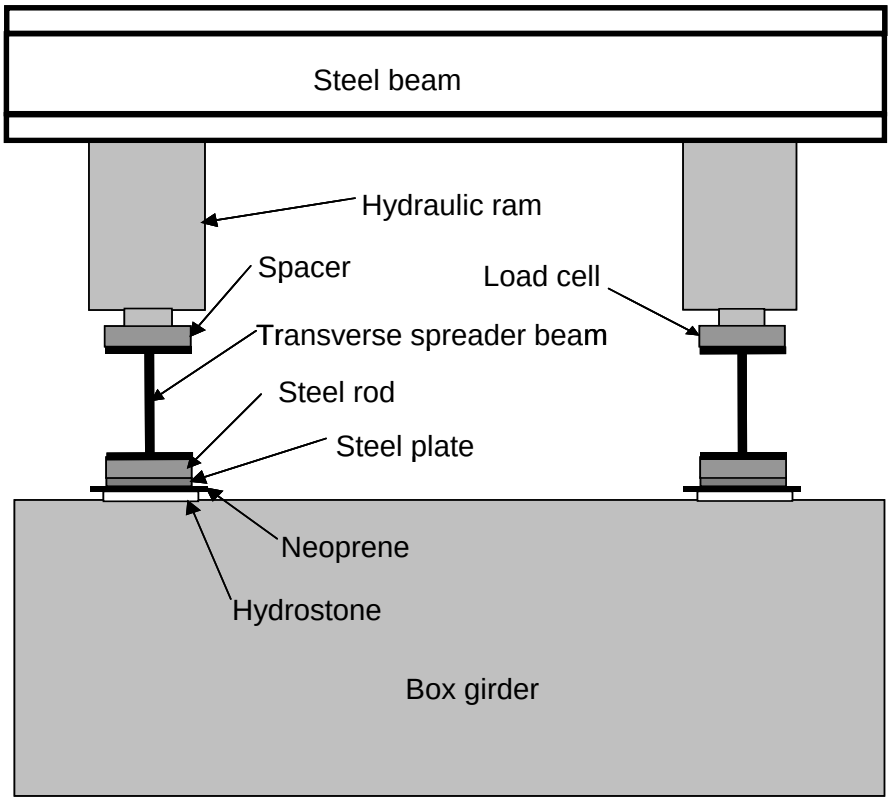

Figure 3.2 Detail of loading setup for shear-dominated fatigue specimens (elevation)

Support conditions and loading points remained consistent with the Case 2 support conditions used in the previous shear-dominated static tests performed by Boenig (2000) (Figures 3.4 and 3.5). The single bearing pad, farthest from the

loading points, was centered under the solid intermediate blockout. The double bearing pads, nearest to the loading points, were placed under the end block in the typical field locations, and the span length as tested was 23.04 ft (7.02 m). The loading point nearer to the girder end was 46 in. (1.17 m) from the center of the support, producing a shear span of approximately 2d, where d is the distance from the extreme compression fiber to the centroid of the longitudinal tension reinforcement. The bonded length of the prestressing strands, from the end of the girder to the center of the bearing pad, was 9.5 in. (0.24 m). A portion of each compression strut (one compression strut per web) fell within each of the following regions (Appendix A): the solid end block and the top flange, thus increasing the combined web thickness in these regions from 10 in. (0.25 m) to the entire width of the girder, 48 in. (1.22 m); and the internal void chamfers, thus varying the combined web thickness in this region from 10 in. (0.25 m) to 16 in. (0.41 m). For a description of compression strut, and an explanation of the strut-and-tie-model, see MacGregor (1997).

Figure 3.3 Loading setup for shear-dominated fatigue specimens

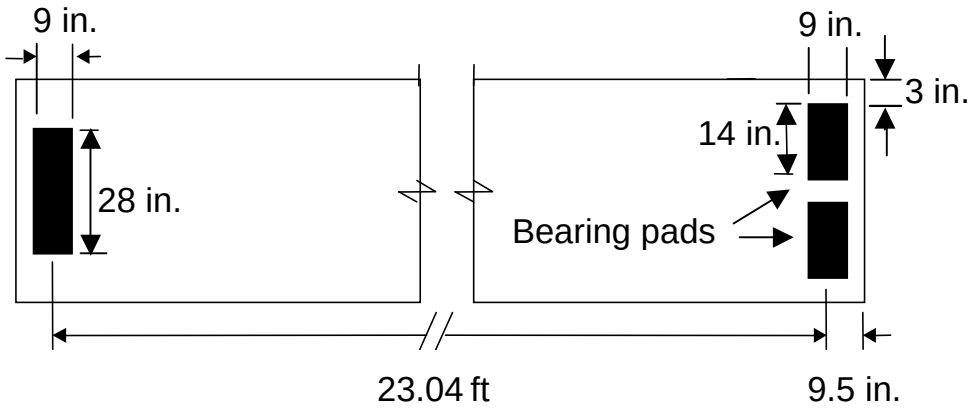

Figure 3.4 Plan of bearing pad placement for shear-dominated fatigue tests

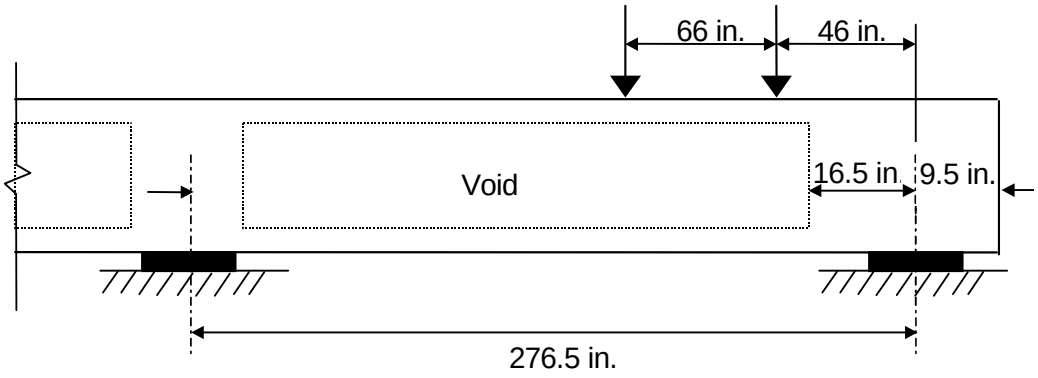

Figure 3.5 Support conditions and loading points for shear-dominated fatigue tests

3.5 SYSTEM CONTROL

A closed-loop system, shown schematically in Figure 3.6, was used to control applied loads during tests. An MTS controller monitored the load on specimens through the load cell, compared it with the command signal, and supplied the appropriate corrective signals to the valve driver controlling the flow of fluid through the hydraulic rams. If the load deviated from the command signal by some pre-set limit, the controller was programmed to stop the test by removing pressure from the hydraulic rams. These limits, as well as the command signal, required occasional adjustments during each test to maintain smooth and continuous application of load cycles (Graddy 1995). Sinusoidal loading was used, at frequencies between 0.25 Hz and 1.3 Hz.

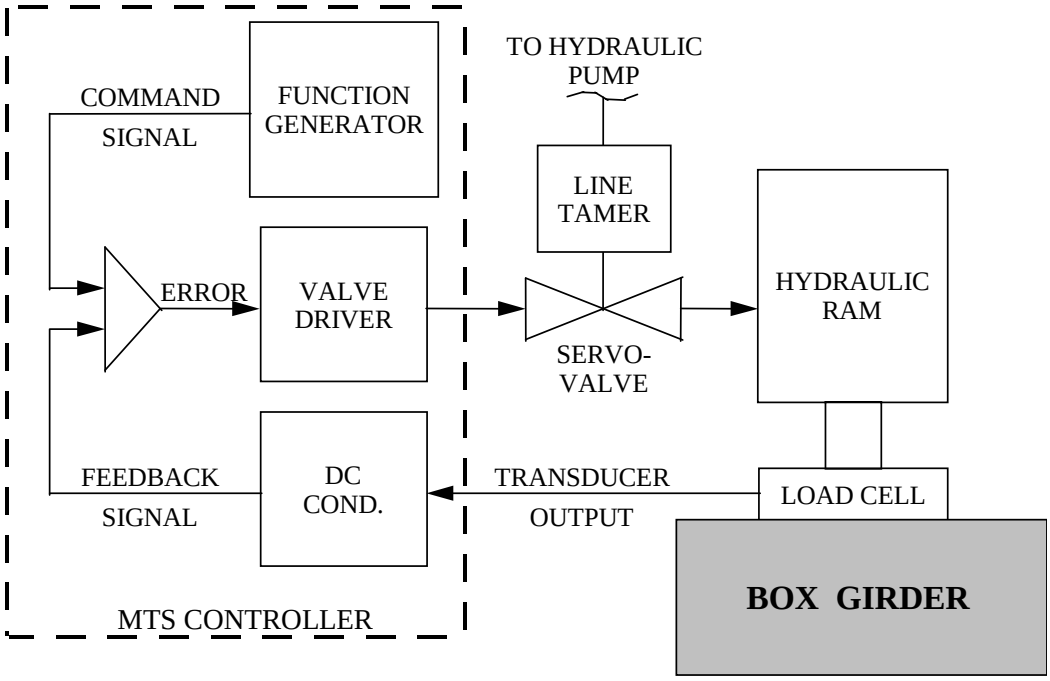

Figure 3.6 Schematic representation of the closed-loop system used for static and fatigue tests (Graddy 1995)

3.6 INSTRUMENTATION AND DATA ACQUISITION

The following is a list of parameters monitored during the testing of specimens BG3N and BG3S: load, cyclic load rate, number of load cycles, deflection between loading points, deflection at supports, slip of prestressing strands, deformation of webs, widening of existing cracks, crack initiation and propagation, and acoustic emission.

3.6.1 Linear Potentiometers

Linear potentiometers were used to measure vertical deflections under each web at a distance 88.5 in. (2.25 m) from the girder end (Figure 3.7), which is

midway between the two hydraulic rams; and on each side of the girder at the support nearest to the load. Linear potentiometers were also used to measure slip of eight prestressing strands (Figures 3.8 and 3.9), as well as web deformation in the shear-critical region.

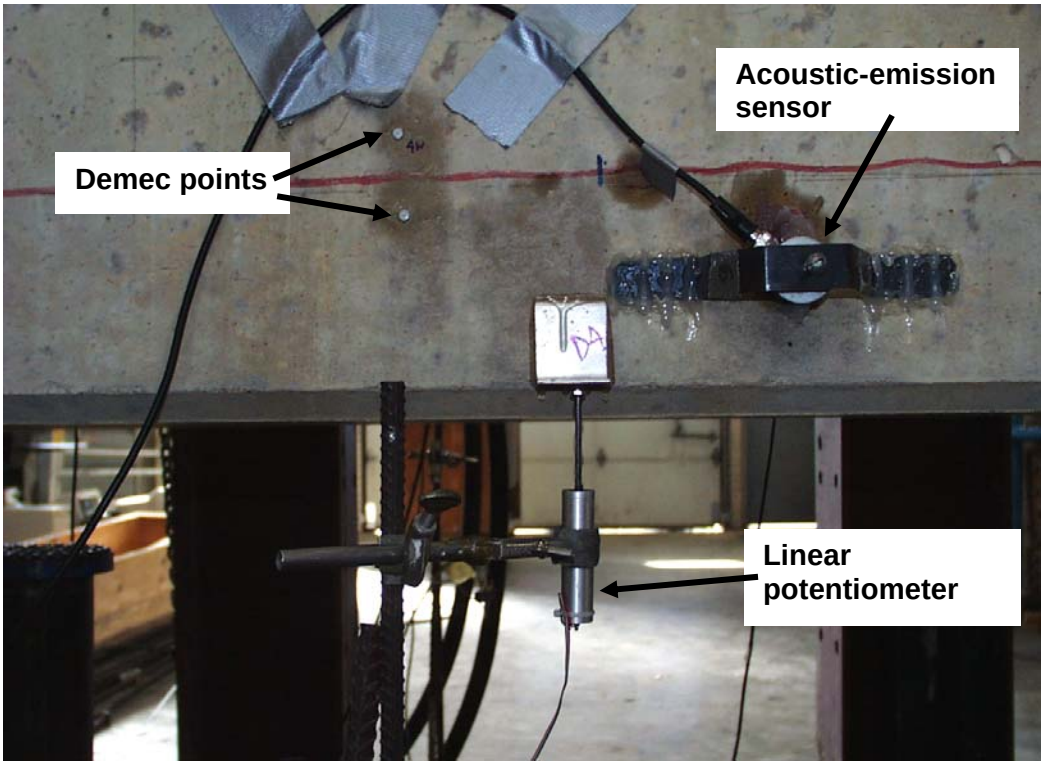

Figure 3.7 Linear potentiometer to measure vertical deflection

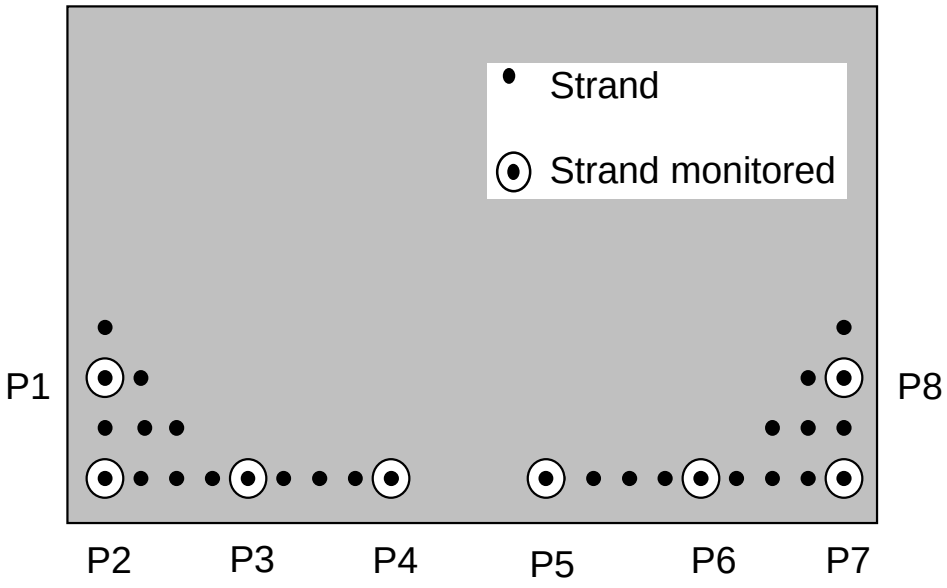

Figure 3.8 Prestressing strand monitored for slip

Figure 3.9 Linear potentiometer to measure slip of prestressing strand

Four linear potentiometers were attached to each of the two webs in the shear-critical region between the support and first loading point to measure web deformation (Figures 3.10, 3.11 and 3.12). Strains were measured in the compression diagonals, tension diagonals, and bottom chords, by attaching steel wires between each potentiometer and its corresponding anchoring hook.

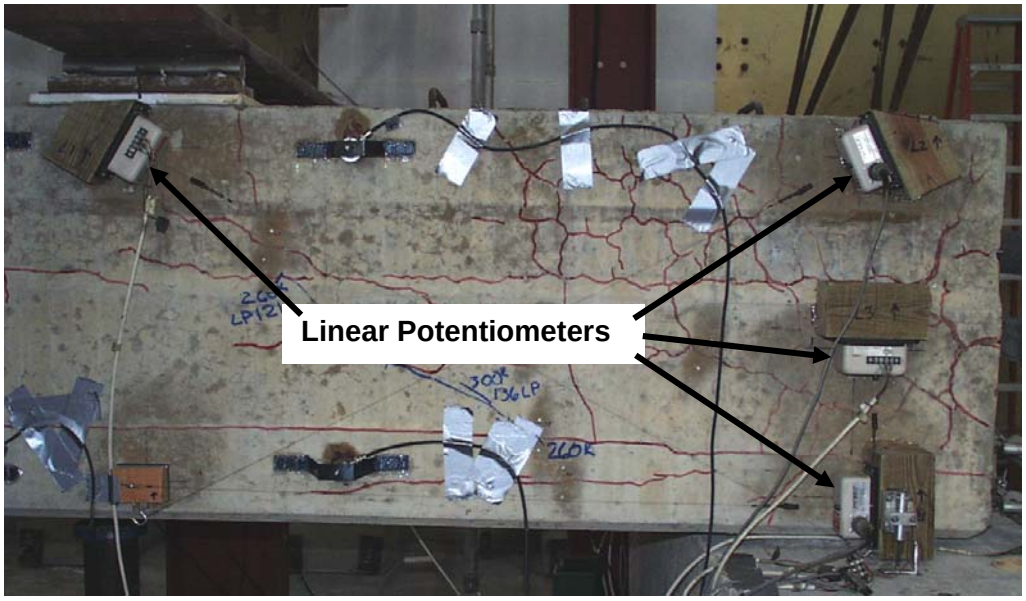

Figure 3.10 Linear potentiometers used to measure web deformations

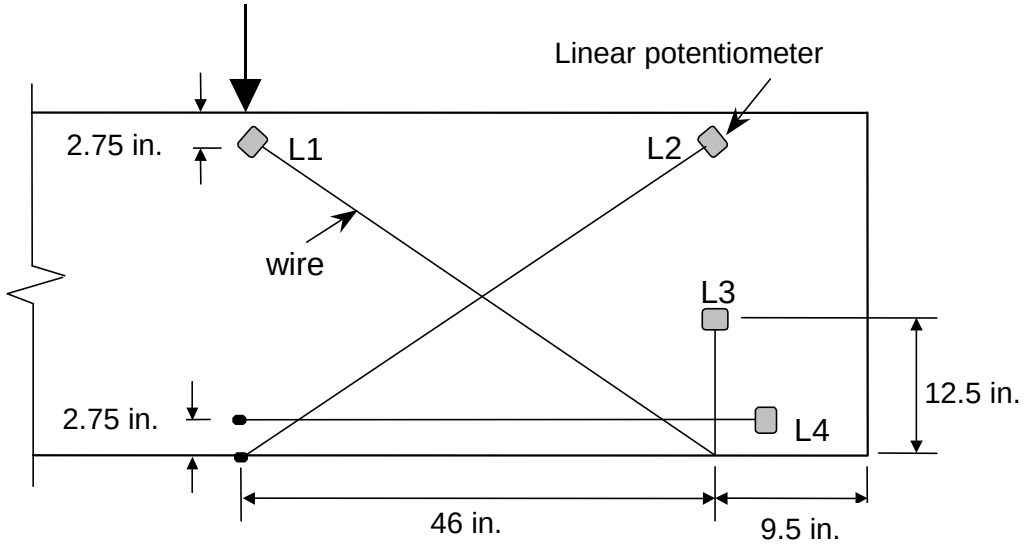

Figure 3.11 Linear potentiometers L1 – L4

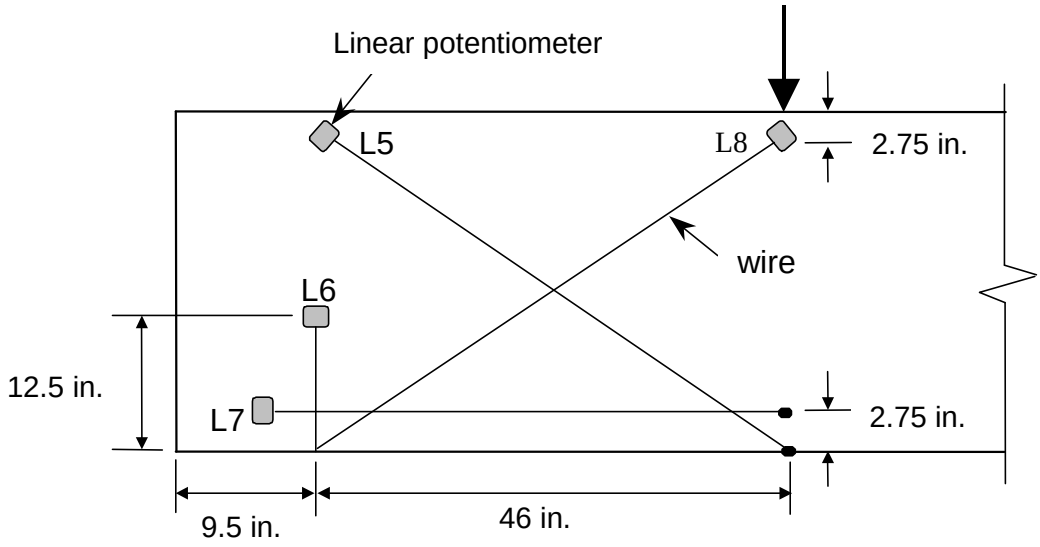

Figure 3.12 Linear potentiometers L5 – L8

One DC voltage source provided an excitation voltage to the linear potentiometers, while the MTS controller provided an excitation voltage to the load cell. Voltages reflecting deflection measurements and load were acquired by a scanner, recorded using a microcomputer, and converted to engineering units using an add-in to a conventional spreadsheet program.

3.6.2 Demountable Mechanical Strain Gauges

Demountable Mechanical Strain Gauges (Demec gauges) were used to monitor changes in crack widths (Figure 3.13). One steel disc was cemented on each side of pre-existing cracks in the shear span to monitor crack widths at pre-determined intervals.

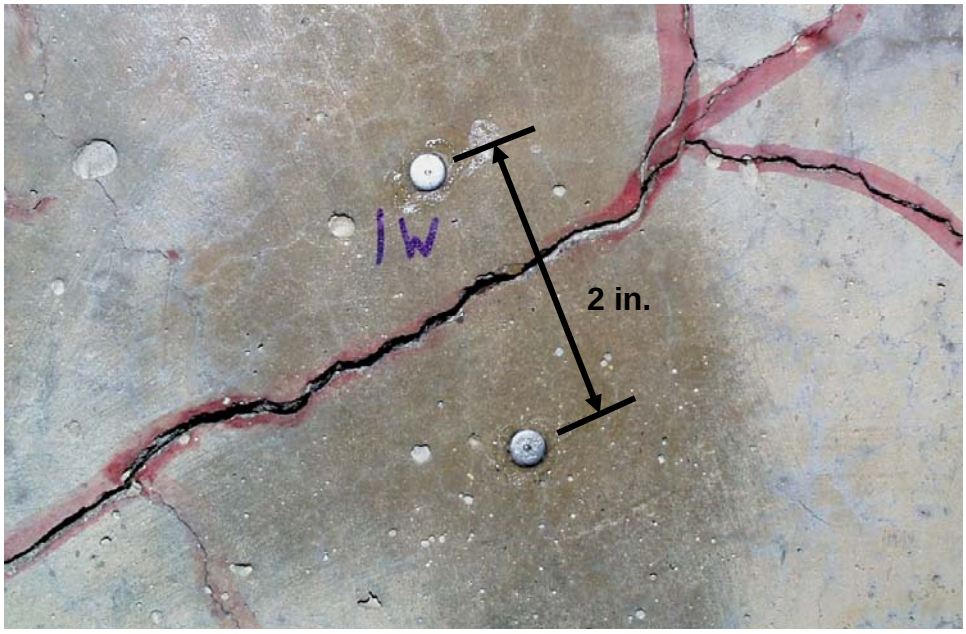

Figure 3.13 Typical Demec measuring points across diagonal crack

3.6.3 Visual Crack Monitoring

The length and width of each visible crack in representative rectangles on the sides of BG3 were measured after selected numbers of load cycles. Rectangles were drawn onto each side of the girder, near the middle of the shear span, with dimensions of 15 in. x 24 in. (0.38 m x 0.61 m) (Figure 3.14).

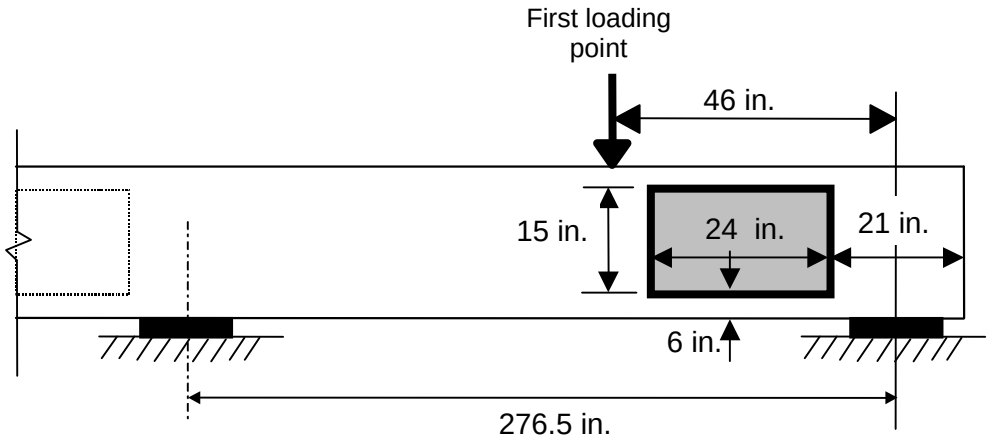

Figure 3.14 Representative rectangle monitored for crack growth

Crack ratio (CR) and damage index (DI) were calculated as follows:

$$CR = \sum wl$$

$$DI = \sum w^2 l$$

where w is the crack width in thousandths of an inch, l is the crack length in inches, and all cracks monitored are within the defined rectangle (Fúnez 1999 and Boenig 2000).

3.6.4 Acoustic-Emission Sensors

Acoustic emission from the concrete was monitored by Chotickai during the testing of the shear-dominated fatigue specimens discussed in this thesis (Figure 3.15).

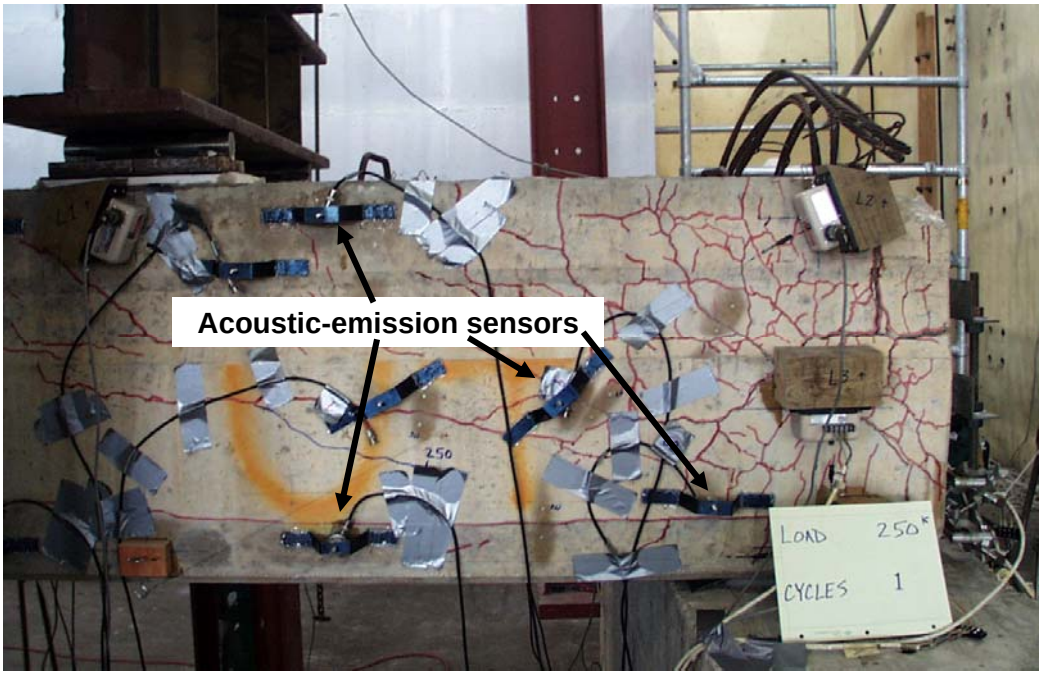

Figure 3.15 Acoustic-emission sensors

3.7 TEST PROCEDURE

3.7.1 Test 1 – Specimen BG3N

A quasi-static load of 260 kips (1160 kN) was applied to the test specimen prior to fatigue loading to pre-crack the section. Although there were pre-existing cracks due to premature deterioration, pre-cracking the section, which entailed

forming inclined cracks in the webs, was done to promote further cracking during the fatiguing of the specimen. The load was slowly increased from 5.0 kips (22 kN) to a level at which visible inclined cracks formed in each web of the girder. The section was then subjected to cyclic loading, from 20 kips (89 kN) to 300 kips (1330 kN). The lower load of 20 kips (89 kN), rather than zero, was chosen to prevent movement of the test specimen. The upper load of 300 kips (1330 kN) was chosen based upon the results of static tests (Boenig 2000). The upper load of 300 kips (1330 kN) was approximately 75 percent of the estimated static load capacity of the girder if no fatiguing had occurred. After pre-determined numbers of loading cycles, the specimen was slowly loaded to 315 kips (1400 kN), 5 percent higher than the fatigue load, and the parameters detailed in Section 3.6 were measured.

The frequency of loading cycles was 0.25 Hz for the first 1000 cycles. After proving adequate performance of the test setup, this frequency was increased to 0.5 Hz from 1000 cycles until failure of the girder at 28,133 cycles. After 1, 100, 1000, and 10,000 cycles, the fatigue loading was stopped, and the quasi-static test to 315 kips (1400 kN) was performed. The load was slowly increased from 5.0 kips (22 kN) to 300 kips (1330 kN), and was held constant at 300 kips (1330 kN) for several minutes to allow the acoustic emissions being monitored to subside. The load was then slowly increased by 5 percent, from 300 kips (1330 kN) to 315 kips (1400 kN), and was again held for several minutes to monitor acoustic emissions. Finally, the load was slowly decreased from 315 kips (1400 kN) to 5.0 kips (22 kN), and was held constant for several minutes.

3.7.2 Test 2 – Specimen BG3S

A quasi-static load of 250 kips (1110 kN) was applied to the test specimen prior to fatigue loading to pre-crack the section, and the procedure is similar to the test performed on Specimen BG3N, explained in Section 3.7.1. The load was slowly increased from 5.0 kips (22 kN) to a level at which visible inclined cracks formed in each web of the girder. The section was then subjected to cyclic loading, from 20 kips (89 kN) to 200 kips (890 kN). As in Test 1, the lower load of 20 kips (89 kN) was to prevent movement of the test specimen. The upper load of 200 kips (890 kN) was chosen to apply a fatigue-shear force much greater than that which would be imposed by a gross truck overload, while still allowing for at least several million cycles prior to failure. After pre-determined numbers of loading cycles, the specimen was slowly loaded to 210 kips (930 kN), 5 percent higher than the fatigue load, and the parameters detailed in Section 3.6 were measured.

The frequency of loading cycles was 1.0 Hz for the first 100,000 cycles. After proving adequate performance of the test setup, the frequency was increased to 1.3 Hz from 100,000 cycles until completion of the fatigue test at 3,328,600 cycles. Fatigue loading was stopped, and the quasi-static tests to 210 kips (930 kN) were performed after the following pre-determined numbers of cycles: 1, 10, 100, 1000, 10,000, 100,000, 200,000, 438,000, 500,000, 763,000, 1 million, 1.25 million, 1.50 million, 1.78 million, 2.02 million, 2.32 million, 2.56 million, 2.78 million, 3.07 million, and 3.33 million. The load was slowly increased from 5.0 kips (22 kN) to 200 kips (890 kN), and was held constant at 200 kips (890 kN)

for several minutes to allow the acoustic emissions being monitored to subside. The load was then slowly increased by 5 percent, from 200 kips (890 kN) to 210 kips (930 kN), and was again held for several minutes to monitor acoustic emissions. Finally, the load was slowly decreased from 210 kips (930 kN) to 5.0 kips (22 kN), and was held constant for several minutes.

After 3,328,600 cycles, the girder was tested quasi-statically to failure, using a stepped loading procedure (Figure 3.16) with intermediate unloading to obtain acoustic emission data. The load was held constant for several minutes after each of the loading and unloading periods, until significant acoustic emissions had subsided. The test procedure was as follows: the girder was first loaded to 200 kips (890 kN) and held, increased to 210 kips (930 kN), reduced to 200 kips (890 kN), increased to 225 kips (1000 kN), reduced to 200 kips (890 kN), and increased to 250 kips (1110 kN). Thereafter, the load was decreased by 25 kips (110 kN), and then increased by 50 kips (220 kN). This pattern was repeated until failure occurred at 365 kips (1620 kN).

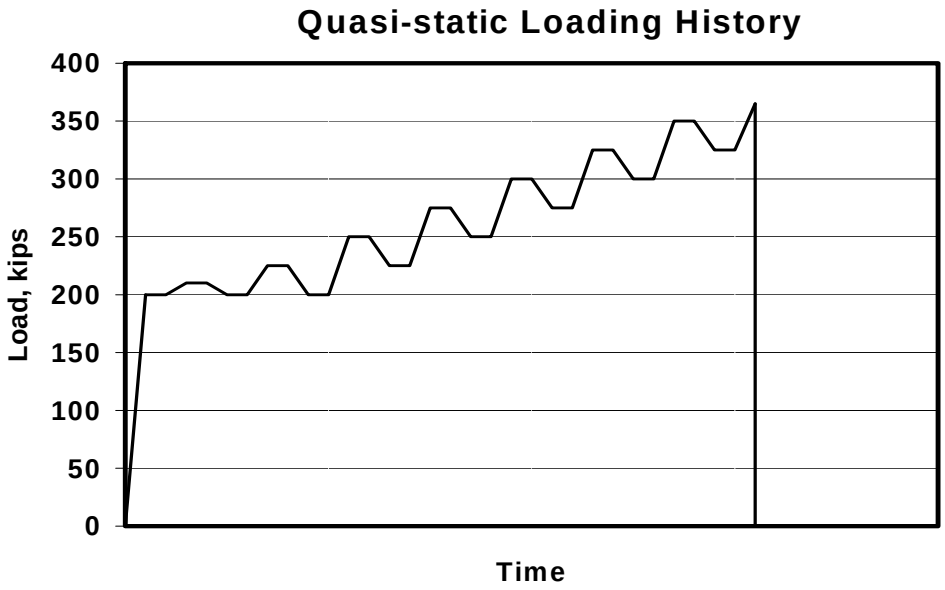

Figure 3.16 Quasi-static loading history for Specimen BG3S

Chapter 4: Test Results

This chapter presents the data gathered and the observations made during the tests described in Chapter 3.

4.1 EXPLANATION OF DATA REDUCTION

The sign conventions used for linear potentiometer data are consistent with the static tests previously performed and documented in Boenig (2000), and are explained below. Positive displacement of the linear potentiometers used to measure vertical deflections (Potentiometers D1 - D4) represents downward deflection of the girder. Positive displacement for strand-slip data (Potentiometers P1 – P8) represents strand retraction. Positive displacement for web deformation (Potentiometers L1 – L8) represents tension in the concrete.

During testing, many small, irregular measurements (< 0.005 in. or 0.1 mm) were recorded by the linear potentiometers, near the lower limit of the sensitivity of these devices. Values smaller than 0.005 in. (0.1 mm) are considered insignificant, and may be explained by instrument fluctuations, slight movement in the instrument mountings, or both.

Linear potentiometers measuring strand-slip indicated large displacements at the end of the test, but these are perhaps not indicative of actual girder behavior. The abrupt girder failure caused some instruments to slip off the ends of the strands; therefore, only displacements that could be confirmed by visual

inspection are presented in this chapter. Appendix C includes a representative sample of all the data collected during the shear-dominated fatigue tests.

4.2 RESULTS OF SHEAR-DOMINATED FATIGUE TESTS

4.2.1 BG3N

The pre-existing cracks in the east and west webs of BG3N are shown in Figures 4.1 and 4.2 respectively. These cracks, and all of the cracks in the following figures have been highlighted to clearly show their locations and lengths.

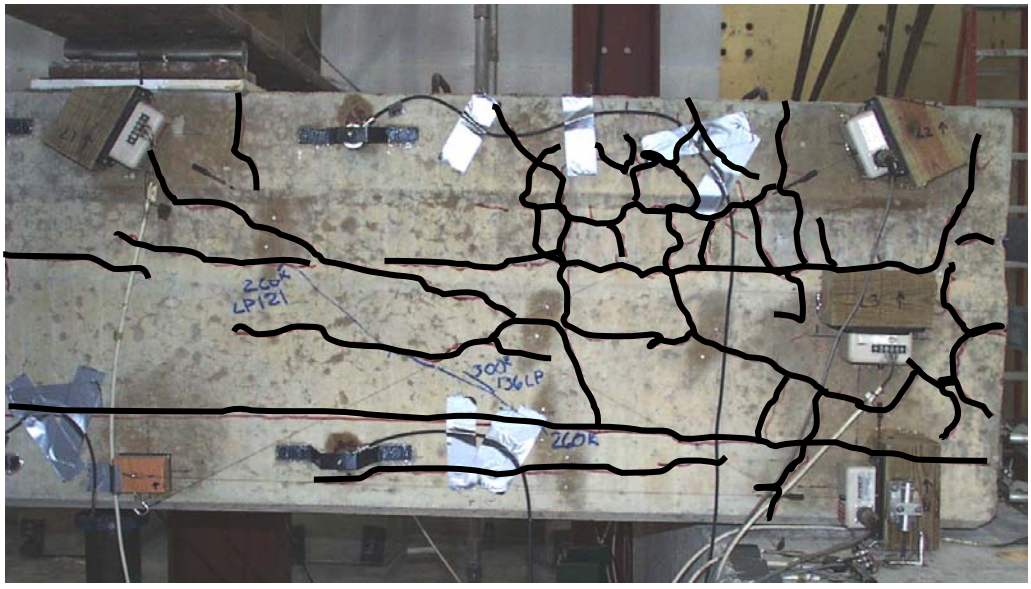

Figure 4.1 Pre-existing cracks in the east web of BG3N

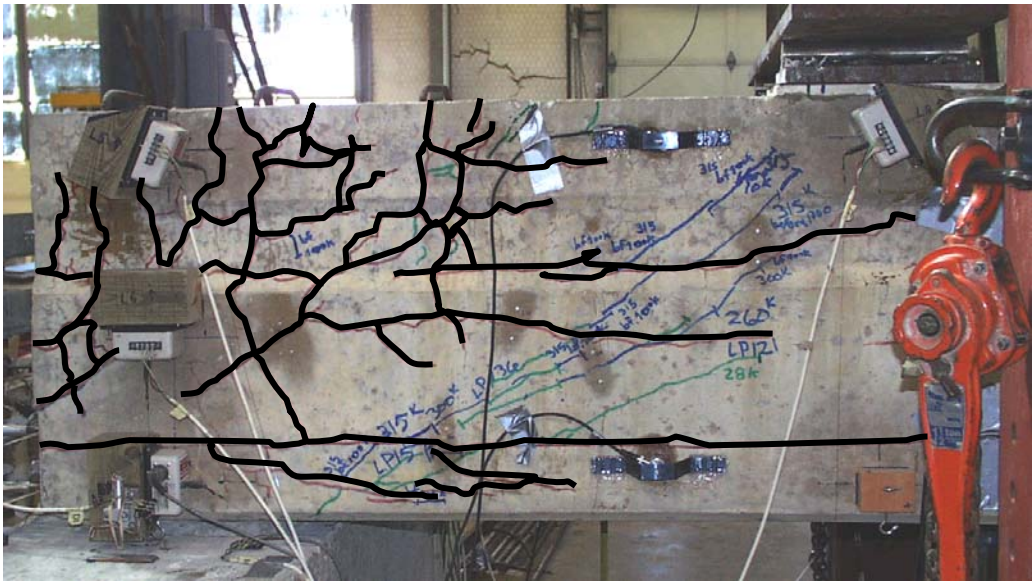

Figure 4.2 Pre-existing cracks in the west web of BG3N

Testing of BG3N began at 11 AM on September 23, 2000. A quasi-static test was performed to pre-crack the girder before beginning the fatigue test, and the first cracks were visible in both the east and west webs at approximately 260 kips (1160 kN). These cracks were diagonal, and were located near a line connecting the first loading point and the bearing pad (Figures 4.3 and 4.4).

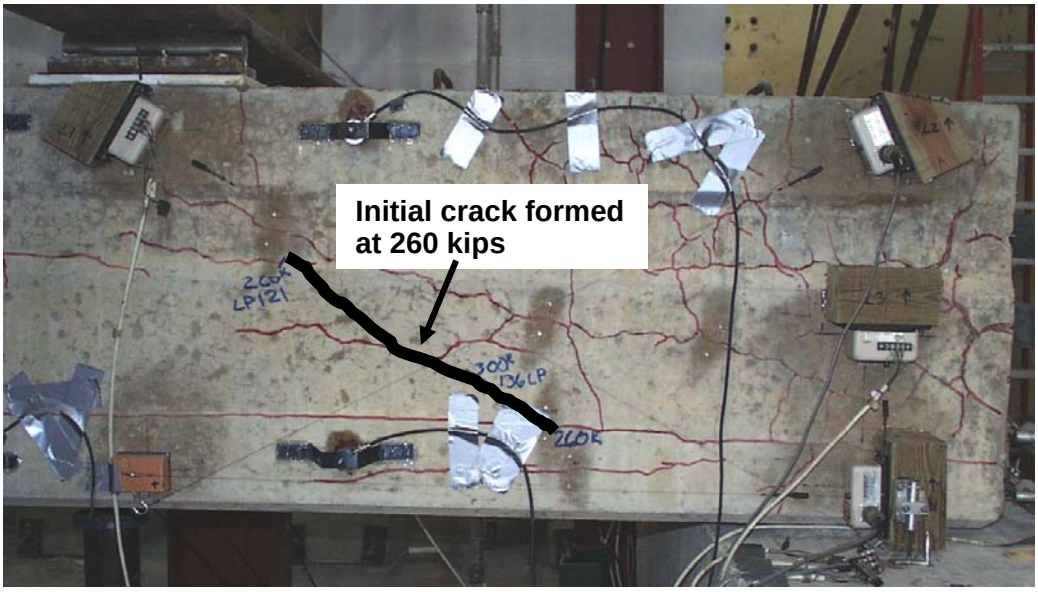

Figure 4.3 Shear-induced crack in the east web of BG3N under a static load of 260 kips (1160 kN)

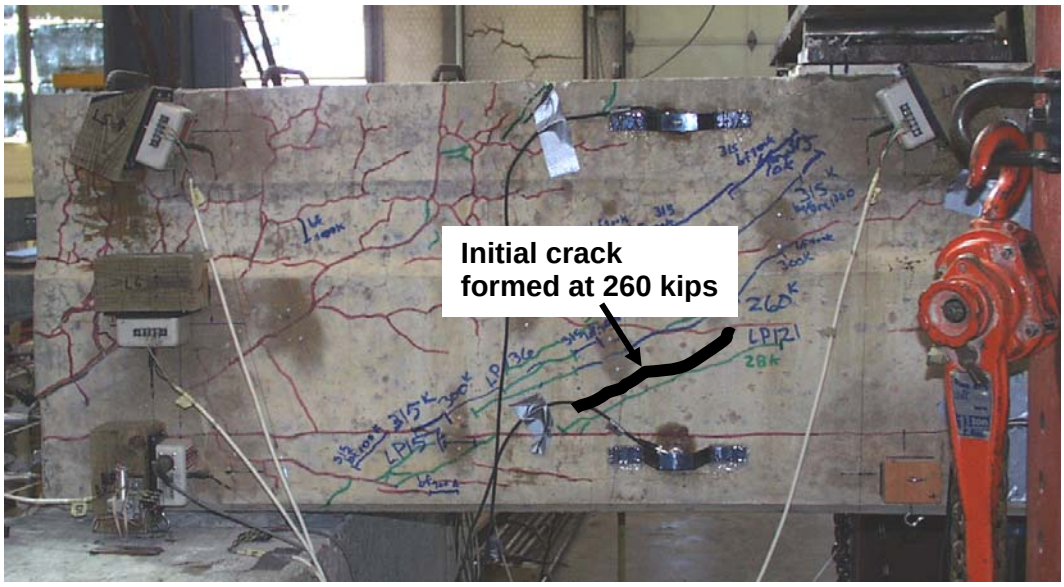

Figure 4.4 Shear-induced crack in the west web of BG3N under a static load of 260 kips (1160 kN)

After these cracks were marked, the load was increased to 300 kips (1330 kN), new cracks were marked, and instrument readings were recorded. Finally, the load was increased to 315 kips (1400 kN), at which point additional diagonal cracks formed in the region between the first loading point and the bearing pad (Figures 4.5 and 4.6).

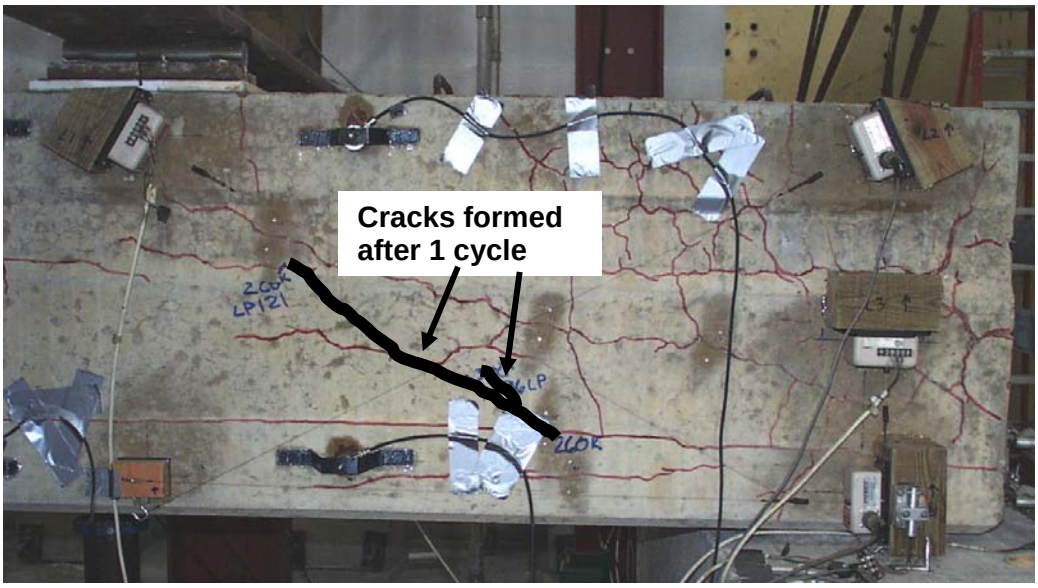

Figure 4.5 Shear-induced cracks in the east web of BG3N after one load cycle, and under a static load of 315 kips (1400 kN)

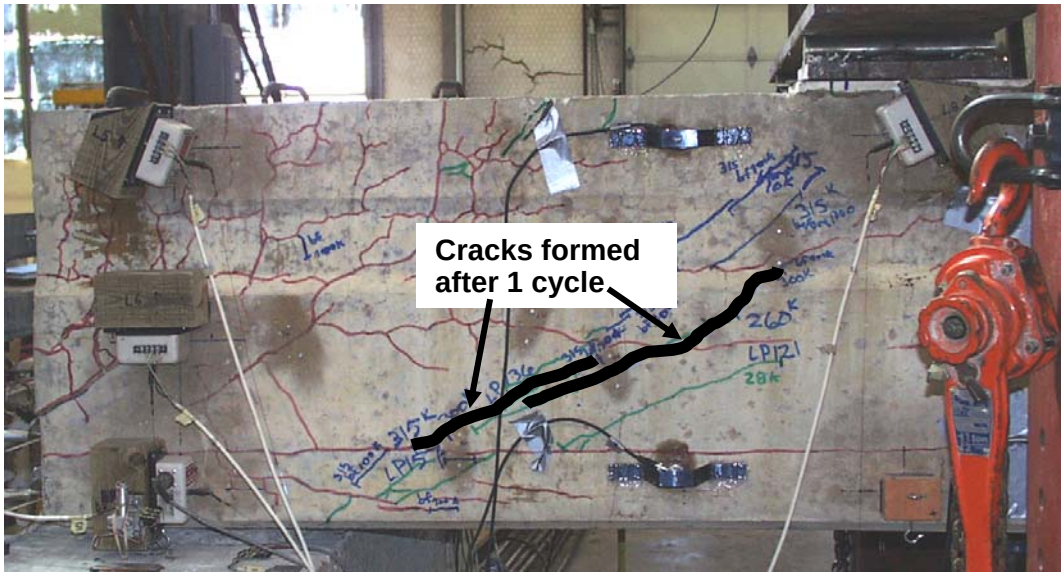

Figure 4.6 Shear-induced cracks in the west web of BG3N after one load cycle, and under a static load of 315 kips (1400 kN)

The fatigue loading procedure and periodic quasi-static loadings proceeded as detailed in Section 3.7.1. During this loading procedure, additional diagonal cracks formed in the same region. Some of these were extensions of existing diagonal cracks, and others were new cracks parallel to the existing diagonal cracks (Figures 4.7 and 4.8).

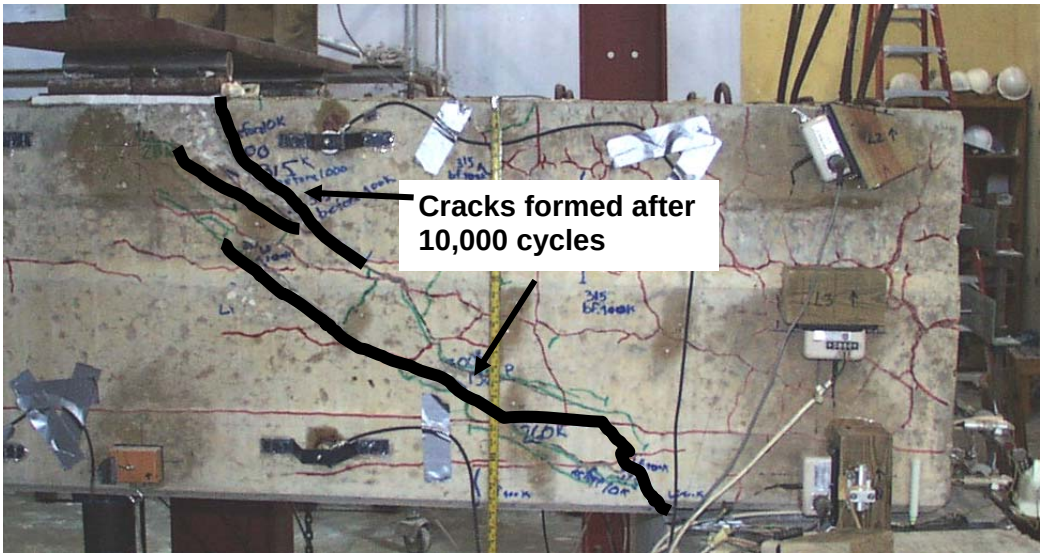

Figure 4.7 Shear-induced cracks in the east web of BG3N after 10,000 load cycles, and under a static load of 315 kips (1400 kN)

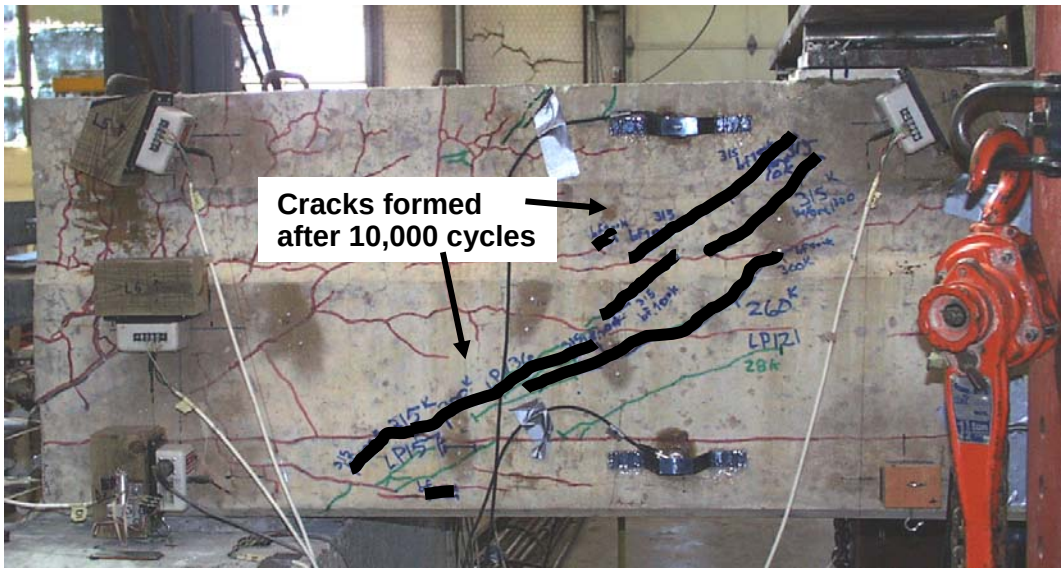

Figure 4.8 Shear-induced cracks in the west web of BG3N after 10,000 load cycles, and under a static load of 315 kips (1400 kN)

After 10,000 load cycles, the girder had moved 0.75 in. (19 mm) south in relation to the test frame and support blocks, while remaining centered in the east-to-west direction. To rectify this situation, the transverse spreader beams were re-centered and the entire test setup was inspected. The concrete support blocks were not adjusted, however, due to the difficulty involved with suspending the girder and moving the blocks simultaneously. There was no damage to the test setup, and modifications were made to restrain the girder from moving again. A steel chain was used to hold the girder stationary in relation to the test frame for the remainder of the load cycles (Figure 4.9). After the chain was placed, there was no significant girder movement for the remainder of the test.

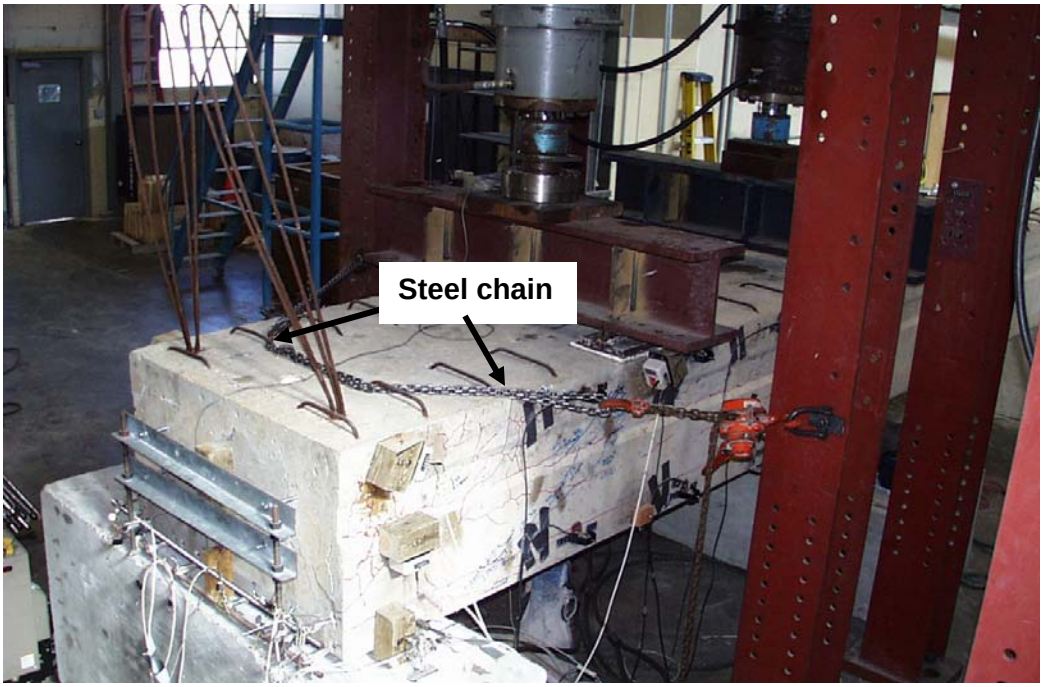

Figure 4.9 Longitudinal girder restraint placed after 10,000 load cycles

Existing cracks began to open much wider after approximately 20,000 load cycles, particularly in the east web. Cracks at the bottom of the east web opened to 0.125 in. (3 mm) wide under the 300 kip (1330 kN) cyclic load.

The MTS controller automatically stopped the test at 4 AM on September 25, 2000, after 28,133 cycles, when the pre-set DC error limit was exceeded. The east web of the girder had failed first, causing the controller to stop the test before completely failing the west web (Figures 4.10, 4.11 and 4.12). The mode of failure was yielding of the vertical reinforcing steel (stirrups) in the east web due to fatigue. Fatigue of the stirrups was caused by a combination of repeated tension and local bending at the interface of the widest diagonal crack (Figure 4.13). The west web, although diagonally cracked through the bottom of the girder, did not exhibit yielded stirrups because the cracks did not open as wide as those on the east face. After removal of concrete, corrosion was evident in the stirrups and prestressing strands in the east web, however, concrete was not removed to view the reinforcement in the west web due to future NDE to be performed on this side by another student. Corrosion of the stirrups and prestressing strands in the east web verified that the cracking was severe enough to allow moisture into the steel reinforcement.

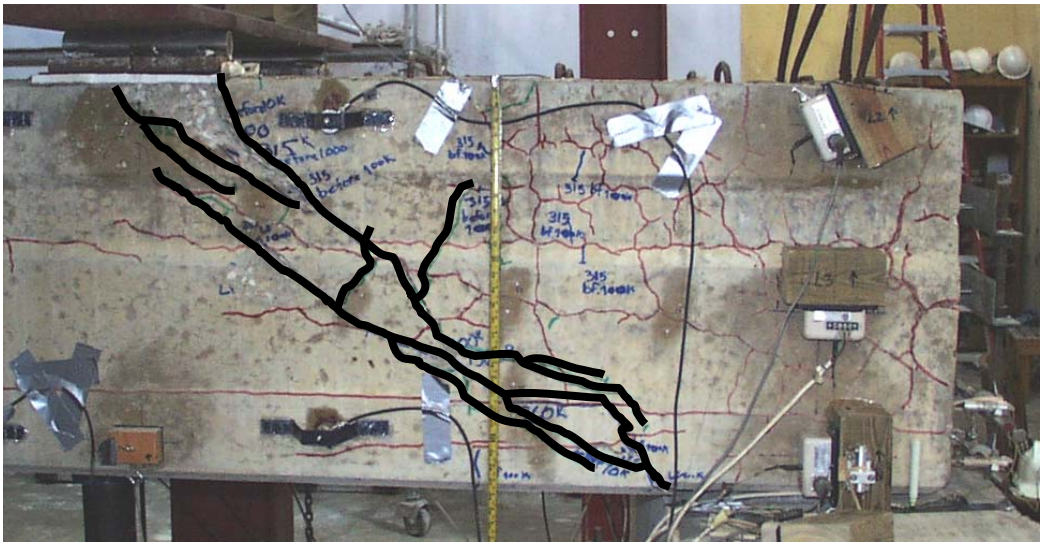

Figure 4.10 Complete failure of the east web of BG3N after 28,133 load cycles from 20 kips (90 kN) to 300 kips (1330 kN)

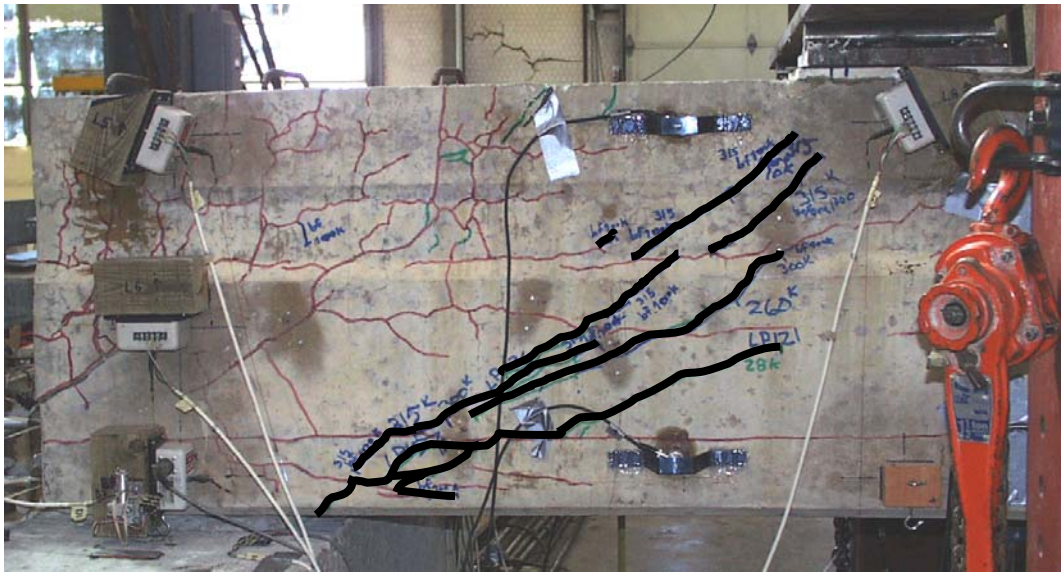

Figure 4.11 West web of BG3N after complete failure of the east web at 28,133 load cycles from 20 kips (90 kN) to 300 kips (1330 kN)

Figure 4.12 Displaced concrete section at the bottom of the east web of BG3N at failure

Figure 4.13 Fractured shear reinforcement (stirrup) in the east web of BG3N at failure, after removal of concrete

4.2.1.1 Data Acquired from Linear Potentiometers

There was no significant slip of prestressing strands during the test. This was verified by visual inspection after each quasi-static loading, and after failure of the girder.

Vertical deflections were measured under each web at a distance 88.5 in. (2.25 m) from the girder end (midway between the two hydraulic rams) after 100, 1000, and 10,000 load cycles. Vertical deflections under each web, and the average of these two deflections, are plotted versus number of load cycles (Figure 4.14).

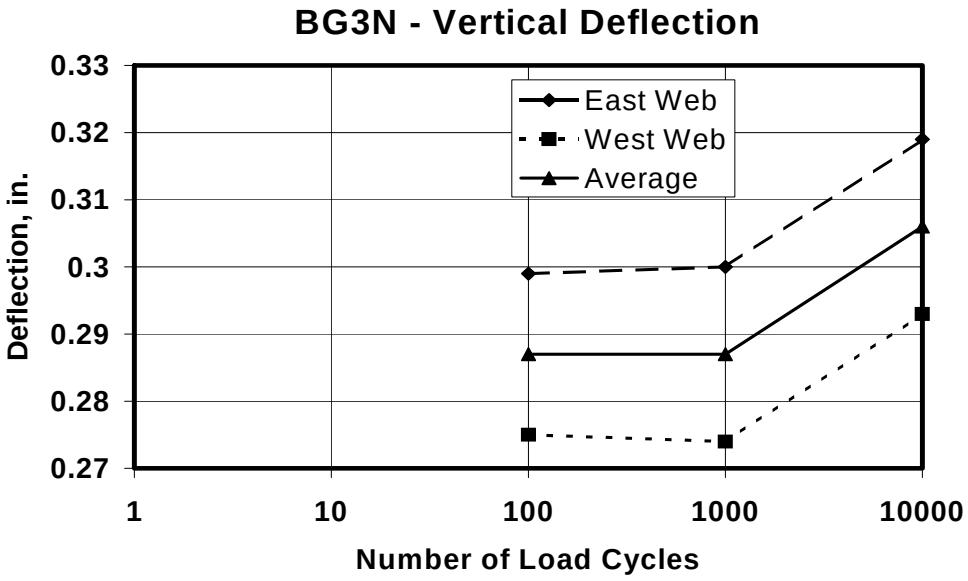

Figure 4.14 Vertical deflection vs. number of load cycles for BG3N

Deformations were measured in the compression diagonals, tension diagonals, and bottom chords (Figures 3.10, 3.11, and 3.12). Figure 4.15 shows

the shortening of the compression diagonal (from L1 data), the extension of the tension diagonal (from L2 data), and the extension of the bottom tension chord (from L4 data) in the east web of BG3N with the increasing number of load cycles.

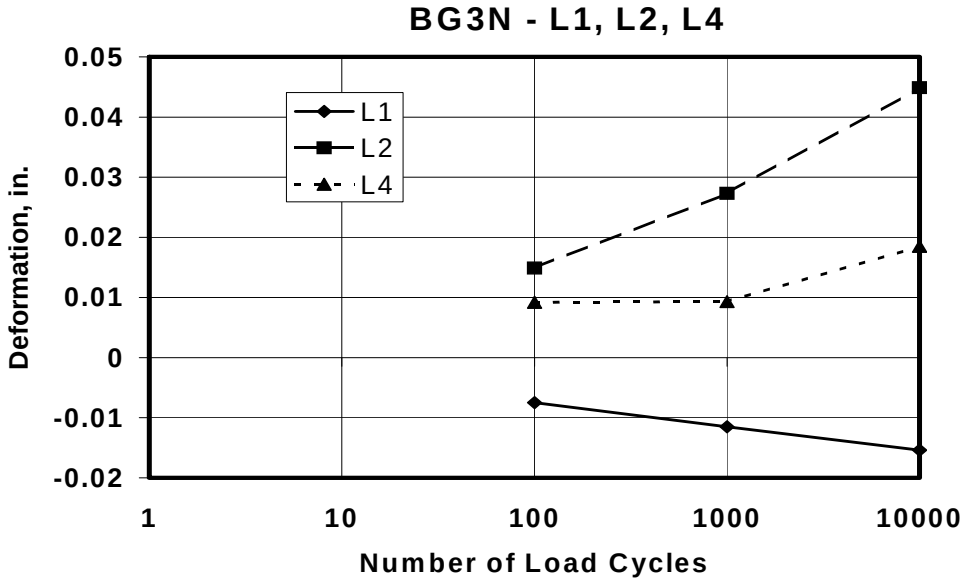

Figure 4.15 Deformation of the diagonals and bottom chord in the east web of BG3N

The total web deformation index was proposed by Boenig (2000) to combine the absolute values of the displacement ratios of the diagonals and bottom chords detailed above. This index allows overall web deformation to be compared between shear test specimens, and girder flexibility to be correlated with concrete modulus of elasticity. Figure 4.16 shows the total web deformation index for the east web of BG3N, and is defined below:

Total web deformation index = (Strain L1 + Strain L2 + Strain L4) x 10,000

where:

- Strain L1 is the absolute value of the length change in compression diagonal L1 divided by the gauge length of L1,
- Strain L2 is the absolute value of the length change in tension diagonal L2 divided by the gauge length of L2, and
- Strain L4 is the absolute value of the length change in bottom chord L4 divided by the gauge length of L4.

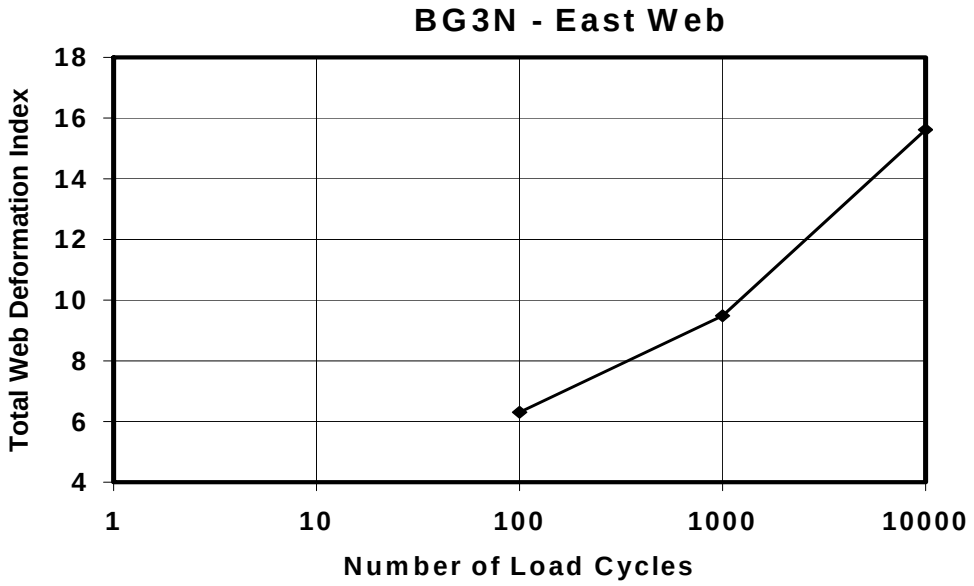

Figure 4.16 Total web deformation index in the east web of BG3N

Vertical deformations in the solid end block, directly above the support on each side of the girder, were also measured (L3 and L6 data). These measurements, however, were not accurately recorded due to instrument error in

this range of very small length change. Therefore, these data are not presented here.

Figure 4.17 shows the shortening of the compression diagonal in the west web of BG3N (from L8 data). The compression diagonal is the only measurement in the west web that produced valid results. The tension diagonal and bottom chord measurements in the west web were not accurately measured due to instrument error in this range of very small length change. Therefore, these data are not presented, and consequently, total web deformation index for the west web is not presented.

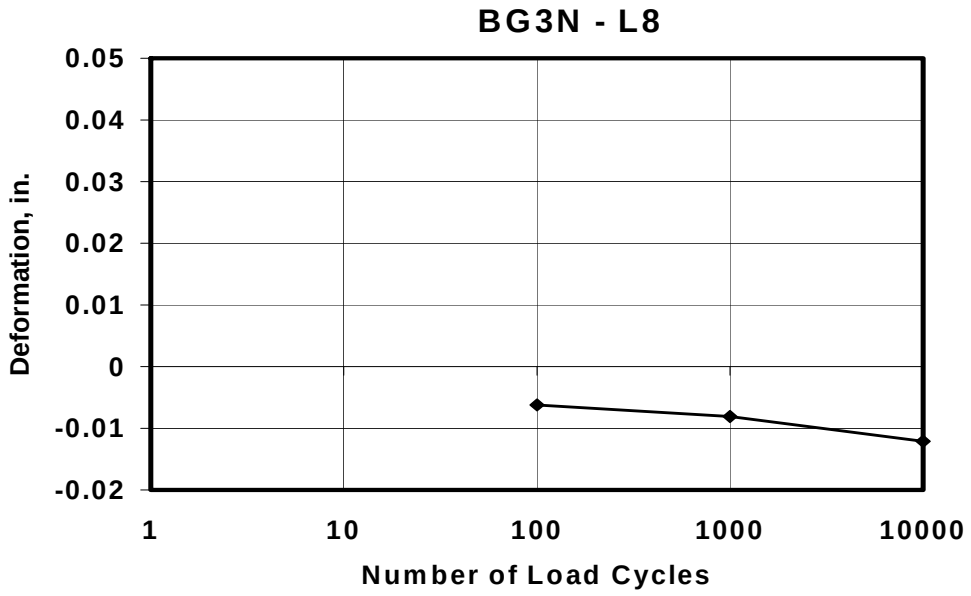

Figure 4.17 Shortening of the compression diagonal in the west web of BG3N

4.2.1.2 Data Acquired from Demountable Mechanical Strain Gauges

Demec gauges were used to monitor changes in crack widths, specifically the changes in width of the widest cracks within the shear-critical regions of both the east and west webs (Figure 4.18). The widest initial crack in the shear-critical region of the east web was monitored with Demec Point 3E. From zero load cycles to 10,000 load cycles, the crack width at Point 3E increased by 0.020 in. (0.50 mm). The widest initial crack in the shear-critical region of the west web was monitored with Demec Point 3W. From zero load cycles to 10,000 load cycles, the crack width at Point 3W decreased by 0.002 in. (0.05 mm). Although Point 3W decreased slightly in width, Point 6W, a narrower parallel crack monitored in the same region, increased in width by 0.002 in. (0.05 mm). Width changes varied for the ten remaining cracks monitored. These crack widths increased very slightly, decreased slightly, or remained constant. Overall, there was very little change in the existing crack widths during fatigue testing. This was not unexpected, because new parallel cracks formed in the same region.

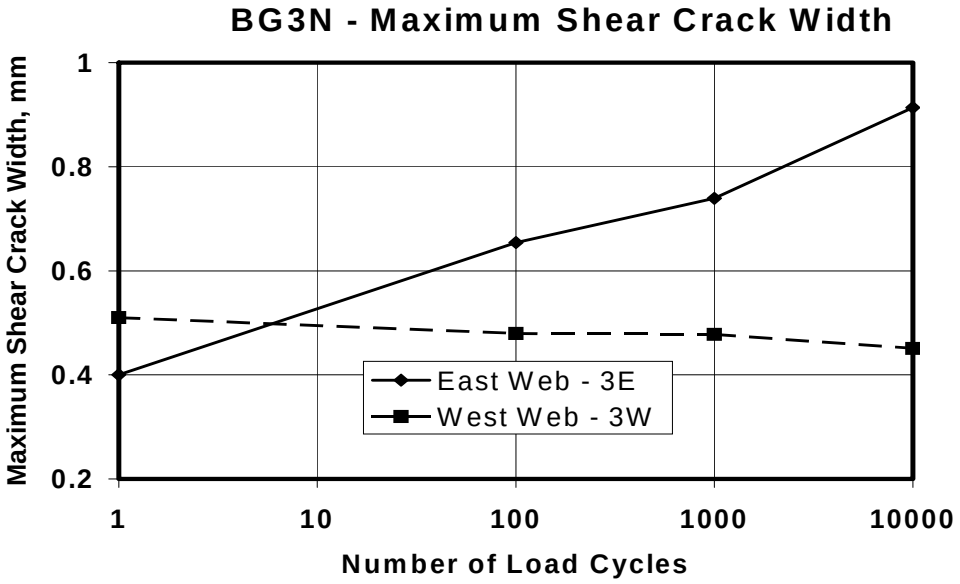

Figure 4.18 Changes in maximum shear crack widths in both webs of BG3N

4.2.1.3 Data Acquired from Visual Crack Monitoring

Crack ratio (CR) and damage index (DI) were monitored as defined in Section 3.6.3. Figure 4.19 shows the change in crack ratio with the number of load cycles, and Figure 4.20 shows the change in damage index with the number of load cycles. The total increases in crack ratio and damage index during fatigue testing were more pronounced in the east web. The increase in east-web crack ratio was 56 percent, and the corresponding change in damage index was 154 percent.

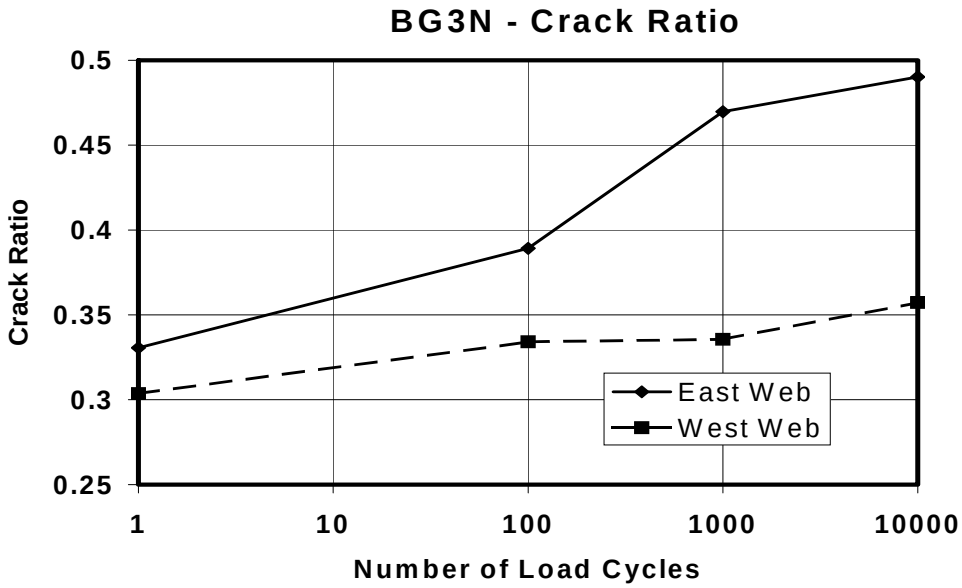

Figure 4.19 Change in crack ratio for BG3N

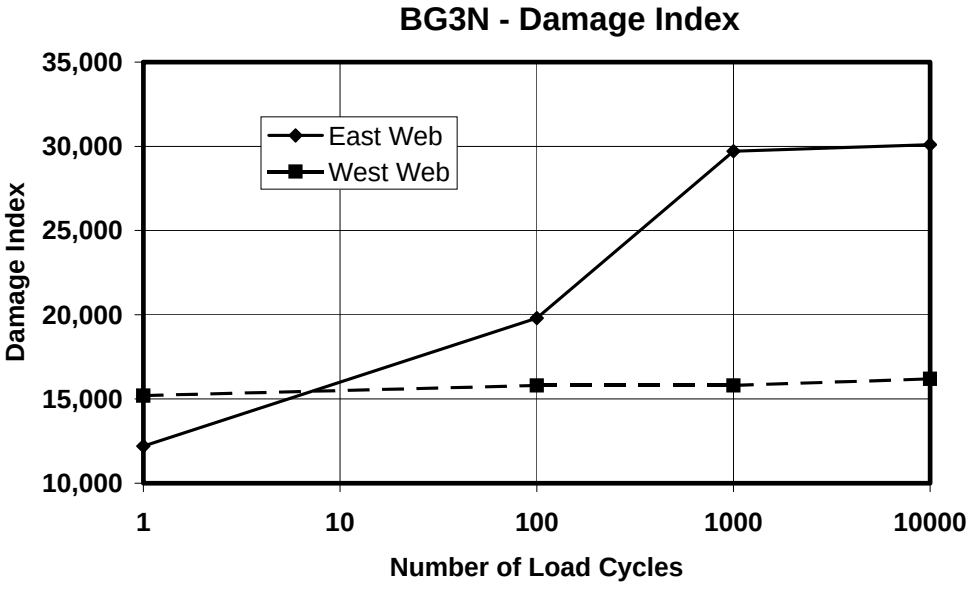

Figure 4.20 Change in damage index for BG3N

4.2.2 BG3S

The pre-existing cracks in the east and west webs of BG3S are shown in Figures 4.21 and 4.22.

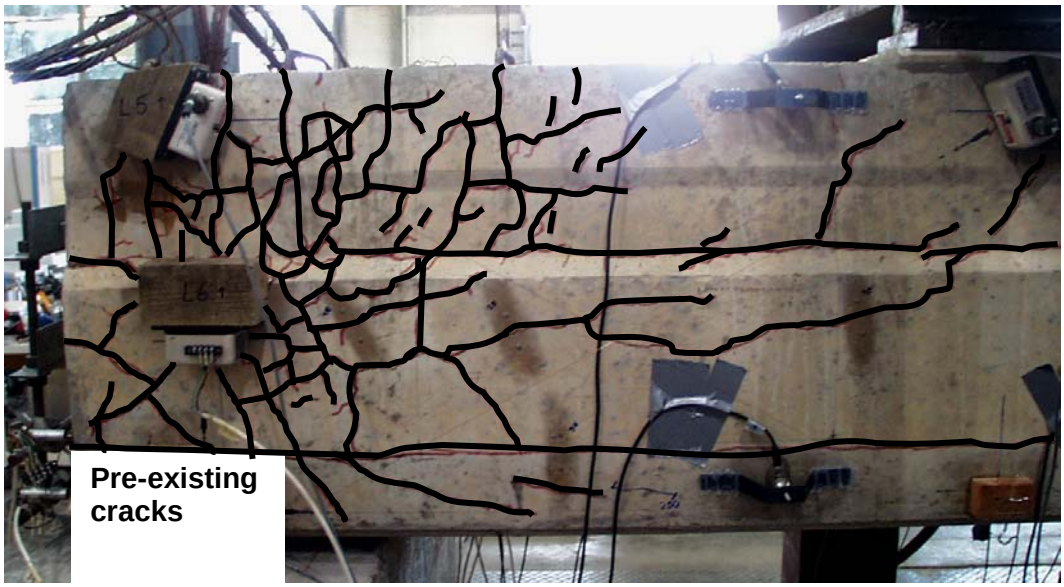

Figure 4.21 Pre-existing cracks in the east web of BG3S

Figure 4.22 Pre-existing cracks in the west web of BG3S

Testing of BG3S began at 3 PM on October 14, 2000. A quasi-static test was performed to pre-crack the girder before beginning the fatigue test, and the first cracks were visible at approximately 230 kips (1020 kN) in the west web, and 250 kips (1110 kN) in the east web. The one short crack that formed in the east web was nearly horizontal, and was located in the bottom flange (Figure 4.23). The cracks that formed in the west web were diagonal and along a line between the first loading point and the bearing pad (Figure 4.24).

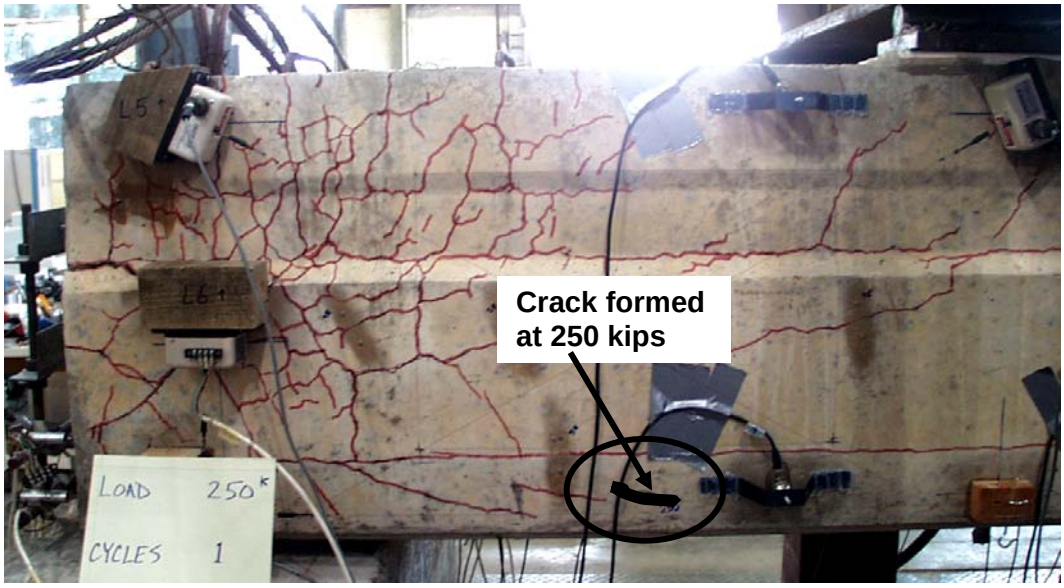

Figure 4.23 Shear-induced crack in the east web of BG3S under a static load of 250 kips (1110 kN)

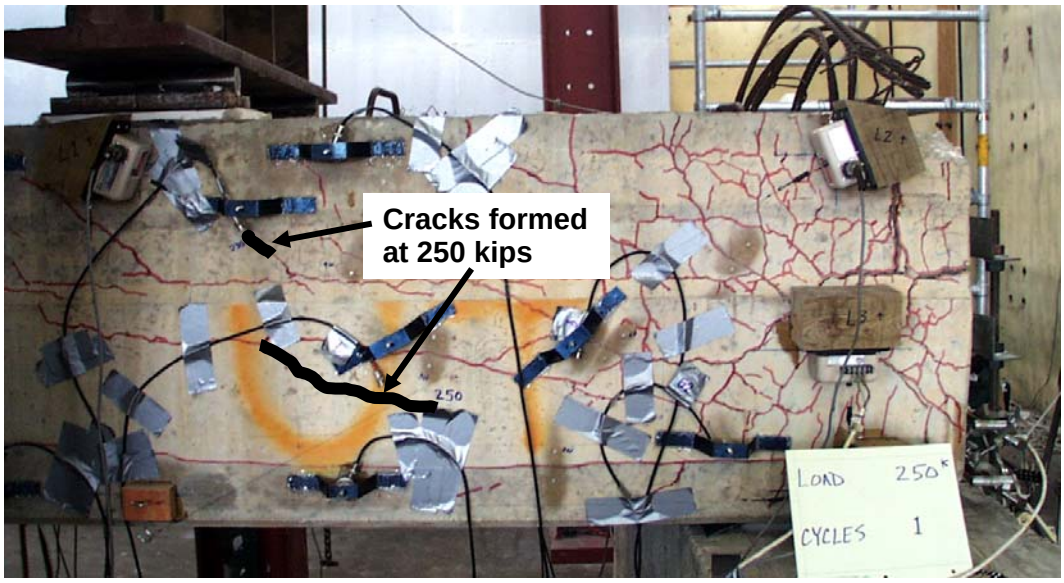

Figure 4.24 Shear-induced cracks in the west web of BG3S under a static load of 250 kips (1110 kN)

After these cracks were marked, the load was returned to zero. The fatigue loading procedure and periodic quasi-static loadings then proceeded as detailed in Section 3.7.2. During this loading procedure of 3,328,600 load cycles, only slight additional diagonal cracking formed, and most of this additional cracking was short extensions of existing diagonal cracks (Figures 4.25 and 4.26).

Figure 4.25 Shear-induced cracks in the east web of BG3S after 3,328,600 load cycles

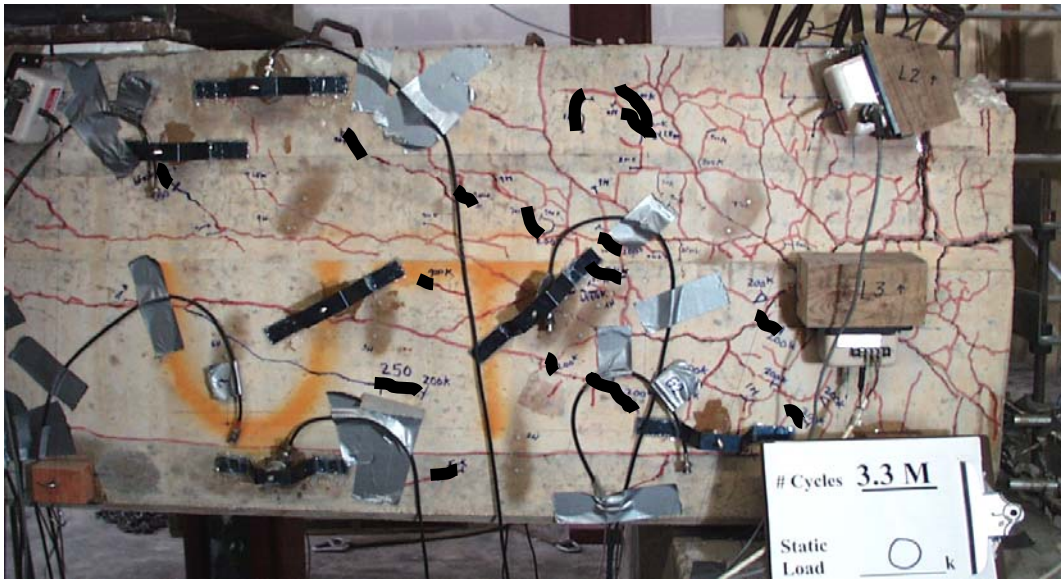

Figure 4.26 Shear-induced cracks in the west web of BG3S after 3,328,600 load cycles

Fatigue testing was stopped at 6 PM on November 15, 2000, after 3,328,600 cycles, and minimal additional visible damage to the girder. At this point in the test, it was evident that under the cyclic load of 20 kips (90 kN) to 200 kips (890 kN) the girder would probably not fail in fatigue for many more cycles.

Approximately thirty minutes after ending the cyclic loading, the girder was tested quasi-statically to failure, using a stepped loading procedure with intermediate unloading as detailed in Section 3.7.2. During quasi-static loading, additional diagonal cracking formed in the same diagonal strut region. Some of the additional cracks were extensions of existing diagonal cracks, and others were new cracks parallel to the existing diagonal cracks. Between 300 kips (1330 kN) and 325 kips (1450 kN) in the quasi-static loading, cracking was audible, and the

east web experienced worse cracking than the west web. At approximately 320 kips (1420 kN), one crack in the east web propagated through the bottom flange. During the loading increment from 325 kips (1450 kN) to 350 kips (1560 kN), there was again audible cracking, yet not as much as during the previous loading step. The additional cracking that formed during the stepped quasi-static loading is shown under a static load of 350 kips (1560 kN) in Figures 4.27 and 4.28.

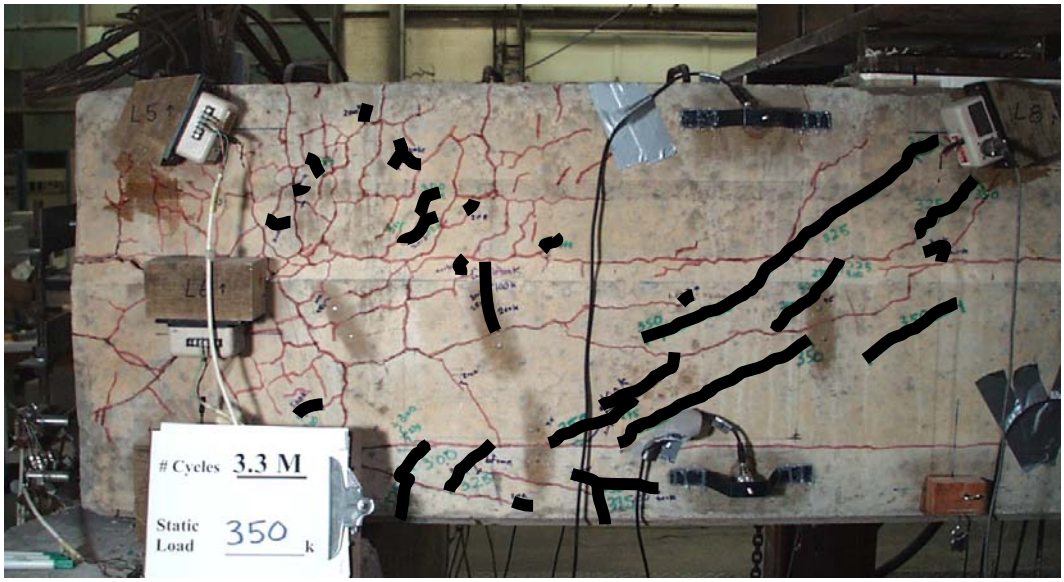

Figure 4.27 Shear-induced cracks in the east web of BG3S after 3,328,600 load cycles, and under a static load of 350 kips (1560 kN)

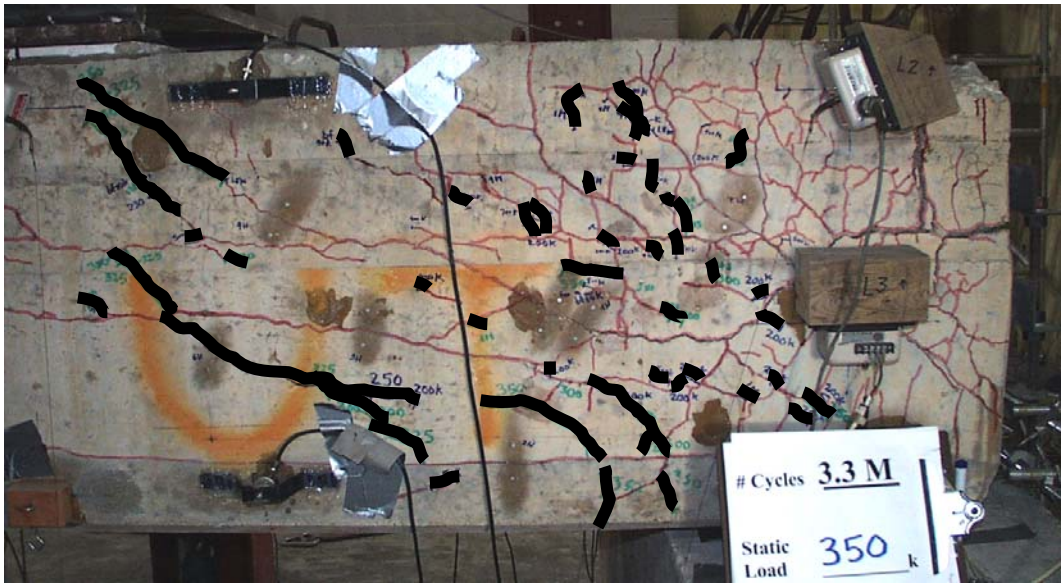

Figure 4.28 Shear-induced cracks in the west web of BG3S after 3,328,600 load cycles, and under a static load of 350 kips (1560 kN)

The girder was unloaded from 350 kips (1560 kN) to 325 kips (1450 kN), and the load was again increased. There was more audible cracking at approximately 360 kips (1600 kN), and loud popping in the final three seconds prior to complete failure at 365 kips (1620 kN). The west web failed slightly prior to the east web when the concrete cover spalled off, exposing the reinforcing steel. At this point, the concrete in the diagonal compression strut crushed, and almost immediately the concrete cover in the east web began to delaminate and spall. The diagonal compression strut in the east web also crushed; although the concrete cover delaminated, it did not spall as severely as on the west side (Figures 4.29 and 4.30). For a description of compression strut, and an explanation of the strut-and-tie-model, see MacGregor (1997). Corrosion was evident in the stirrups and prestressing strands in both the east and west webs,

which again verified that the cracking was severe enough to allow moisture into the steel reinforcement.

Figure 4.29 Failure of the east web of BG3S after 3,328,600 load cycles and a 365 kip (1620 kN) quasi-static load

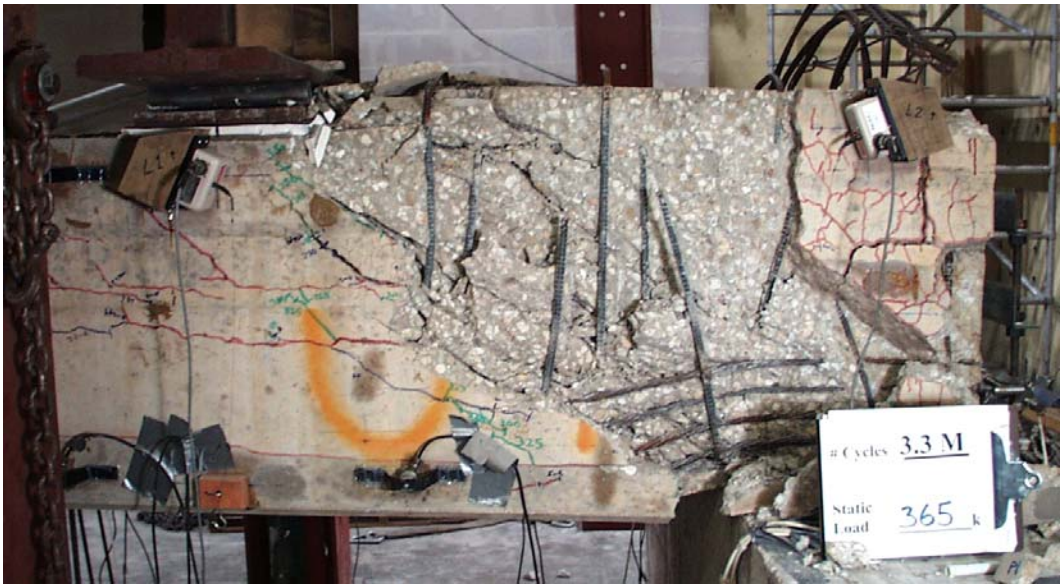

Figure 4.30 Failure of the west web of BG3S after 3,328,600 load cycles and a 365 kip (1620 kN) quasi-static load

The actual quasi-static loading history of BG3S to failure is shown in Figure 4.31.

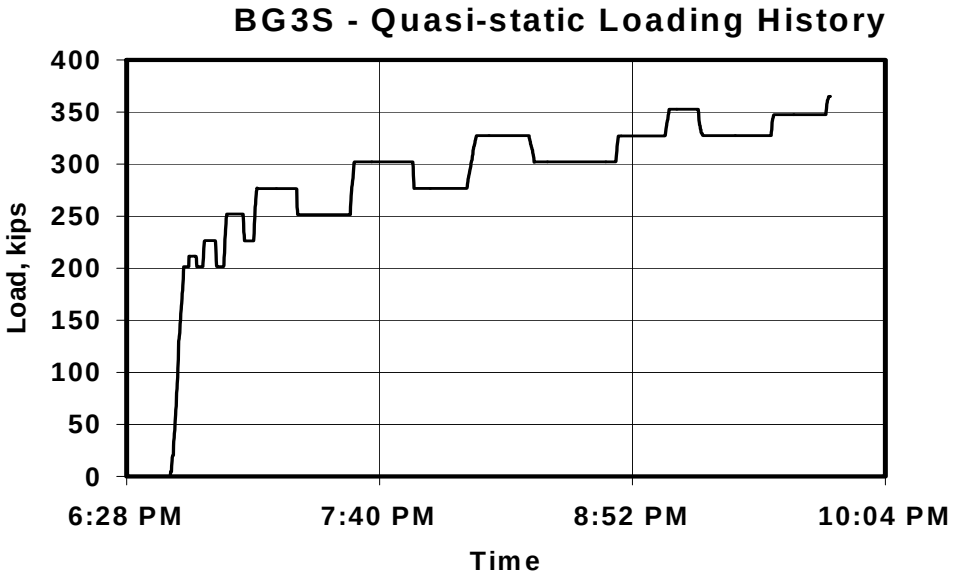

Figure 4.31 Actual quasi-static loading history of BG3S to failure

4.2.2.1 Data Acquired from Linear Potentiometers

There was no significant slip of prestressing strands during the fatigue test. In the final moments of the quasi-static test to failure, however, as the concrete cover spalled off and the web concrete crushed, several interior prestressing strands and all of the strands nearest to the exterior surfaces of the webs slipped (Figure 4.32). The amount of slip was not measured accurately by the linear potentiometers because as the girder failed, the potentiometers slipped off of the ends of the prestressing strands. Slip was verified by visual inspection, and was manually measured to be between 0.125 in. (3 mm) and 0.25 in. (6 mm) for the

Figure 4.32 Slip of exterior prestressing strands after failure of BG3S

interior strand, and approximately 0.5 inch (13 mm) for the exterior strand.

Vertical deflections were measured under each web at a distance 88.5 in. (2.248 m) from the girder end (midway between the two hydraulic rams) after pre-determined numbers of load cycles detailed in Section 3.7.2, and throughout the quasi-static loading to failure. Vertical deflections under each web, and the average of these two deflections, are plotted versus number of load cycles (Figure 4.33).

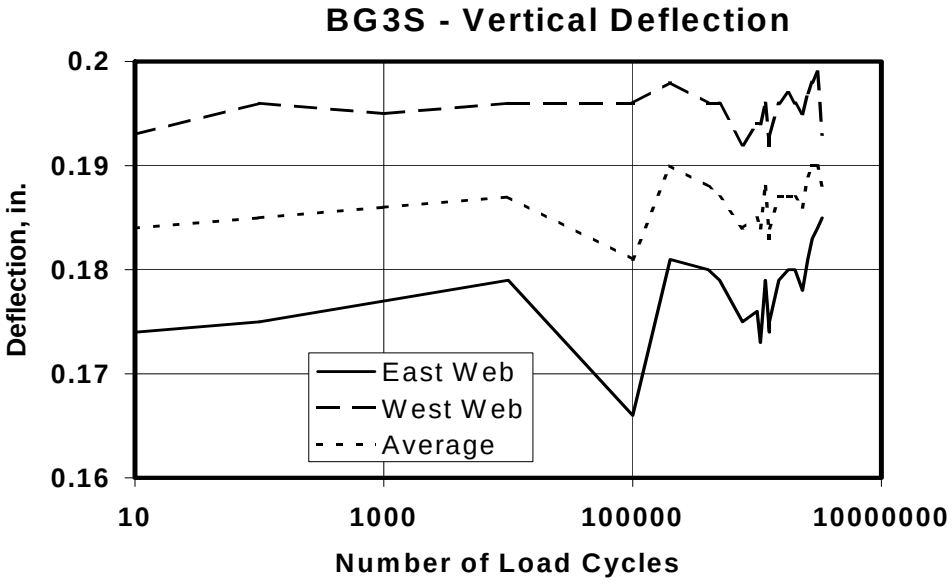

Figure 4.33 Vertical deflection vs. number of load cycles for BG3S

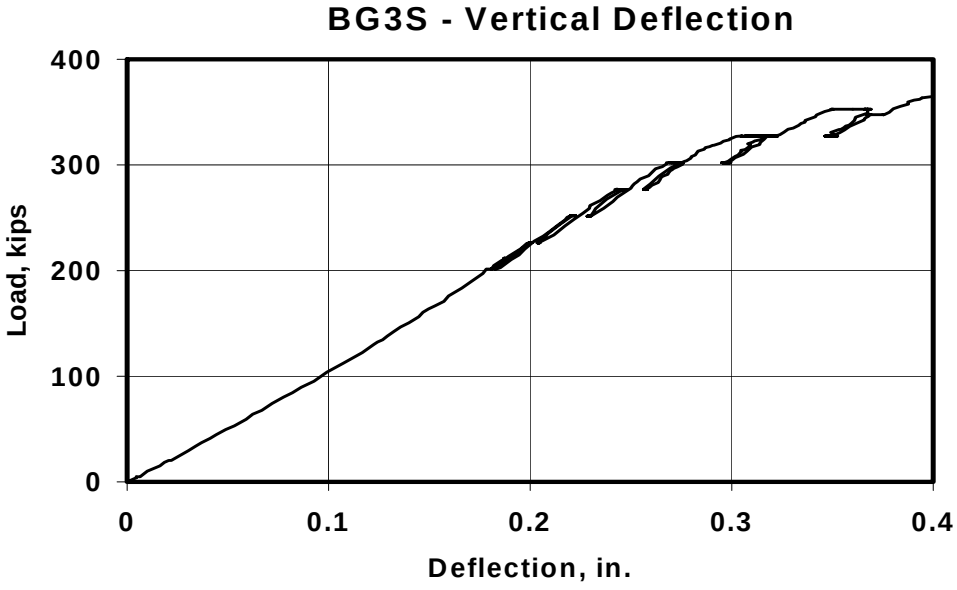

Figure 4.34 Quasi-static loading of BG3S to failure

The difference between the average deflection after one load cycle, and nearly 3.3 million cycles was only 0.006 in. (0.15 mm). Therefore, the change in vertical deflection with respect to the number of load cycles is very small. Vertical deflections were similarly measured during quasi-static loading to failure, and are plotted versus load (Figure 4.34).

Deformations were measured in the compression diagonals, tension diagonals, and bottom chords (Figures 3.10, 3.11, and 3.12). In both webs, the deformations in these locations were too small to be measured accurately with the linear potentiometers being used. Throughout fatigue testing, the deformations were smaller than the threshold of sensitivity of the instruments, which confirmed that the changes in web deformation with respect to the number of load cycles were insignificant. Therefore, these data are not presented, and consequently, total web deformation index is not presented.

Web deformations as described above were similarly measured during quasi-static loading to failure. The shortening of compression diagonals, extension of tension diagonals, and extension of the bottom chords in the shear-critical regions of both webs are shown in Figures 4.35, 4.36, and 4.37. Measurements were recorded until a load of 325 kips (1450 kN) was achieved, at which time the linear potentiometers measuring web deformation were removed in anticipation of the girder failure.

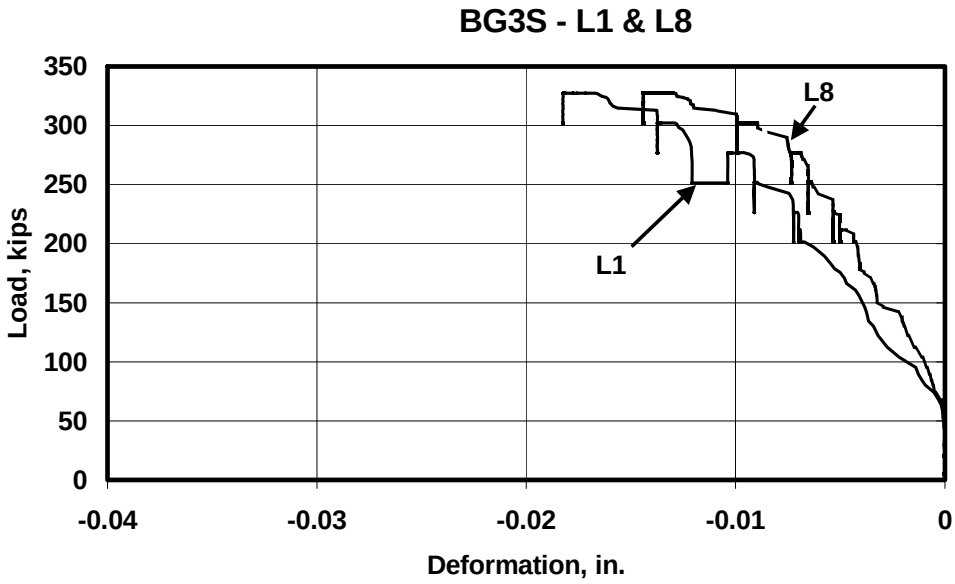

Figure 4.35 Shortening of the compression diagonals in the webs of BG3S

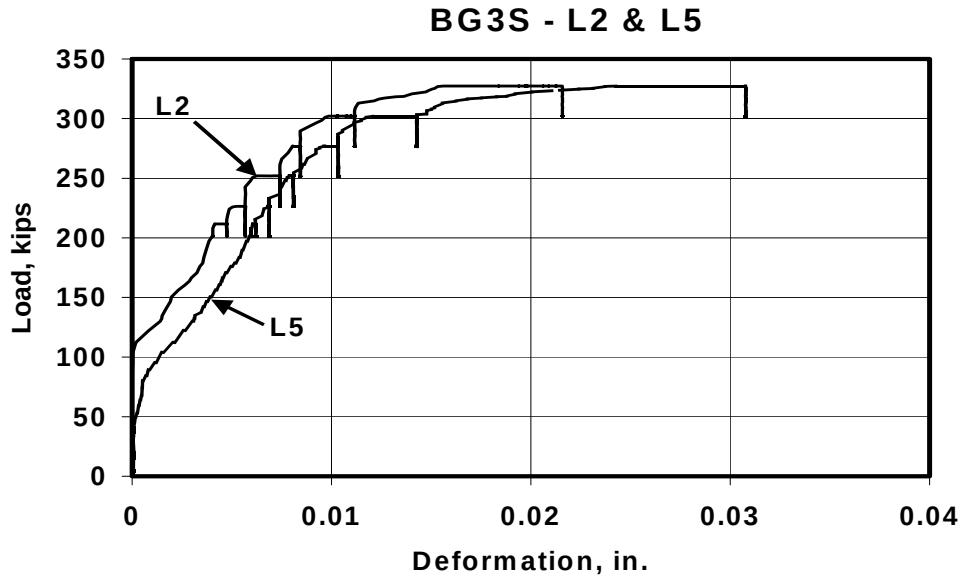

Figure 4.36 Extension of the tension diagonals in the webs of BG3S

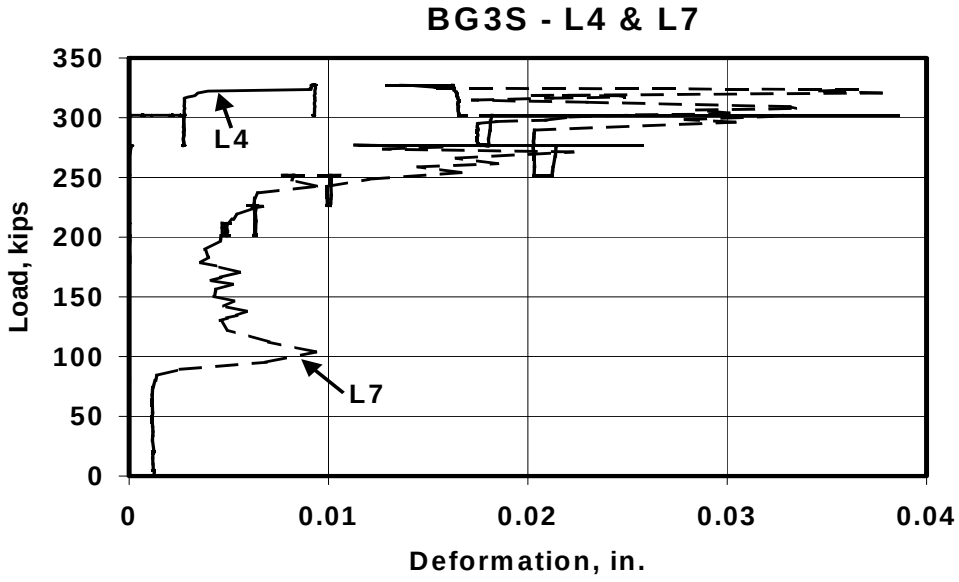

Figure 4.37 Extension of the bottom chords in the webs of BG3S

4.2.2.2 Data Acquired from Demountable Mechanical Strain Gauges

Demec gauges were used to monitor changes in crack widths, specifically the change in width of the widest cracks within the shear-critical regions of both the east and west webs (Figure 4.38). The widest initial crack in the shear-critical region of the east web was monitored with Demec Point 2E. From zero load cycles to 3,328,600 load cycles, the crack width at Point 2E increased by 0.003 in. (0.08 mm). The widest initial crack in the shear-critical region of the west web was monitored with Demec Point 1W. The crack width at Point 1W also increased slightly, 0.003 in. (0.08 mm), from zero load cycles to 3,328,600 load cycles. Of the five cracks monitored on the east side and the seven cracks monitored on the west side, only one crack width in addition to Points 2E and 1W increased significantly. Point 4E, a much narrower crack, increased 0.003 in.

(0.08 mm). The widths of the ten remaining monitored cracks increased very slightly, decreased slightly, or remained constant. Overall, there was very little change in any crack widths due to the fatigue testing.

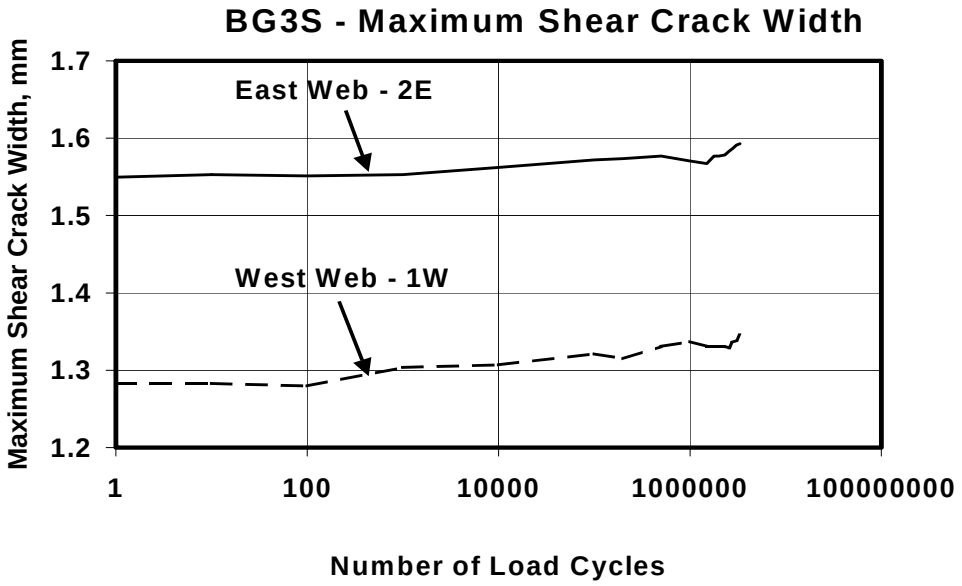

Figure 4.38 Changes in maximum shear crack widths in both webs of BG3S

4.2.2.3 Data Acquired from Visual Crack Monitoring

Crack ratio (CR) and damage index (DI) were monitored as defined in Section 3.6.3. Figure 4.39 shows the change in crack ratio with the number of load cycles, and Figure 4.40 shows the change in damage index with the number of load cycles. There was very little damage caused by the fatigue testing, subsequently there was very little change reflected in the crack ratio or damage index with increased numbers of load cycles. Figures 4.39 and 4.40 graphically show significant increases between measurements at 100,000 and 200,000 load

cycles. The total increases in crack ratio and damage index during fatigue testing were more pronounced in the west web. The increase in west web crack ratio was 12 percent, and the corresponding change in damage index was 14 percent.

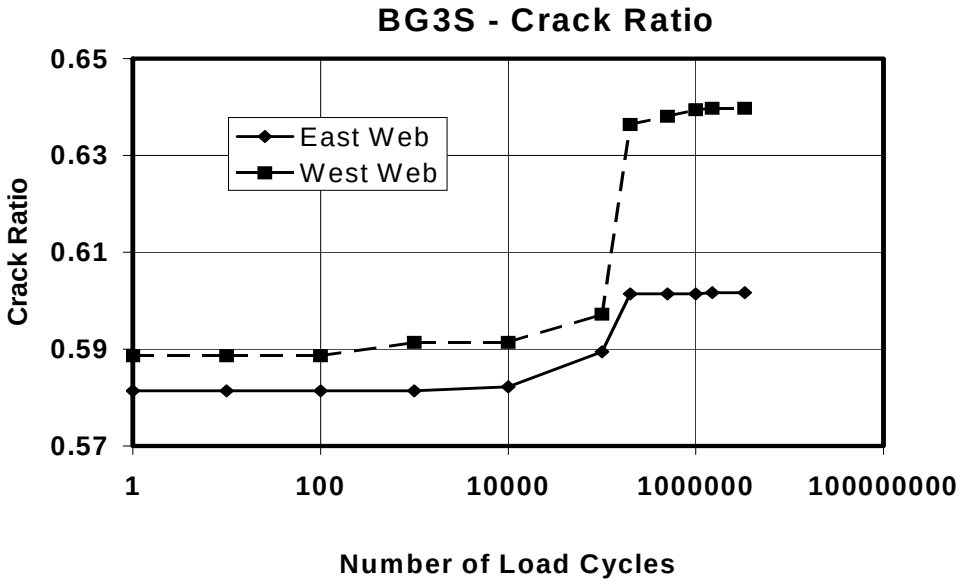

Figure 4.39 Change in crack ratio for BG3S

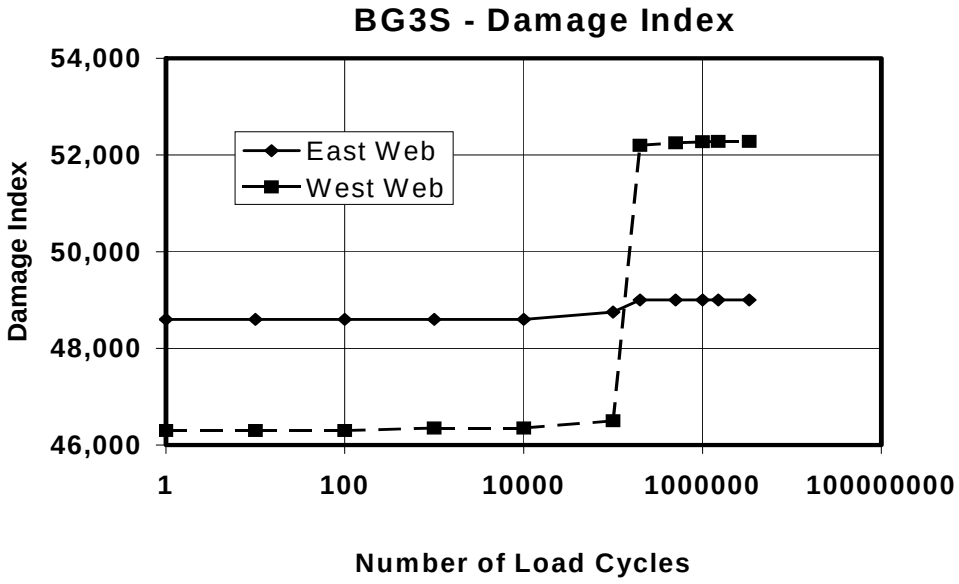

Figure 4.40 Change in damage index for BG3S

No Tables

Chapter 5: Significance of Test Results

In this chapter, the experimental results from the two shear-dominated fatigue tests presented in Chapter 4 are evaluated and compared with predicted results. In Section 5.1, shear forces from applied fatigue testing loads are compared with calculated shears resulting from AASHTO design service loads. Section 5.2 presents the experimental results by plotting applied shear force range for the specimens against the number of load cycles required to cause shear failure (S-N curves). Section 5.3 compares the behaviors of the two shear-dominated fatigue specimens. Finally, Section 5.4 compares shear-transfer mechanisms and failure modes of the shear-dominated fatigue specimens.

5.1 COMPARISON OF TEST LOADS WITH AASHTO SERVICE LOADS

Applied maximum shears and shear ranges for the test specimens are compared with shears resulting from AASHTO live-plus-impact service loads. Critical AASHTO live loads were determined by calculating and comparing the shear forces produced by the specified HS20-44 (MS18) standard truck loading, standard lane loading equivalent to truck trains, and Alternate Military Loading. The HS20-44 (MS18) standard truck loading is used with the minimum distance of 14 ft (4.27 m) between the rear two sets of axles to provide the critical loading condition for shear.

Using a simple span of 68.25 ft (20.80 m) from center to center of supports, representing the test specimens' in-service conditions, the maximum

live-load shear for the HS20-44 truck loading is V_{LL} = 62.1 kips (276 kN). The impact factor for a 68.25 ft (20.80 m) span is 30 percent, which yields a shear due to live-plus-impact load of 80.7 kips (359 kN). Using the AASHTO distribution of wheel loads, each girder experiences a shear due to live-plus-impact load of 29.3 kips (130 kN). For this span length, the calculated dead-load shear per girder due to self-weight of the girder, cast-in-place slab, and railing is 43 kips (191 kN). The combined shear at the support due to dead load and live-plus-impact load is approximately 73 kips (325 kN). Therefore, the AASHTO design shear range of an in-service bridge with these dimensions is from 43 kips (191 kN) to 73 kips (325 kN), a range equal to 30 kips (133 kN).

Shear at the support during fatigue testing ranged from 21 kips (93 kN) to 221 kips (983 kN) for BG3N, a range equal to 200 kips (890 kN), and from 21 kips (93 kN) to 150 kips (667 kN) for BG3S, a range equal to 129 kips (574 kN). These ranges of shear force are respectively 6.7 times and 4.3 times higher than the AASHTO design shear ranges calculated above. Both of the fatigue tests subjected the girders to fatigue-shear forces and shear-force ranges that were much greater than those that would be imposed by gross truck overloads, therefore, much more severe than the bridge girders would ever normally experience.

5.2 PRESENTATION OF TEST RESULTS USING S-N CURVES

To predict the capacity of a bridge girder under fatigue loading, the relationship between the ranges of applied shear force and the number of load

cycles to failure must be known. This relationship can be illustrated by an S-N curve, described below and shown schematically in Figure 5.1.

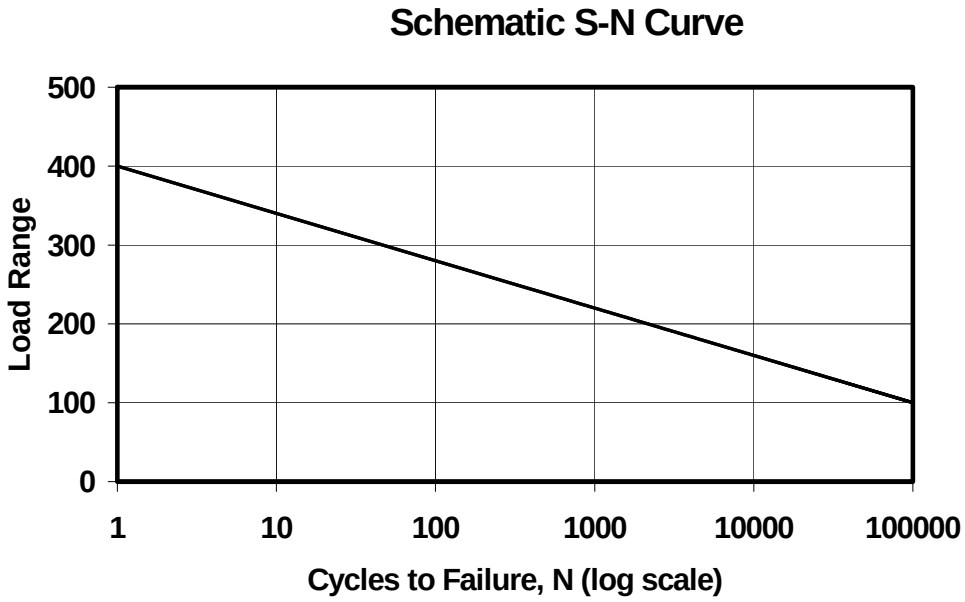

Figure 5.1 Schematic S-N curve

The first point on an S-N curve, at one load cycle, is the experimentally determined static capacity of the girder. The remainder of the S-N curve can be established using fatigue testing. Next, the anticipated number of fatigue cycles for the service life of the bridge in question can be determined by estimating the Average Daily Truck Traffic (ADTT). The ordinate of the S-N curve for that number of cycles is the load range that the bridge can withstand. Conversely, given the anticipated load range, the number of cycles to failure can be estimated.

Applied shear force ranges for the two fatigue tests described in this thesis, and for the three quasi-static tests performed by Boenig (2000), were

plotted against the number of load cycles to cause shear failure. The five data points were plotted using a logarithmic scale for the horizontal axis (number of cycles to failure, N), and the resulting S-N curve exhibited a linear relationship between applied shear force range (or shear stress range), and the number of cycles to failure.

Table 5.1 summarizes the experimental and calculated values associated with the five tests detailed above, where V is the shear force range at the girder support, and N is the number of cycles to failure.

Table 5.1 S-N data for quasi-static and fatigue test specimens

Specimen	V (kips)	N
BG1S	302	1
BG2S	269	1
BG4S	269	1
BG3N	200	28,133
BG3S	129	>3,328,600

Note: 1 kip = 4.45 kN

The data presented in Table 5.1 were analyzed by taking the logarithm of the number of cycles to failure (N), and performing a linear regression analysis.

The best-fit line through the S-N data, calculated by least-squares regression, is shown in Figure 5.2. Although this S-N curve is based upon only five data points, the calculated reliability is acceptable, as indicated by an R^2 value of 0.94.

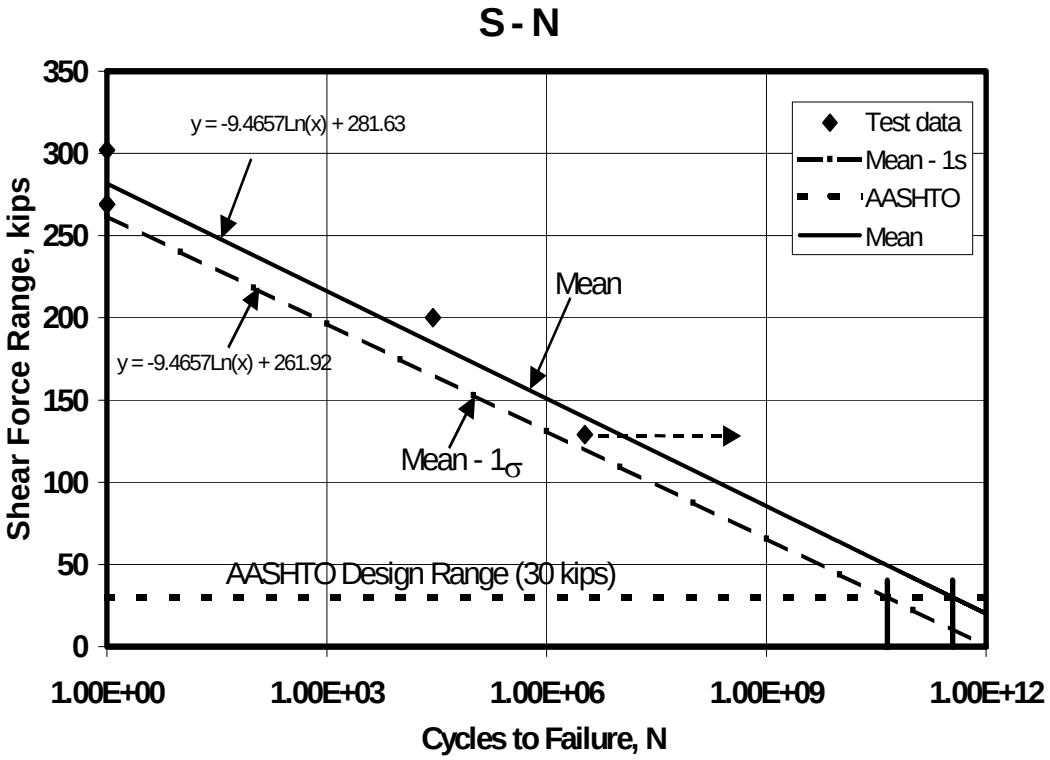

Figure 5.2 S-N curve for box girder test specimens

The mean line was extrapolated forward to 1 x 10^{12} cycles to obtain an estimate of the fatigue-force range required to produce failure under worst-case AASHTO truck load cycles for a bridge. A realistic number of truck load cycles during the service life of a bridge is 5 – 8 million, based upon 100,000 trucks per year for 50 to 75 years. An unrealistically high estimate of truck load cycles during the service life of a bridge is 45 – 70 million, based upon an Average Daily

Truck Traffic (ADTT) of 2500 trucks per day for 50 to 75 years. It is also conservative to assume that every truck load is a constant-amplitude, worst-case AASHTO design shear load, rather than a more realistic variable-amplitude fatigue load. An in-service bridge would normally experience varying truck loads, and typically never experience the highest design loads one hundred percent of the time.

The final point on the S-N curve (from BG3S data) also leads to conservative comparisons because the fatigue test was stopped at 3,328,600 cycles, without allowing the girder to fail. The actual number of cycles to failure (N) for the shear-force range of 129 kips (574 kN) is unknown, but is greater than 3,328,600 (denoted by the dashed arrow to the right of this data point in Figure 5.2). For a larger actual value of N, the best-fit line to the S-N curve would be even more horizontal (smaller slope), and actual values for range of shear force on the S-N curve will be higher, giving an even larger safety factor with respect to the AASHTO design shear force range.

The lower, dashed line parallel to the best-fit line represents a uniform downward offset of 1 standard deviation, based on a calculated coefficient of variation equal to 6.6 percent in the three quasi-static tests performed by Boenig (2000), and assumed to be similar for the two fatigue tests.

The final step in analyzing the S-N curve is to compare the mean minus one standard deviation offset line with the AASHTO design shear force range. Using a realistic number of truck load cycles of 5 to 8 million, the maximum acceptable shear force range in the girder, represented by the offset line, is equal

to 114 kips (507 kN). This value is 3.8 times higher than the AASHTO design range of 30 kips (133 kN). Even when an unrealistically high number of truck load cycles of 70 million is used, the acceptable shear force range in the girder is still equal to 91 kips (405 kN), 3.0 times higher than the AASHTO design range. If the mean and mean minus one standard deviation lines are projected forward, they intersect the AASHTO design range line at 350 billion and 45 billion respectively. These values far exceed the number of truck load cycles during the service life of a bridge.

Nominal shear stresses resulting from applied loads, although not plotted on an S-N curve in this thesis, were calculated using the following equation:

$$v = \frac{V}{b_w d}$$

where

- v = nominal shear stress range acting on failure planes, psi
- V = shear force range at girder support, lb.
- b_w = girder web width, in.
- d = distance from extreme compression fiber to centroid of longitudinal tension reinforcement, in.

These nominal stresses can then be normalized to a dimensionless quantity by dividing by $\sqrt{f_c}$, where f_c is the tested concrete compressive strength and has units of psi (MPa). Table 5.2 shows the results of such a normalization.

Table 5.2 Normalization of shear stresses for quasi-static and fatigue test specimens

Specimen	V (kips)	$b_w d$ ($in.^2$)	v (psi)	f_c (psi)	$\frac{v}{\sqrt{f_c}}$	N
BG1S	302	235	1310	8430	14.3	1
BG2S	269	235	1170	5210	16.3	1
BG4S	269	235	1170	5910	15.3	1
BG3N	200	235	851	*	*	28,133
BG3S	129	235	549	*	*	>3,328,600

Note: 1 in. = 25.4 mm, 1 kip = 4.45 kN, 1 ksi = 6.89 MPa
* f_c not available

For BG1S, BG2S, and BG4S, f_c was determined by testing concrete core samples removed from the untested ends of the respective quasi-statically tested girders (Boenig 2000). Core samples were not taken from the fatigue specimens because the concrete in both ends of BG3 was damaged during testing, and removing cores from the shear-critical region before testing would have invalidated the fatigue test results. Although it is generally convenient to use shear stresses normalized with respect to f_c for purpose of comparison, without f_c

values for test specimens BG3N and BG3S, it was not possible to do so in this study.

5.3 BEHAVIOR OF SHEAR-DOMINATED FATIGUE SPECIMENS

The behaviors of BG3N and BG3S are compared with shear transfer mechanisms and failure modes, using visual observations and numerical results from the physical testing. Decreased girder stiffness, and potentially decreased strength and service life, can be correlated to increases in the following parameters: vertical deflection; total web deformation index; crack ratio; damage index; and maximum shear-crack width. The most useful laboratory measures to compare changing girder stiffness appear to be vertical deflection and the total web deformation index, provided that the instrumentation is sensitive enough to accurately record small deformations. Stiffness of in-service bridges, however, can more easily be measured indirectly, by correlating changes in overall shear crack widths, crack ratios, and damage indices with experimental lab results. These field methods are practical because they do not require complex instrumentation.

In addition to the parameters detailed above, concrete compressive strength and modulus of elasticity decrease as the degree of deterioration increases. Furthermore, if visual damage can be correlated with reductions in concrete compressive strength and modulus of elasticity, then visual damage can also be correlated to reductions in structural capacity.

BG3N was subjected to heavier fatigue loads (and a larger shear-force range) than BG3S, and consequently exhibited a greater decrease in stiffness as the number of load cycles increased. Results from the fatigue test performed on BG3N also indicate a greater increase in damage to the shear-critical region, evident from the increasing visual indices of crack ratio and damage index. The following comparisons can only be made, however, if the tested girders exhibit significant increasing structural damage: vertical deflection vs. number of load cycles; total web deformation index vs. number of load cycles; maximum shear crack width vs. number of load cycles; crack ratio vs. number of load cycles; damage index vs. number of load cycles; vertical deflection vs. crack ratio; total web deformation index vs. crack ratio; vertical deflection vs. damage index; and total web deformation index vs. damage index.

BG3S, which was subjected to lower fatigue loads than BG3N, did not exhibit significant structural damage, and therefore did not exhibit significant changes in the correlations listed above. The lack of significant changes in girder stiffness and damage are still valuable observations, however, considering the gross overload conditions for the duration of 3,328,600 load cycles. These favorable test results are important because both of the specimens tested, and representative in-service girders, exhibit the most severe concrete deterioration in the shear-critical regions near the girder ends.

Even with the most severe concrete deterioration in the shear-critical regions near the girder ends, there was no significant slip of prestressing strands in either of the two test specimens. This was due to several factors. First, the

solid end block in the girder is 26 in (0.66 m) long, which exceeds the transfer length of the prestressing strands (ACI 318-99 and AASHTO 1996). The girders also have a 14 in. (0.36 m) length of bonded prestressing strand in the anchorage zone behind the face of the support, outside of the shear and moment region. Another factor in the insignificant strand slip is that a substantial transverse clamping force acts on the prestressing strands due to the vertical reaction at the support, and increases frictional resistance between the prestressing strands and the concrete. Gross strand slip, while not observed in these tests, is still a possible failure mechanism. Slip of prestressing strands will be further investigated in a separate part of this research project, using strand pull-out tests performed on slices removed from different regions of four box girders described in Section 3.3.

Additional information was learned by quasi-statically loading BG3S to failure. The quasi-static load test of BG3S experimentally determined the ultimate shear-force capacity to be 268 kips (1190 kN). This value is comparable to the values obtained from the three quasi-static tests performed by Boenig (2000), in which no prior fatigue loading was performed. The ultimate shear-force capacities of the three previous test specimens were 309 kips (1370 kN) for BG1S, and 276 kips (1230 kN) for BG2S and BG4S. Visually, the damage in BG3 was comparable to the damage in BG2S and BG4S, and significantly worse than the damage in BG1S. Therefore, it is noteworthy that the decrease in ultimate capacity was less than 4 percent when compared with comparable girders that had never experienced fatigue loading.

In addition to the ultimate capacity, the quasi-static load test of BG3S produced significant data regarding vertical deflection and web deformation. As shown in Figures 4.34 through 4.37, the curves representing vertical deflection vs. load, and web deformations vs. load, become more horizontal with increasing load. This is consistent with the expected behavior of both reinforced concrete and prestressed concrete.

5.4 SHEAR TRANSFER AND FAILURE MODES OF SHEAR-DOMINATED FATIGUE SPECIMENS

5.4.1 Mechanisms for Shear Transfer

In an uncracked section, shear is transferred by diagonal tension in the concrete, and the nominal shear strength provided by concrete at this point is equal to V_{cw}. When the principal tensile stress in the web exceeds the tensile strength of the concrete, web-shear cracking results. After diagonal cracks form in the web, shear is transferred by a combination of tensile stress in the shear reinforcement (stirrups), aggregate interlock along the crack surfaces, dowel action, and stress in the concrete compressive zone. Because these transfer mechanisms are interrelated, it is difficult to quantify the shear contributions of the individual components. Furthermore, the nominal shear strength provided by concrete (V_c) in prestressed concrete girders varies with the effective prestress force in the girder. High compressive stresses, present as a result of the prestress force, reduce the principal tensile stress and prevent web-shear cracks from immediately propagating through the bottom flange. The prestressing strands also

act as reinforcement to further prevent crack propagation through the bottom flange. By preventing cracking through the bottom flange, the likelihood of strand slip at the girder ends is also reduced. It is difficult, however, to determine the effective stress in the prestressing strands (f_{se}) because of the variability in the initial stress level in the strands and also in their prestress losses over time.

Shear transfer in a cracked section can also be viewed as a strut-and-tie model, in which the concrete acts as a diagonal compression strut, the prestressing strands as a bottom tension chord, and the stirrups as vertical tension members. To analyze the section using strut-and-tie-model, the following values must be estimated: concrete compressive strength (f_c); effective stress in the prestressing tendons (f_{se}); bond between prestressing strands and concrete; and stress in the stirrups.

The basic mechanism described for shear transfer is applicable to fatigue loading conditions as well, but evaluation of shear strength becomes even more difficult as V_c decreases with an increasing number of load cycles. This reduction in V_c is due in part to deterioration of aggregate interlock along the crack interface resulting from abrasion caused by repeated opening and closing of the cracks. An explanation of how the shear components are interrelated and difficult to quantify is presented below. As V_c is reduced, whether from deterioration of aggregate interlock or by increased crack widths, more stress is transferred into the stirrups crossing the cracks, and the nominal shear strength provided by the shear reinforcement (V_s) is increased accordingly. If these diagonal cracks widen further under fatigue loading, the axial stress in the stirrups increases near the

crack, the stirrups debond from the concrete near the crack, or both. As this happens, transverse shear and bending stresses are also induced into the stirrups at the locations of the inclined cracks due to horizontal widening of the cracks.

For these reasons, fatigue loading makes the analysis of stress in the stirrups even more difficult. Although the fatigue behavior of reinforcing steel tested in air is well understood, less is known about the fatigue behavior of reinforcing steel embedded in concrete. Because it is difficult to measure or calculate the stress in the stirrups, it is not possible to calculate the shear fatigue strength of prestressed concrete members with any certainty. Information reported by ACI Committee 215 (1997), however, can help determine if fatigue failure of the component materials or the system (prestressed member) is probable. From previous studies of shear fatigue in prestressed concrete members, it appears that the stress range in the shear reinforcement is crucial to understanding the probability of shear fatigue, and is presented below.

Shear fatigue failure is unlikely if the level of tensile stress in the shear reinforcement remains below the generally accepted endurance limit of the steel, which for Grade 60 reinforcing steel is approximately 24 ksi (165 MPa) (MacGregor 1997). Shear fatigue failure is also unlikely if the stress range in the reinforcing steel remains below the generally accepted limit of 20 ksi (138 MPa) during fatigue loading of 1 million or more cycles involving tensile stresses (MacGregor 1997). Again, these stress values are difficult to determine, making it difficult to evaluate the fatigue shear strength of a member.

5.4.2 Comparison of Shear Transfer and Failure Modes between Test Specimens BG3N and BG3S

From Section 5.4.1, it is apparent that evaluating the fatigue shear strength of prestressed concrete members is difficult. Therefore, the calculations performed to estimate fatigue shear strength of BG3N and BG3S provide only estimates, and are not thoroughly reviewed in this section. A conservative approach, however, is to assume that $V_c = 0$, and to calculate the level of stress in the shear reinforcement accordingly. It is not usually possible to determine the exact quantity and location of shear reinforcement; therefore, it is also conservative to assume some percentage of effective shear reinforcement less than the design value. Using these conservative assumptions yields higher calculated stress levels in the shear reinforcement.

5.4.2.1 BG3N

In this first test, as diagonal web cracks widened with cycling, V_c was reduced, increasing the stress in the shear reinforcement crossing the cracks. The applied shear force at the support was 221 kips (983 kN), compared with the calculated $V_c = 129$ kips (572 kN) for the uncracked section, and the calculated nominal shear strength, $V_n = 223$ kips (992 kN). These calculations are presented in Appendix B. Although they are based on the estimated values discussed in Section 5.4.1, it is apparent that V_c was exceeded and the stirrups were required to carry a high percentage of the load. These calculations were unconservative, assuming that all of the stirrups were properly placed at a 6 in. (0.15 m) spacing and were fully effective. From visual inspection of the failed girder, it is evident that not all of the stirrups in the shear-critical region were properly spaced or fully

effective (Figures 5.3 and 5.4). Therefore, the stirrup stress was even higher than the calculated values in Appendix B, which assumed correct stirrup spacing.

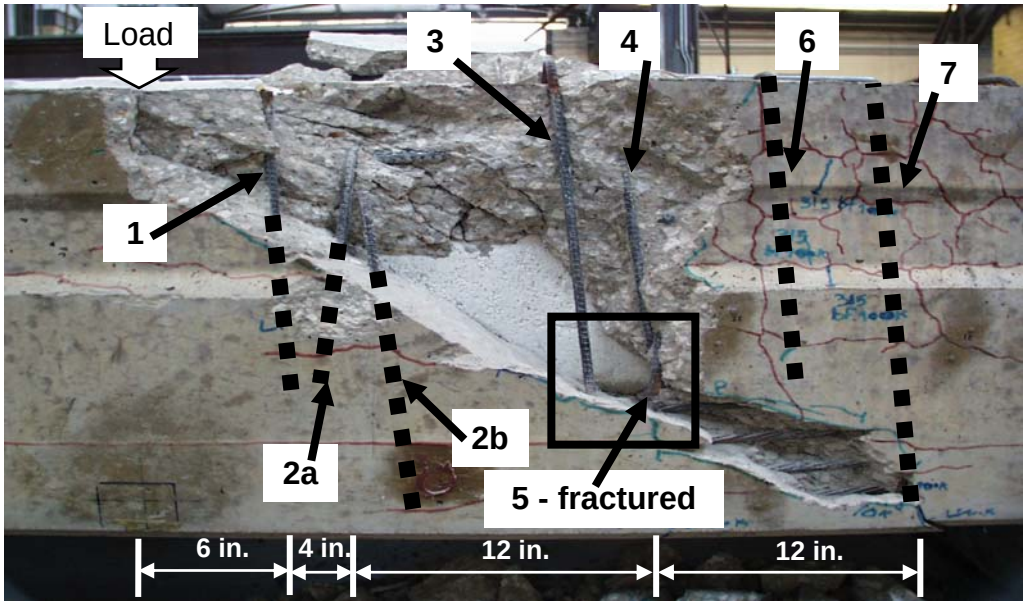

Figure 5.3 In-situ reinforcement for shear-critical region of BG3N (east web), after removal of concrete

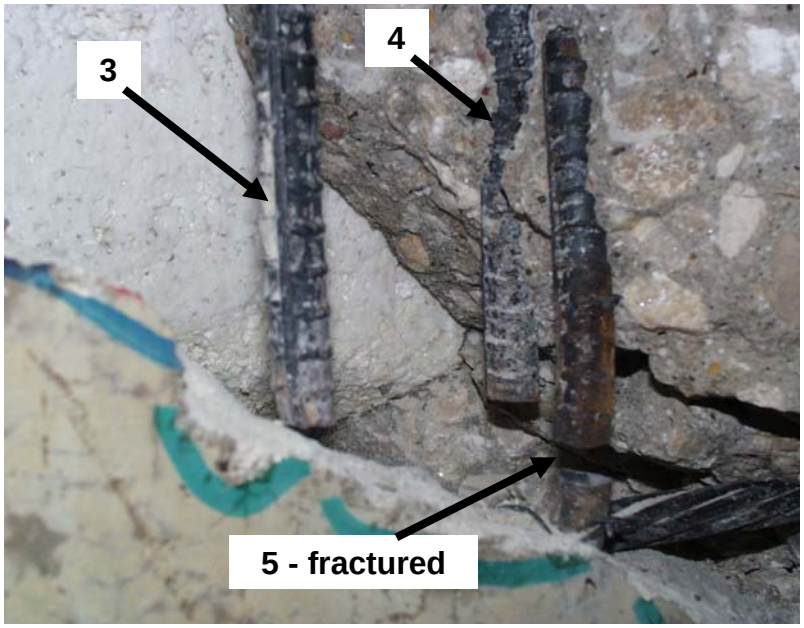

Figure 5.4 Detail of rectangular area in Figure 5.3

Presented below is a description of the shear reinforcement for the shear-critical region in the east web of BG3N. The stirrups are all bar size # 4, ASTM A615 Grade 60 (420 MPa), and are referenced using the numbering system in Figures 5.3 and 5.4. The dotted lines in Figure 5.3 represent the approximate locations of embedded stirrups, based on the locations of the exposed portions of the stirrups. The regions of concrete above and below the failure plane are referred to as upper and lower respectively.

Stirrup 1: upper embedment, 8 in. (0.20 m); lower embedment, 11 in. (0.28 m); at failure plane, 6 in. (0.15 m) horizontally from center of loading point;

Stirrup 2a: upper embedment fully developed by a continuous horizontal leg at its upper end; lower embedment, 10 in. (0.25 m) (2a is the U-shaped top half of a two-piece spliced hoop); at failure plane, 9 in. (0.23 m) horizontally from center of loading point

Stirrup 2b: upper embedment, 5 in. (0.13 m); lower embedment with hook fully developed bar (2b is the U-shaped bottom half of a two-piece spliced hoop); at failure plane, 11 in. (0.28 m) horizontally from center of loading point

Stirrup 3: does not cross the failure plane

Stirrup 4: does not cross the failure plane

Stirrup 5: fractured; at failure plane, 22 in. (0.56 m) horizontally from center of loading point

Stirrup 6: does not cross the failure plane

Stirrup 7: does not cross the failure plane

Four stirrups crossed the failure plane (Figures 5.3 and 5.5): Stirrups 1 and 2a are assumed to be fully effective; Stirrup 2b partially effective; and Stirrup 5 fully effective and fractured. The shear reinforcement is not evenly distributed, however, as Stirrups 1, 2a, and 2b cross the failure plane within 10 in. (0.25 m) from the center of the first loading point, causing this region to act as a pivot for the cracked section. The only other reinforcement crossing the failure plane was Stirrup 5, 22 in. (0.56 m) from the loading point.

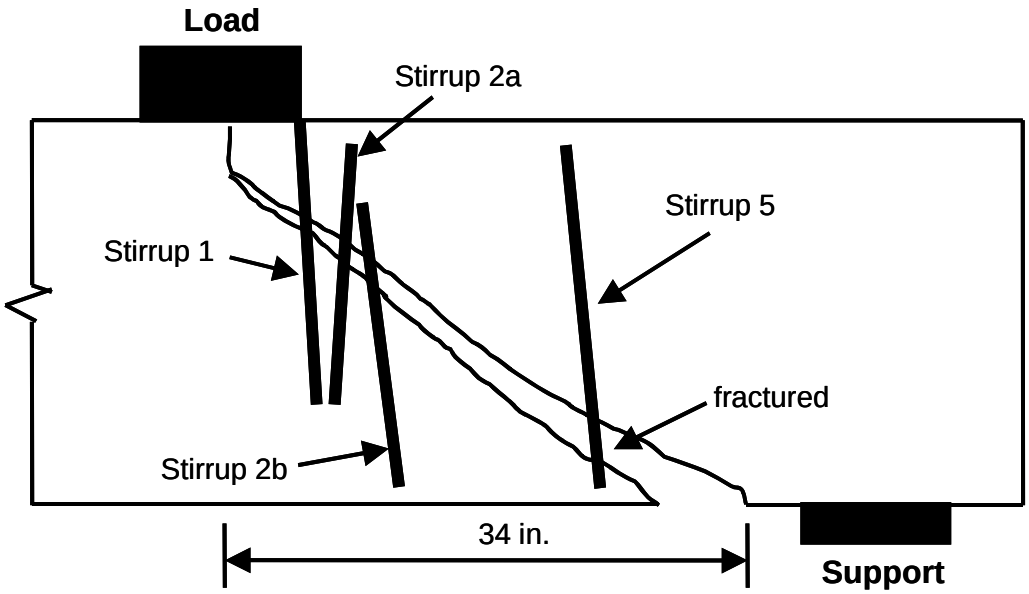

Figure 5.5 Shear reinforcement crossing the failure plane

The loading and support conditions shown in Figure 5.5 produced a failure mechanism in which the section of girder to the right of the diagonal crack, rotated counter-clockwise about the loaded point. That rotation tended to make

the diagonal crack wider at the bottom than the top, and therefore produced higher elastic stresses in stirrups located farther away from the loaded point. As a result of that mechanism plus the as-built location of the stirrups, the closely spaced Stirrups 1, 2a and 2b, located close to the load, were not highly stressed, while Stirrup 5, located farthest from the load, was very highly stressed, and eventually fractured.

For simplicity in calculating shear stresses, however, it is assumed that the three fully effective bars had equal tensile stress, and that Stirrup 2b was 50 percent effective (3.5 stirrups crossing the failure plane per web). Also, it is assumed that the west web had the same shear reinforcement configuration. Using the procedure detailed in Appendix B, V_s = 84 kips (374 kN), compared with the previously calculated 94 kips (417 kN).

In either case, the stirrups were subjected to many cycles of repeated loading at a stress range close to the yield point of the steel, far exceeding the generally accepted endurance limit of 24 ksi (165 MPa) and the generally accepted safe stress range of 20 ksi (138 MPa). In addition to the tensile stress in the stirrups, transverse shear and bending stresses were also present. This was visually evident from the horizontal movement across the widest diagonal crack that opened repeatedly to a width of 0.125 in. (3 mm) under the 300 kip (1330 kN) cyclic load. Visual inspection of the test specimen (presented above and in Section 4.2.1), and the calculations presented above, confirm that the mode of failure was fatigue of the shear reinforcement.

5.4.2.2 BG3S

This second test used a lower fatigue load and load range, and consequently caused very little additional damage to the girder. The existing diagonal shear cracks opened and closed, but did not significantly increase in length or width as the number of load cycles increased. For this reason, V_c remained more effective than in the previous test, and the level of stress in the stirrups likely remained below the generally accepted endurance limit of 24 ksi (165 MPa). Calculations based on estimated values verified that the level of stress was near the generally accepted endurance limit of 24 ksi (165 MPa), and the stress range was also near the generally accepted limit of 20 ksi (138 MPa). From calculations based on the assumptions that $V_c = 0$ and stirrup spacing is 6 in., it is possible that these stress limits were exceeded, but apparently not enough to cause significant damage even after 3,328,600 cycles.

Because no significant damage was observed after 3,328,600 cycles, the specimen was tested quasi-statically to failure. Visual inspection of the test specimen, presented in Section 4.2.2, verified that the mode of failure was crushing of the diagonal concrete compression struts in the webs.

Chapter 6: Summary, Conclusions and Recommendations

6.1 SUMMARY

This thesis describes part of the work associated with TxDOT Study 1857, "Structural Assessment of In-Service Bridges with Premature Concrete Deterioration." The overall study focuses on seven specific tasks that were outlined in the project proposal (Klingner 1998):

1) Conduct field investigation to confirm and monitor existing premature concrete deterioration and the rate of increase of such deterioration, where numerical measures of this increase include crack width and crack density.
2) Conduct laboratory investigations of local effects of premature concrete deterioration. Perform tests on cores and slices removed from several girders with varying degrees of deterioration, and perform full-scale tests to failure on prestressed concrete girders.
3) Develop nondestructive evaluation (NDE) techniques for determining degree and type of concrete deterioration.
4) Develop petrographic techniques for assessing the severity of concrete deterioration, and establish the relationship between various types of deterioration in structural effectiveness, and various changes in internal structure. TxDOT personnel will perform this task, using cores extracted from the laboratory specimens. No work has been completed on this task by The University of Texas at Austin.

5) Develop engineering models for evaluating the global reduction in capacity of a structural element due to local premature concrete deterioration.

6) Develop an overall methodology for predicting the probable loss in capacity over time of a deteriorated structural element, based on external evidence, NDE, and engineering models.

7) Develop recommended actions for TxDOT to handle any given case of premature concrete deterioration. Using the results of Tasks 1-6, provide specific guidelines for assessing the probable capacity of a structure as a function of time.

The particular focus of this thesis is to determine the effects of premature concrete deterioration on shear-fatigue strength of pre-cracked, prestressed concrete girders; to predict the service life of pre-cracked girders in shear-critical loading configurations using S-N curves established from data collected during two full-scale fatigue tests; and to determine the possible shear-fatigue failure modes. Also, to determine the overall level of damage, S-N data from the two shear-dominated fatigue tests are related to measured girder stiffness, crack widths, and visual damage indices. The theoretical background of premature concrete deterioration, while not the focus of this thesis, is reviewed.

6.2 CONCLUSIONS

1) Premature concrete deterioration is the result of an internal expansion mechanism in the concrete. Its basic causes are Delayed Ettringite Formation (DEF) and Alkali-Silica Reaction (ASR), which usually occur together in some degree. Both mechanisms are accelerated by exposure to water (Boenig 2000) (Chapter 2).

2) The reduced shear capacity of a prestressed concrete bridge girder with premature deterioration can be estimated, or its service life predicted, using an experimentally established S-N curve. The S-N curve can be established by plotting the shear force range, the load range, or the normalized shear-stress range against the number of cycles to failure (N), where the horizontal axis is logarithmic (Section 5.2).

3) Under service loads, in-service box girders of the same type and with concrete deterioration similar to that of the two specimens tested in fatigue, should have a shear service life at least as long as their intended design life, and probably significantly longer, provided that the concrete deterioration is arrested, and the prestressing strands and reinforcing steel are protected from further corrosion. This conclusion is based upon the results of the two laboratory tests that subjected girders to fatigue-shear forces that were much greater than those that would be imposed by gross truck overloads. Using the conservative S-N curve established from these experimental test results, and a realistic number of truck load cycles of 5 to 8 million, the maximum acceptable shear force range in the girder is 3.8

times higher than the AASHTO design shear range of an in-service bridge with these dimensions. Even when an unrealistically high number of truck load cycles of 70 million is used, the acceptable shear force range in the girder is still 3.0 times higher than the AASHTO design range. If the conservative S-N curve is projected forward, it intersects the AASHTO design range line at 45 billion cycles, greatly exceeding the number of truck load cycles during the service life of a bridge (Section 5.2).

4) The failure mode of prestressed concrete girders subjected to shear fatigue overloads may be fatigue of the shear reinforcement in tension and transverse bending near diagonal cracks, debonding of shear reinforcement from the concrete near cracks, or both. Failure occurs after shear cracks have opened significantly due to progressive deterioration. Because the cracks tend to widen with time, it is possible to monitor deterioration using visual inspection (Section 5.4.1).

5) Shear fatigue failure of prestressed concrete girders with premature concrete deterioration is unlikely if the level and range of stress in the shear reinforcement remain below the endurance limit of the steel (Section 5.4.1).

6) Slip of prestressing strands does not appear to be a likely mode of shear-fatigue failure in this specific type of girder, for several reasons. First, the solid end block is longer than the transfer length of the prestressing strands, and a significant length of bonded prestressing strand lies within the anchorage zone behind the face of the support (outside the shear and

moment region). Second, significant transverse clamping force acts on the prestressing strands due to the vertical reaction at the support, and increases frictional resistance between the prestressing strands and the concrete. Gross strand slip, while not observed in these tests, will be further investigated in a separate part of this research project using strand pull-out tests performed on slices removed from the test specimens (Section 5.3).

7) Decreased girder stiffness, and potential decreases in strength and service life, can be correlated to increases in the following damage parameters: vertical deflection; total web deformation index; crack ratio; damage index; and maximum shear-crack width. Maximum shear-crack width, and the two visual damage indices of crack ratio and damage index, are the most practical damage parameters for field use, because they do not require complex instrumentation (Sections 3.6.3 and 5.3).

8) It is difficult to calculate the nominal shear strength provided by concrete (V_c) in prestressed girders after diagonal shear cracks have formed in the webs. Therefore, it is conservative to assume that $V_c = 0$ in calculating the shear capacity of prestressed girders with premature concrete deterioration. Although it is inconsistent with the physical requirement that the concrete act as an effective diagonal compression strut, this assumption is practical in the context of current AASHTO design provisions for shear (Section 5.4).

~~9.3~~6.3 RECOMMENDATIONS

Formatted: Bullets and Numbering

The following recommendations are made based on the test results of this thesis, along with results from previous research on Project 1857 (Boenig 2000, Fúnez 1999).

1) Cracks in critical regions of prestressed concrete girders should be sealed to prevent corrosion of prestressing strands and reinforcing steel. Wide cracks may be filled with a flexible sealant, and narrower cracks with a low-viscosity, crack-penetrating sealant. In addition to sealing the girders, it is equally important to establish a maintenance program to ensure that the cracks remain sealed.

2) Crack widths, particularly of inclined cracks in shear-critical regions, should be further monitored for in-service structures to determine the rate of deterioration over time. Likewise, representative squares in the shear-critical regions, similar to those drawn on the laboratory specimens, should continue to be monitored in the field girders to calculate and monitor visual damage indices over time.

3) Visual damage indices of in-service girders, in combination with NDE techniques currently being studied in Project 1857, should be used to estimate reduced concrete compressive strength in the shear-critical regions near the girder ends. A method for correlating visual damage indices with f_c is presented by Boenig (2000).

4) Research should be continued in the following areas:

- methods to slow or arrest the concrete deterioration in existing structures;
- correlation between visual damage indices, NDE results, and petrographic studies, with concrete compressive strength; and
- further development of S-N curves for different types of girders and various levels of concrete deterioration.

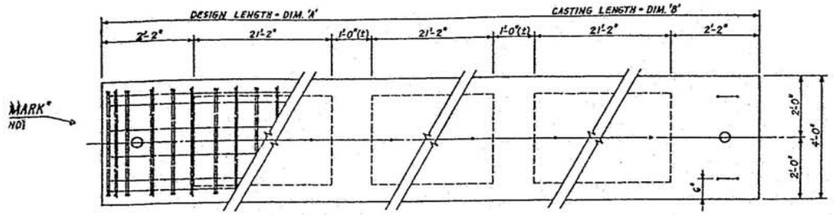

PLAN

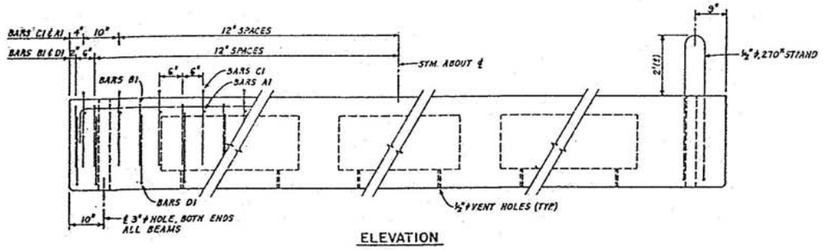

ELEVATION

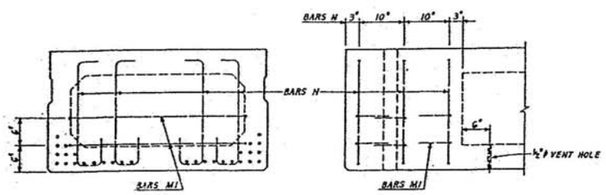

END MAT REINFORCEMENT

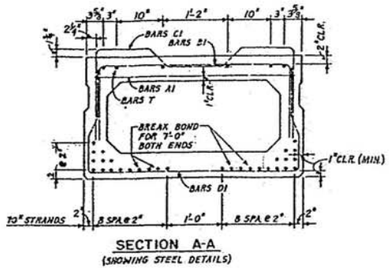

SECTION A-A
(SHOWING STEEL DETAILS)

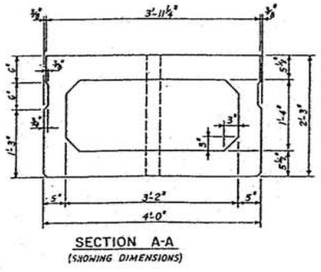

SECTION A-A
(SHOWING DIMENSIONS)

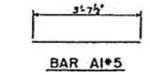

BAR A1 #5

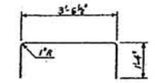

BAR B1 #4

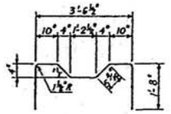

BAR C1 #4

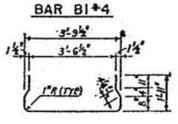

BAR D1 #4

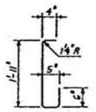

BAR N #5

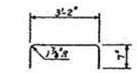

BAR M1 #5

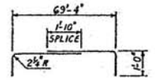

BAR T #6

BOX BEAM REINFORCING BAR SCHEDULE

BEAM MARK	NO. REQ'D.	BAR MARK, SIZE & NO. REQUIRED PER BEAM											
		A1 #5	B1 #4	C1 #4	D1 #4	T #6	M1 #5	N #5					
F7	5	71	72	71	72	6	12	24					
F10	4	71	72	71	72	6	12	24					
F37	54	71	72	71	72	6	12	24					
TOTALS		4173	4536	4173	4536	378	756	1512					

STRAND STRESS SCHEDULE

NO. OF STRANDS	30 - 1/2"ϕ, 270 K
INITIAL LOAD	1000 #/STR. (MIN.)
FINAL LOAD	28.9 K/STR.
RELEASE STRENGTH	5000 PSI
DESIGN STRENGTH	6000 PSI

GENERAL NOTES

1. CONCRETE SHALL BE CLASS 'H' OR 'H-H'.
2. REINFORCING STEEL SHALL BE GRADE 60.
3. DIMENSIONS RELATING TO REINFORCEMENT ARE TO CENTERLINE OF STEEL.
4. THE BOTTOM CORNERS OF ALL BOX BEAMS SHALL BE CHAMFERED ¾.
5. TOPS OF ALL BOX BEAMS SHALL HAVE A ROUGH WOOD FLOAT FINISH.
6. CARDBOARD FORMS FOR VOIDS SHALL BE WATERPROOFED.
7. FORMS FOR VOIDS MAY BE STYROFOAM AT FABRICATOR'S OPTION.
8. REINFORCING STEEL SHALL BE SUPPORTED ON VOID FORMER BY 6"X 6"X REQUIRED THICKNESS PRECAST MORTAR BLOCKS.
9. BOTTOM CORNER STRANDS MAY BE DISPLACED SLIGHTLY DUE TO THE BEND RADIUS OF THE STIRRUP BARS.

DIMENSION SCHEDULE

BEAM MARK	DIM. 'A'	DIM. 'B'
F7	69.86'	69'-10⅜"
F10	69.84'	69'-10½"
F37	69.83'	69'-10⅜"

A. I. & ASSOCIATES, INC.
CONSULTING ENGINEERS

DRAWINGS APPROVED

☒ Approved without modifications
☐ Approved with modifications as shown.

Date 2-8-91
By A.T.

Approval of these drawings does not relieve the contractor of responsibility for correctness of detail.

HELDENFELS BROTHERS, INC.
PRESTRESSED CONCRETE DIVISION
CORPUS CHRISTI SAN MARCOS

PRESTRESSED CONCRETE BEAMS
FABRICATION DRAWINGS

BOX BEAMS

48"X 27"

THD PROJECT I-IR 45-1(253)031

Appendix A: Fabrication Details of Box Girders

Appendix B: Calculations for Predicted Behavior of Shear-Dominated Fatigue Tests

The predicted ultimate static capacity of shear-dominated specimens was calculated using a simplified model of the girder cross-section (Figure B.1) and ACI 318-99. Neglecting the small vertical shear keys in the webs, and the chamfered edges in the polystyrene void, the simplified cross-sectional area was calculated to be 688 in.^{2}. Equation numbers in Appendix B refer to ACI 318-99.

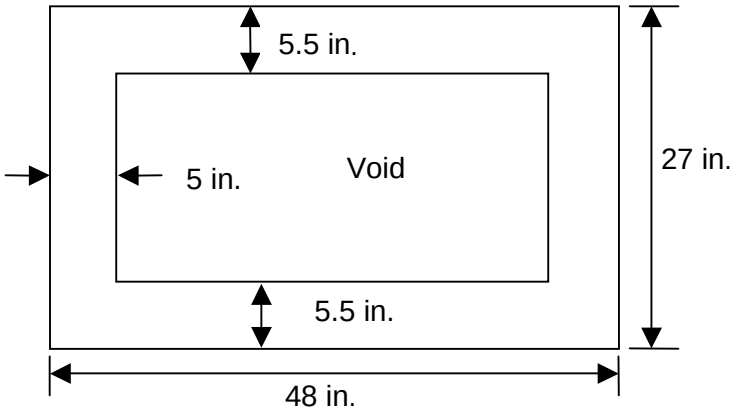

Figure B.1 Simplified girder cross-section used for calculations

The support conditions and loading points shown in Figures 3.4 and 3.5 were used for analysis of the shear-dominated fatigue specimens. Concrete compressive strength (f_c) was assumed to be 6,000 lb/in.^{2} (41.4 MPa), based on core samples removed from girders with similar damage and tested by Boenig (2000).

The nominal shear strength provided by concrete when diagonal cracking results from excessive principal tensile stress in the web is:

$$V_{cw} = \left(3.5\sqrt{f'_c} + 0.3f_{pc}\right)b_w d + V_p = 128{,}700\,\text{lb} \quad (572\ \text{kN}) \qquad (11\text{-}12)$$

where

f_{pc} = compressive stress in concrete (after allowance for all prestress losses) at centroid of cross section resisting externally applies loads or at junction of web and flange when the centroid lies within the flange, lb/in.^{2}

$$f_{pc} = \frac{f_{se}}{A} = \frac{26\ \text{strands}\left(0.153\,\text{in.}^2\right)\left(160{,}000\,\text{lb/in.}^2\right)}{688\,\text{in.}^2} = 925\,\text{lb/in.}^2$$

f_{se} = 160,000 lb/in.^{2} was the assumed value for effective stress in prestressed reinforcement (after allowance for all prestress losses) Note: only 26 of the 30 prestressing strands were assumed to be effective since 4 strands were intentionally debonded over the last 7 ft of the girder.

b_w = 10 in. (combined width of both webs)

d = 23.46 in. (distance from extreme compression fiber to centroid of longitudinal tension reinforcement (26 effective prestressing strands), but need not be less than 0.80h for circular sections and prestressed members)

V_p = 0 (vertical component of effective prestress force at section, lb)

Based on the design of #4 stirrups spaced at 6 in. center-to-center, the nominal shear strength provided by shear reinforcement is:

$$V_s = \left(\frac{A_v f_y d}{s} \right) = \left(\frac{(0.2\text{in}^2) \bullet 2\text{legs} \bullet (60{,}000\text{lb/in.}^2)(23.46\text{in.})}{6\,\text{in.}} \right) \qquad (11\text{-}15)$$

V_s = 93,800 lb (417 kN)

The nominal shear strength of the box girders is:

$V_n = V_c + V_s$ = 223 kips (992 kN) (11-2)

Including the self-weight of the girder (0.75 kip/ft), the maximum applied shear force was 221 kips (983 kN) for BG3N (Test 1), and 150 kips (667 kN) for BG3S (Test 2).

Per ACI calculations, the actual values for V_c, V_s, and V_n were lower than the design values. The actual V_c could be assumed to be zero after the cracks had opened significantly, and the actual V_s was some fraction of the design value, which assumed a stirrup spacing of 6 in. By visual inspection of the failed test specimens, the average spacing of effective shear reinforcement was greater than 6 in. Section 5.4.2.1 details the as-built location of the stirrups for specimen BG3N, and explains the failure mechanism and resulting elastic stresses in the stirrups.

Appendix C: Data from Shear-dominated Tests

After predetermined numbers of fatigue cycles throughout the testing of specimens BG3N and BG3S, quasi-static tests were performed. Representative samples of data collected from the linear potentiometers during these quasi-static tests are presented in this appendix. Although more than 20 quasi-static tests were performed, only portions of the data from seven of these tests are included here.

Complete data from BG3N are included in Section C.1.1 for the quasi-static test after 1 cycle, and a load range of 0 to 315 kips. Portions of data from BG3N are also included for quasi-static tests after 100, 1000, and 10,000 cycles in Sections C.1.2, C.1.3, and C.1.4 respectively. The slip of prestressing strands was smaller than the threshold of sensitivity of the instruments; therefore, sample strand-slip data are presented only from the quasi-static test after 1 cycle.

Representative sample data from BG3S are included in Section C.2.1 for the quasi-static test after 10,000 cycles (load range of 0 to 210 kips) and in Section C.2.2 for the quasi-static test to failure after 3,328,600 cycles (load range of 0 to 365 kips). The eight linear potentiometers measuring web deformation during the test to failure of BG3S were prone to damage, and were therefore removed after 325 kips in anticipation of girder failure. No significant slip of prestressing strands occurred during any of the quasi-static tests of BG3S; therefore those data are not presented. See Figures 3.8, 3.11, and 3.12, for the locations of linear potentiometers P1 – P8, and L1 – L8.

C.1 BG3N

C.1.1 1 Load Cycle

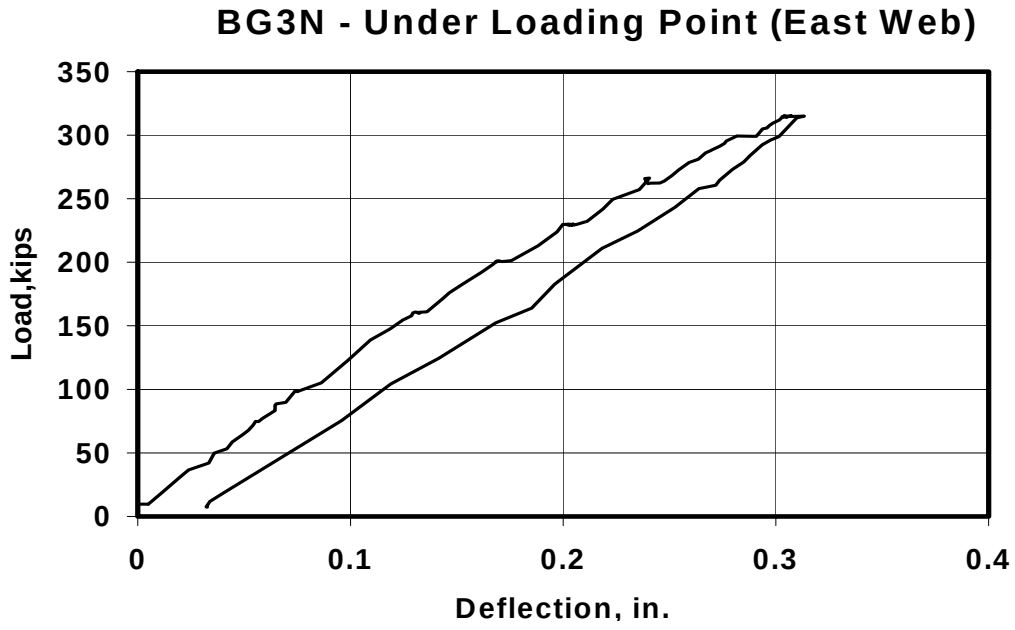

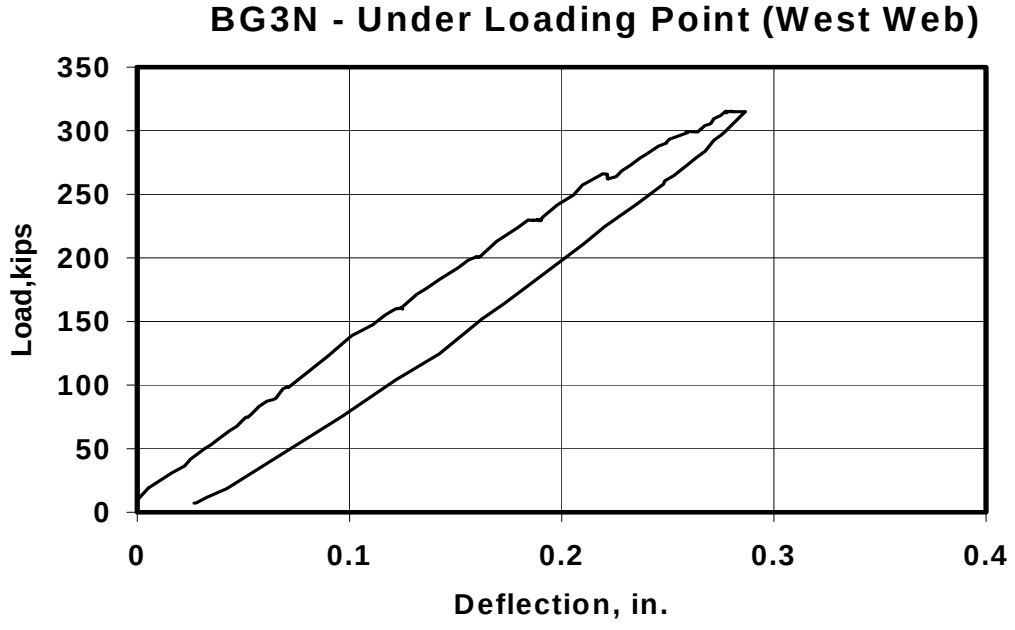

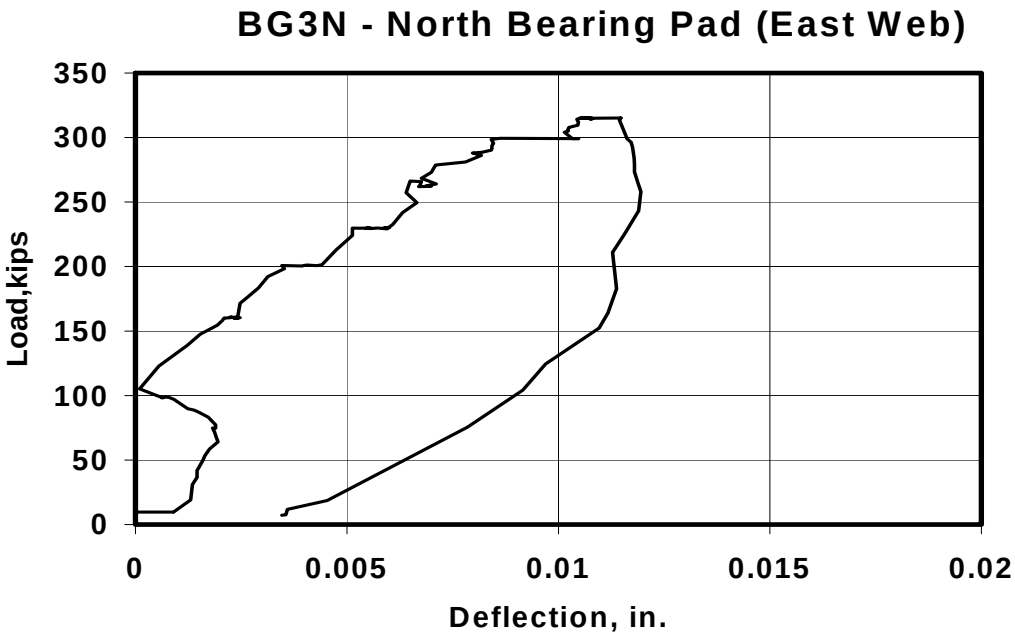
BG3N - North Bearing Pad (East Web)
Load,kips
350
300
250
200
150
100
50
0
0
0.005
0.01
0.015
0.02
Deflection, in.

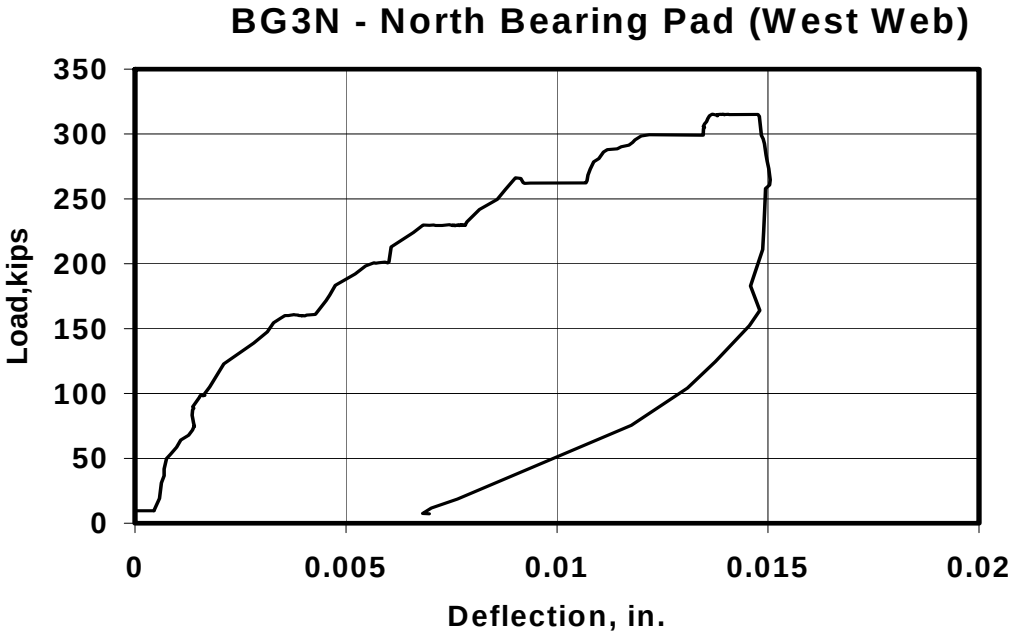
BG3N - North Bearing Pad (West Web)
Load,kips
350
300
250
200
150
100
50
0
0
0.005
0.01
0.015
0.02
Deflection, in.

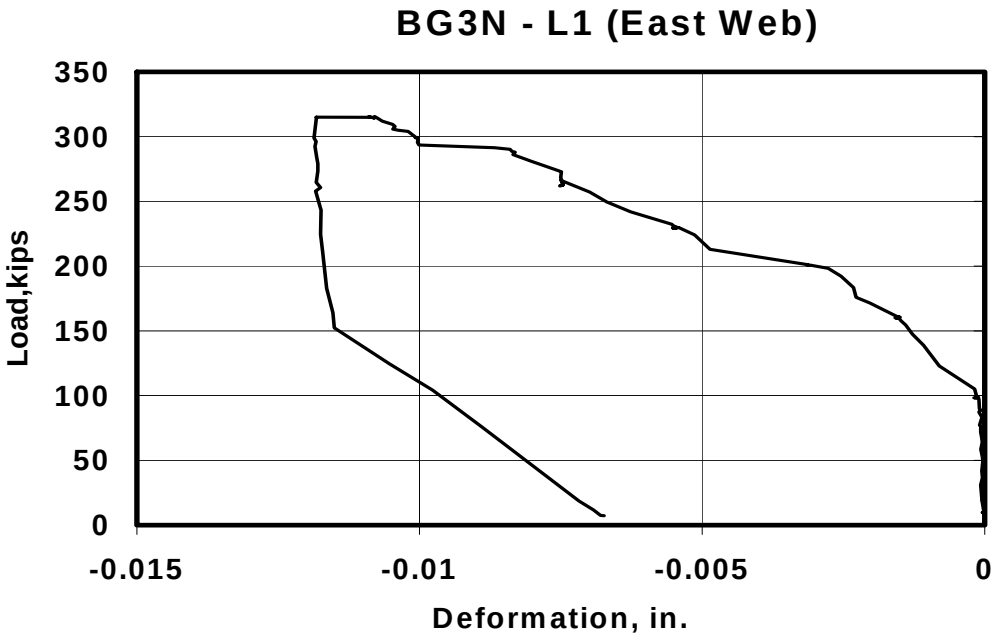
BG3N - L1 (East Web)
350
300
250
200
150
100
50
0
Load,kips
-0.015
-0.01
-0.005
0
Deformation, in.

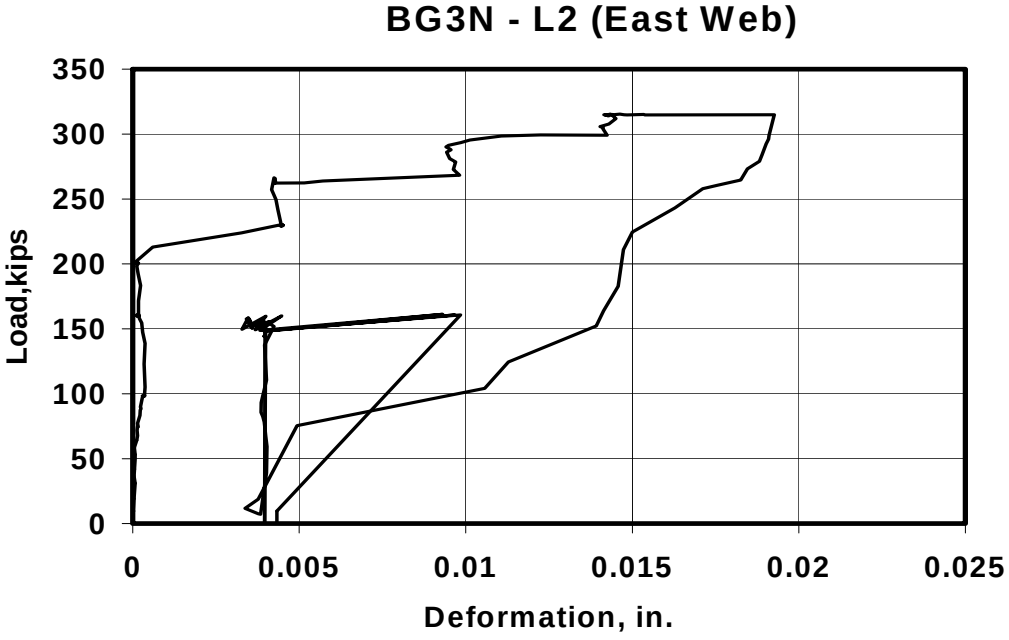
BG3N - L2 (East Web)
350
300
250
200
150
100
50
0
Load,kips
0
0.005
0.01
0.015
0.02
0.025
Deformation, in.

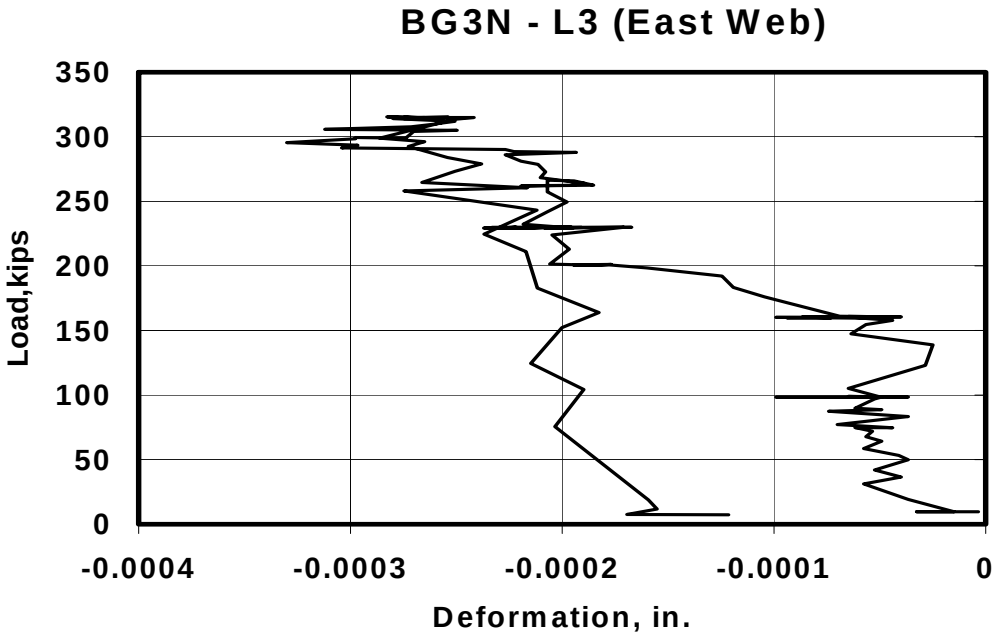
BG3N - L3 (East Web)
Load,kips
350
300
250
200
150
100
50
0
-0.0004
-0.0003
-0.0002
-0.0001
0
Deformation, in.

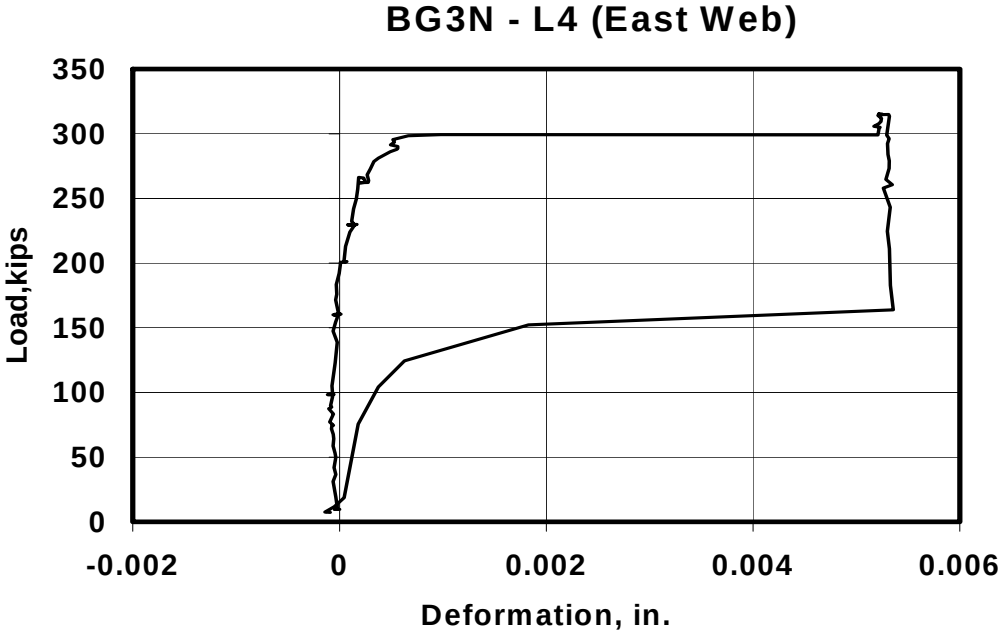
BG3N - L4 (East Web)
Load,kips
350
300
250
200
150
100
50
0
-0.002
0
0.002
0.004
0.006
Deformation, in.

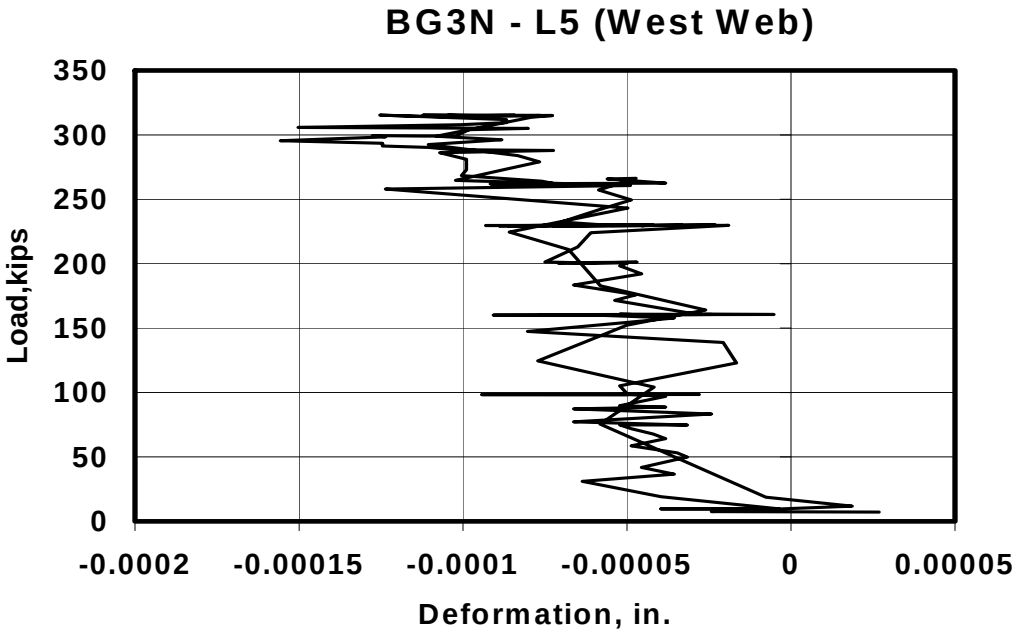
BG3N - L5 (West Web)
Load,kips
350
300
250
200
150
100
50
0
-0.0002
-0.00015
-0.0001
-0.00005
0
0.00005
Deformation, in.

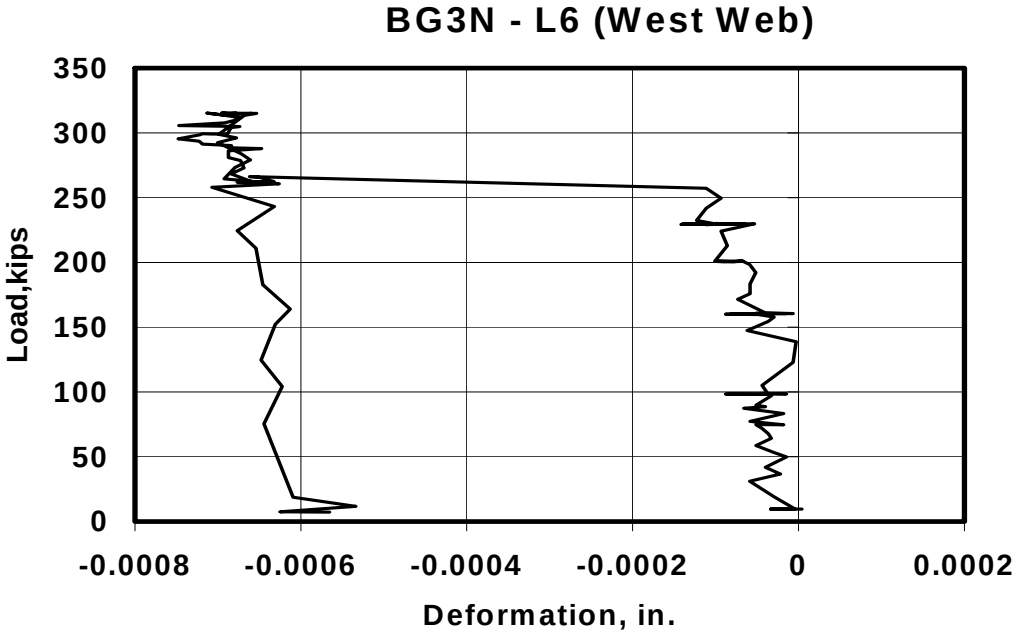
BG3N - L6 (West Web)
Load,kips
350
300
250
200
150
100
50
0
-0.0008
-0.0006
-0.0004
-0.0002
0
0.0002
Deformation, in.

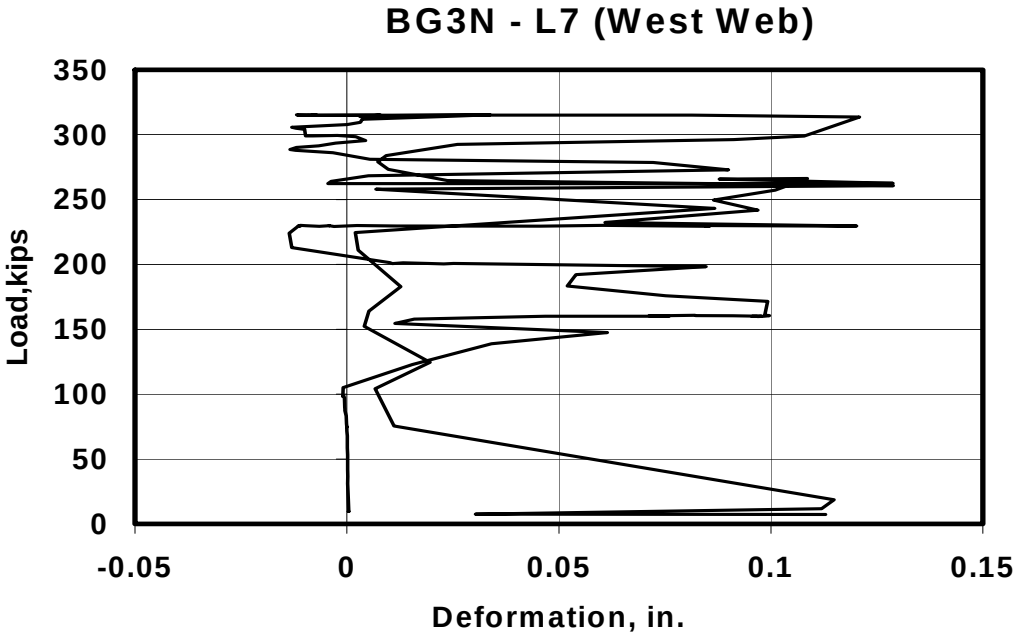
BG3N - L7 (West Web)
Load,kips
350
300
250
200
150
100
50
0
-0.05
0
0.05
0.1
0.15
Deformation, in.

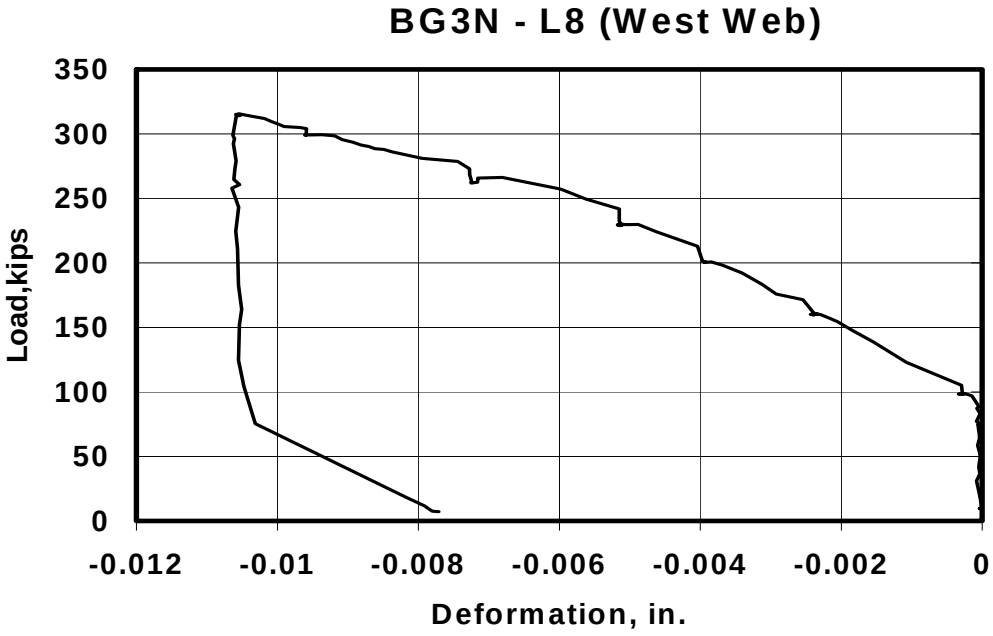
BG3N - L8 (West Web)
Load,kips
350
300
250
200
150
100
50
0
-0.012
-0.01
-0.008
-0.006
-0.004
-0.002
0
Deformation, in.

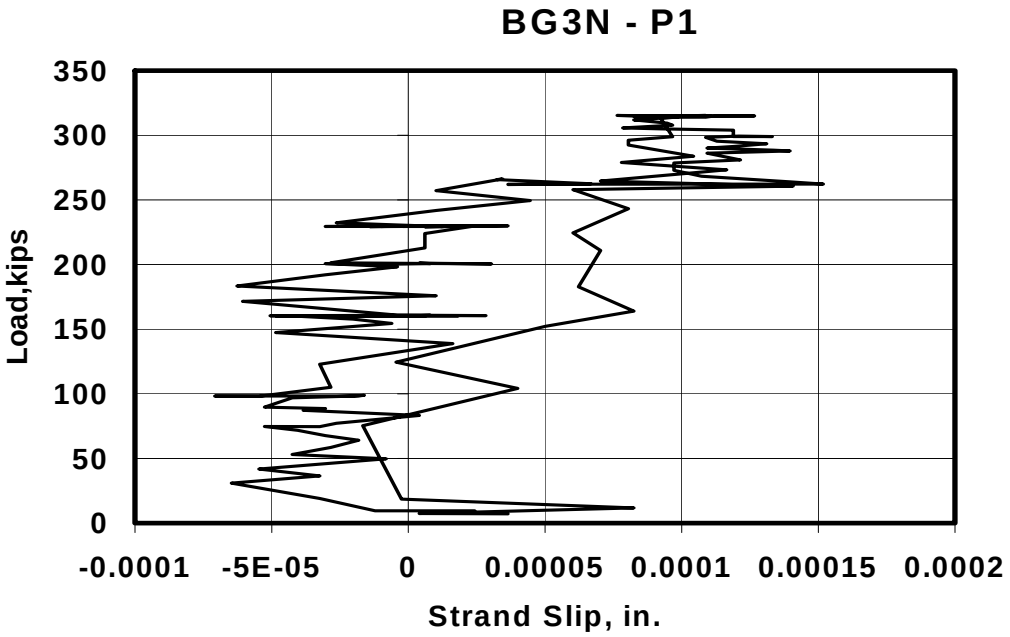
BG3N - P1
Load,kips
350
300
250
200
150
100
50
0
-0.0001
-5E-05
0
0.00005
0.0001
0.00015
0.0002
Strand Slip, in.

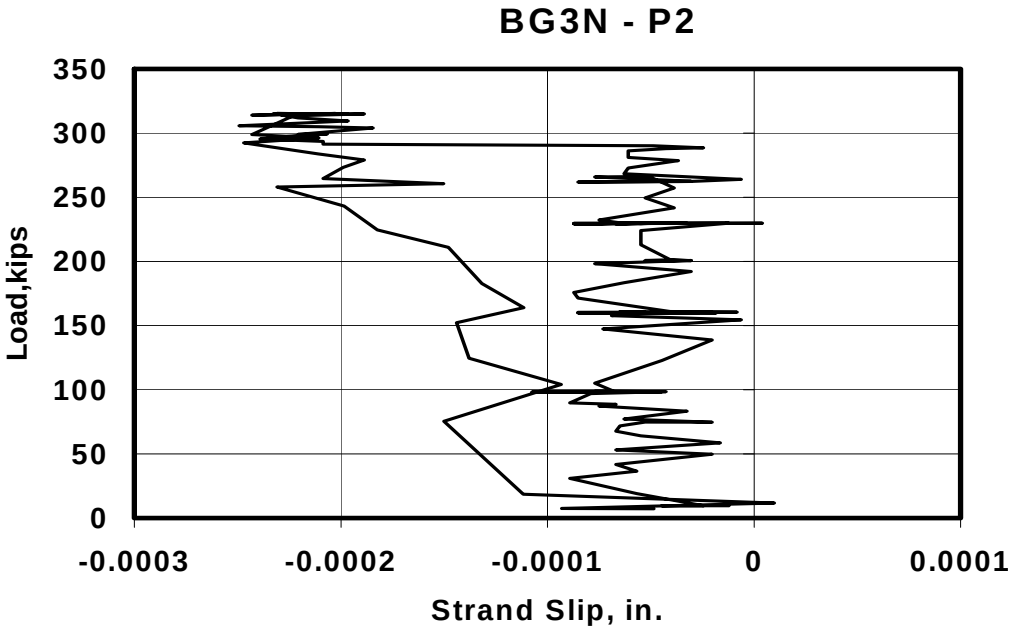
BG3N - P2
Load,kips
350
300
250
200
150
100
50
0
-0.0003
-0.0002
-0.0001
0
0.0001
Strand Slip, in.

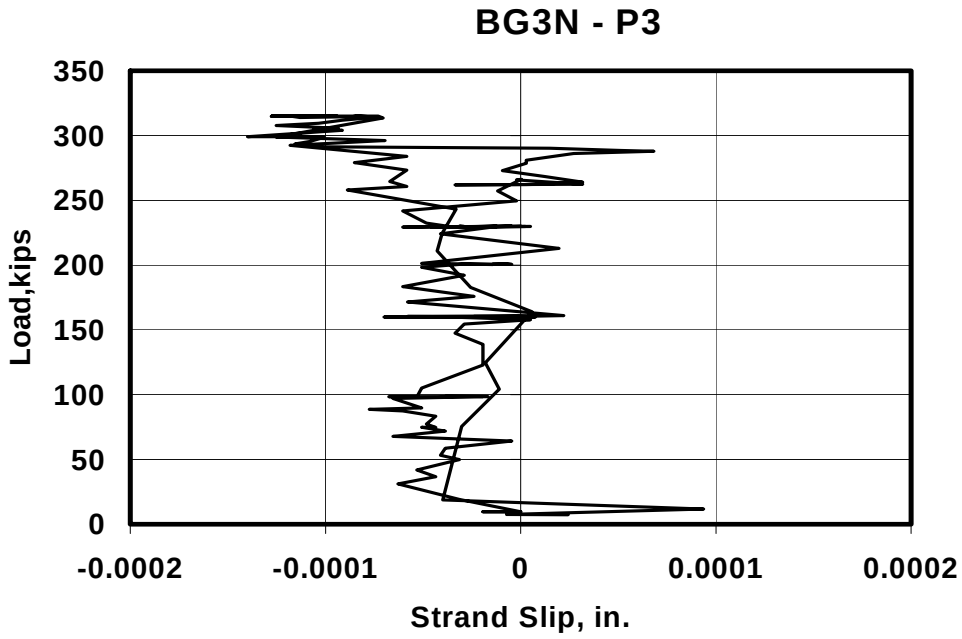
BG3N - P3
350
300
250
200
150
100
50
0
Load,kips
-0.0002
-0.0001
0
0.0001
0.0002
Strand Slip, in.

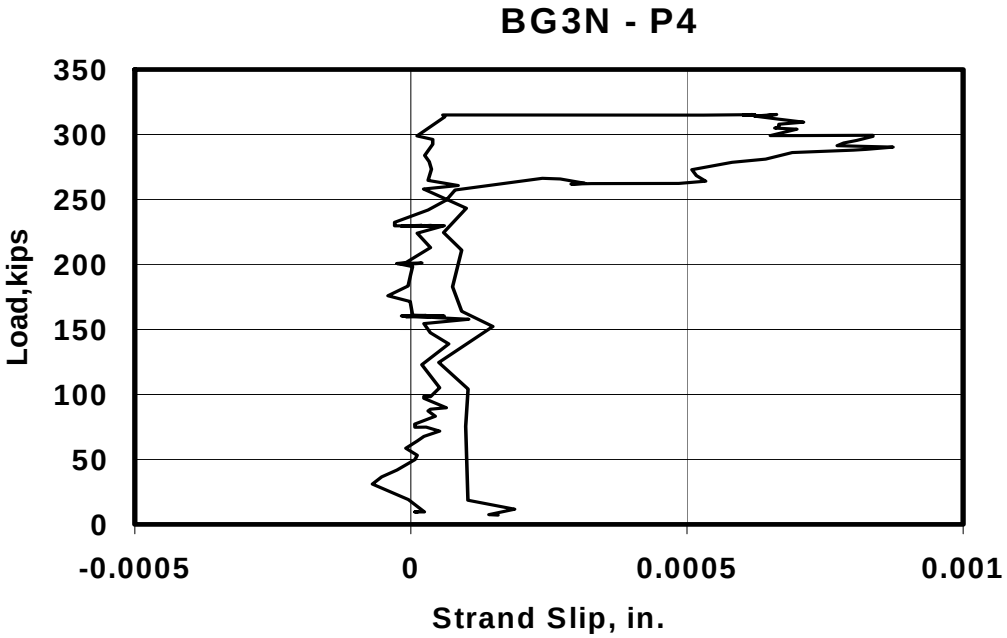
BG3N - P4
350
300
250
200
150
100
50
0
Load,kips
-0.0005
0
0.0005
0.001
Strand Slip, in.

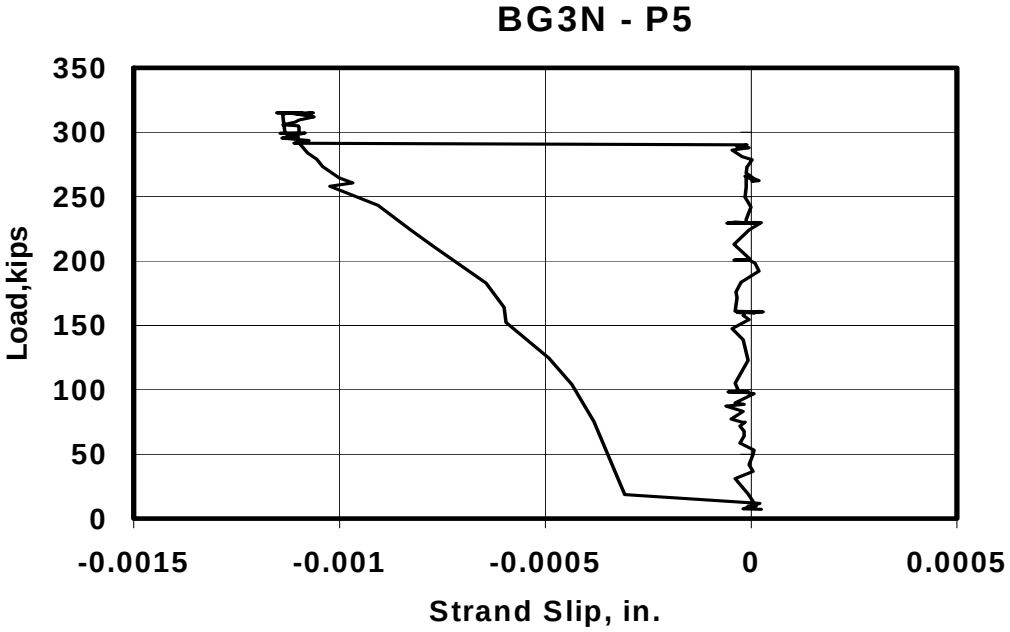
BG3N - P5
350
300
250
200
150
100
50
0
Load,kips
-0.0015
-0.001
-0.0005
0
0.0005
Strand Slip, in.

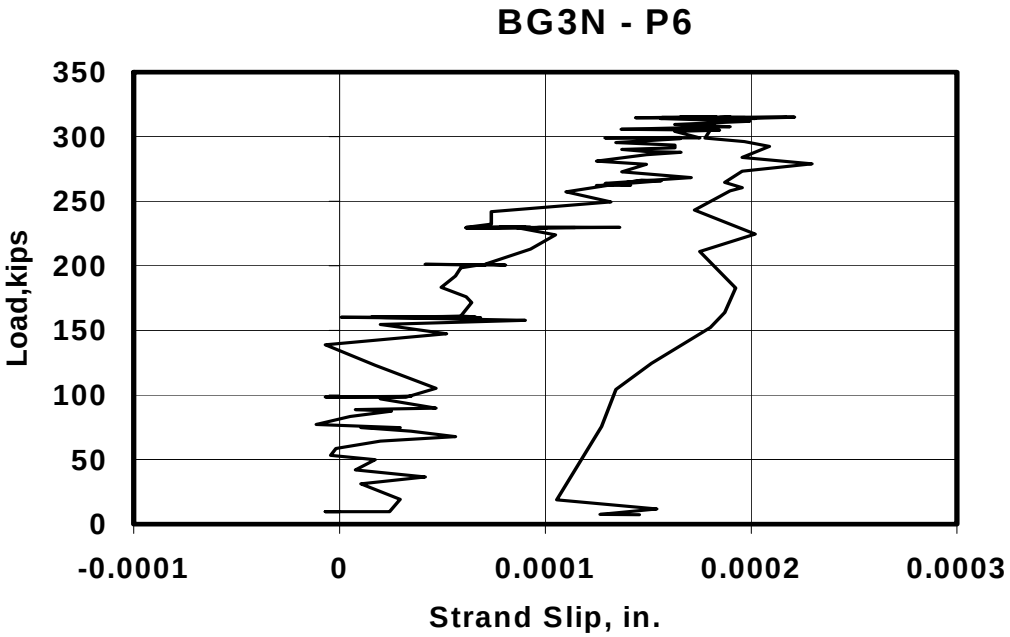
BG3N - P6
350
300
250
200
150
100
50
0
Load,kips
-0.0001
0
0.0001
0.0002
0.0003
Strand Slip, in.

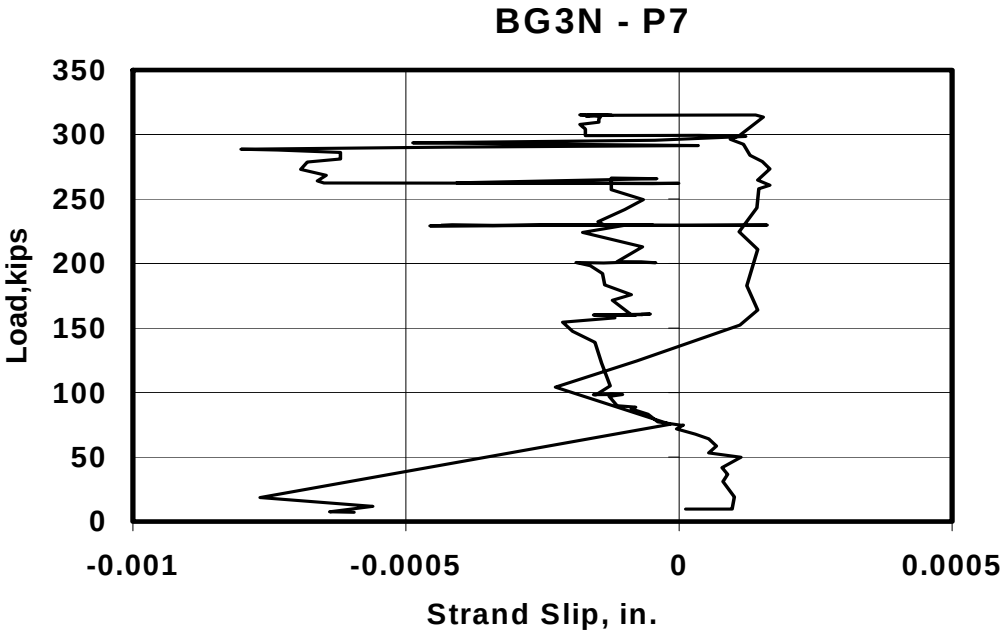
BG3N - P7
350
300
250
200
150
100
50
0
Load,kips
-0.001
-0.0005
0
0.0005
Strand Slip, in.

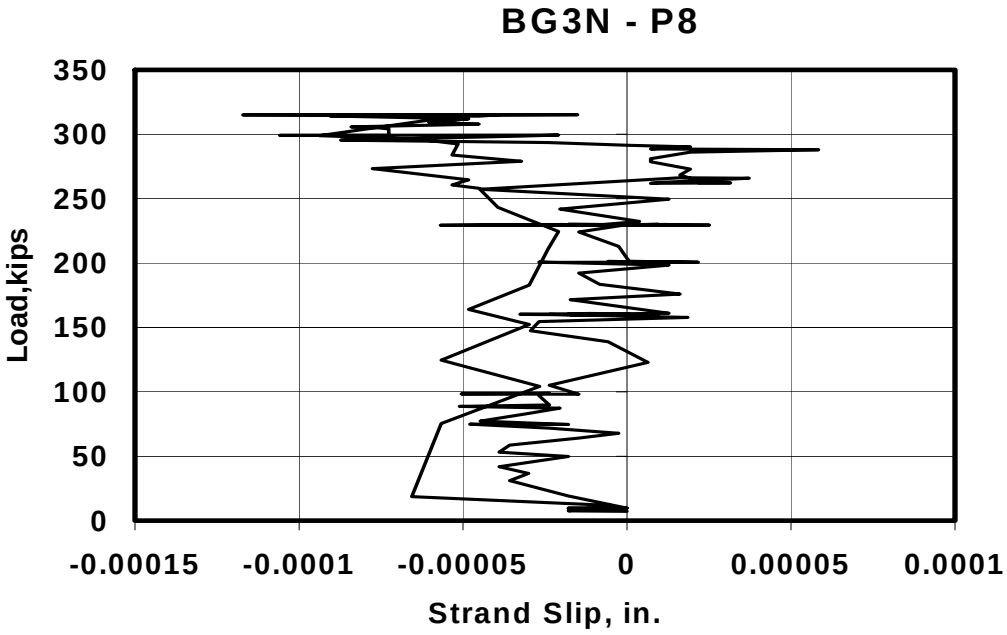
BG3N - P8
350
300
250
200
150
100
50
0
Load,kips
-0.00015
-0.0001
-0.00005
0
0.00005
0.0001
Strand Slip, in.

C.1.2 100 Load Cycles

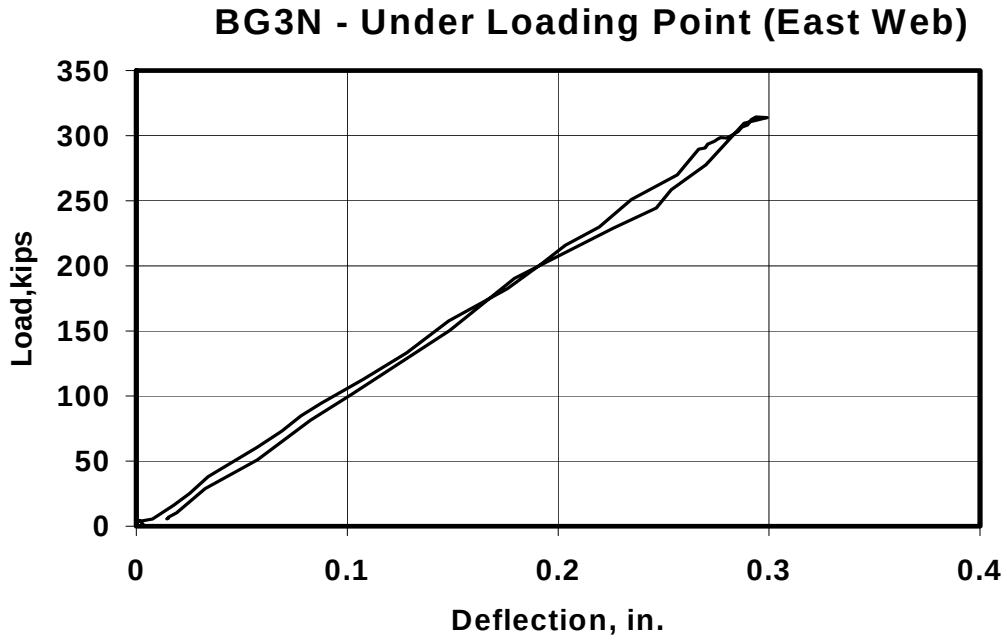

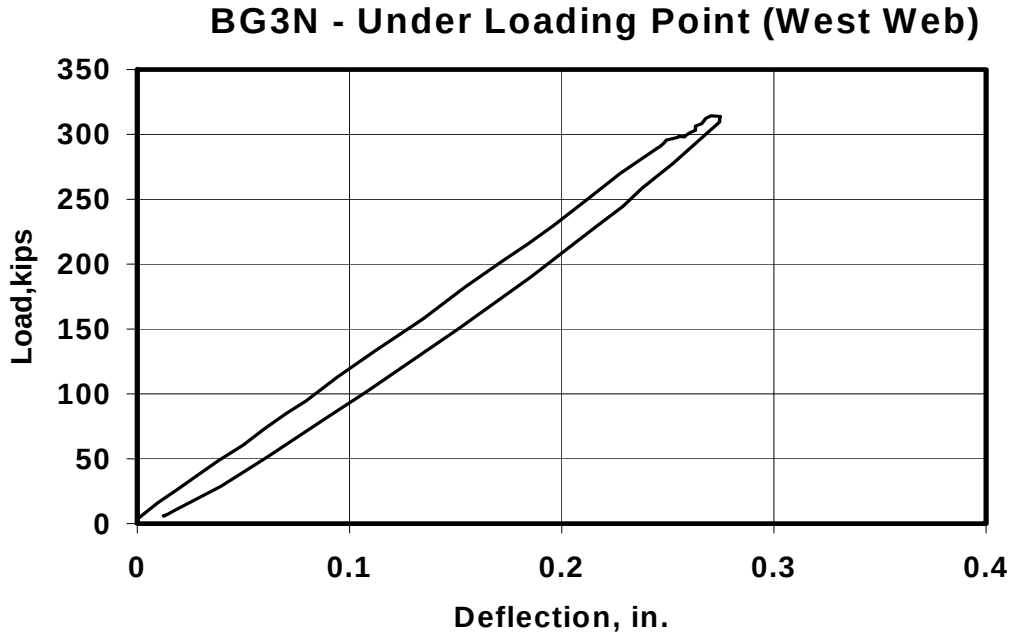

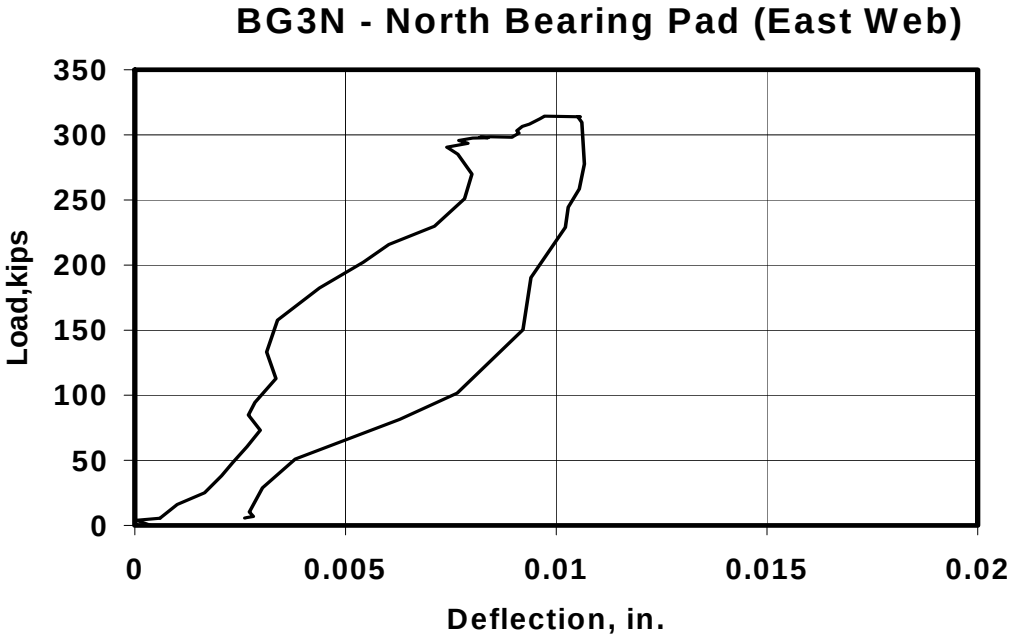
BG3N - North Bearing Pad (East Web)
Load,kips
350
300
250
200
150
100
50
0
0
0.005
0.01
0.015
0.02
Deflection, in.

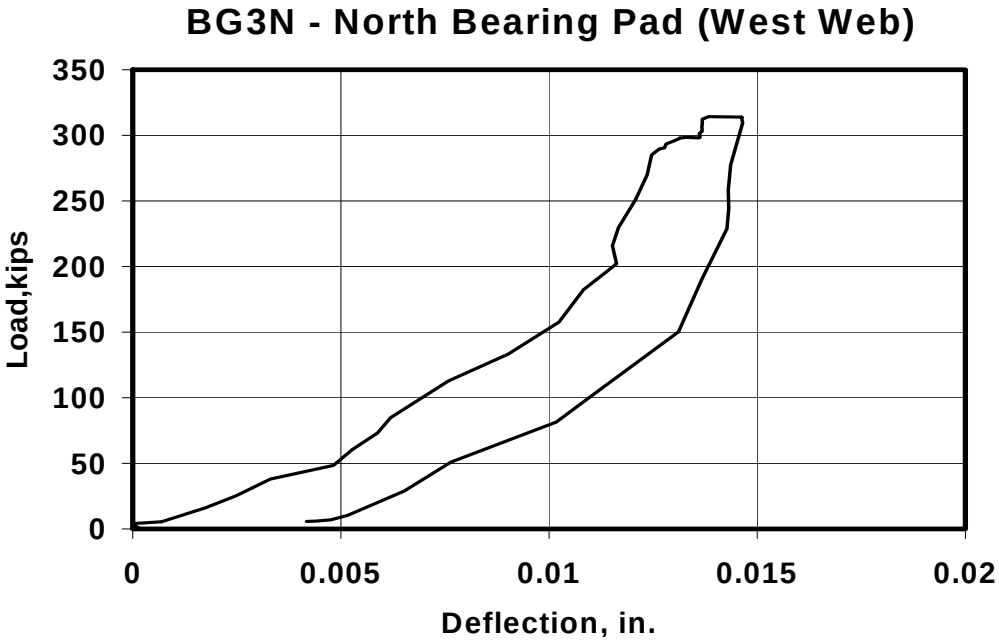
BG3N - North Bearing Pad (West Web)
Load,kips
350
300
250
200
150
100
50
0
0
0.005
0.01
0.015
0.02
Deflection, in.

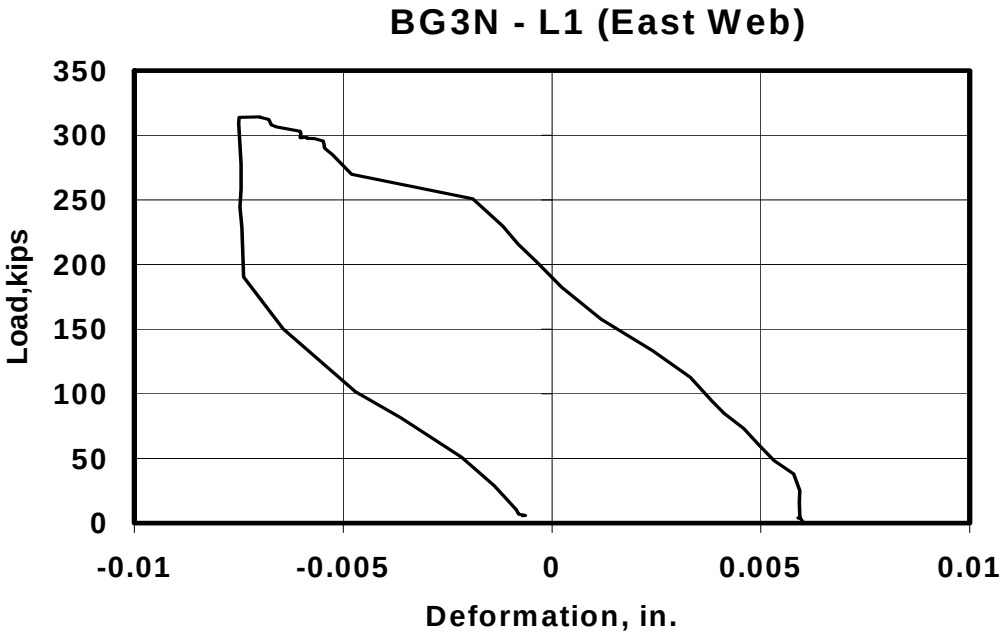
BG3N - L1 (East Web)
Load,kips
350
300
250
200
150
100
50
0
-0.01
-0.005
0
0.005
0.01
Deformation, in.

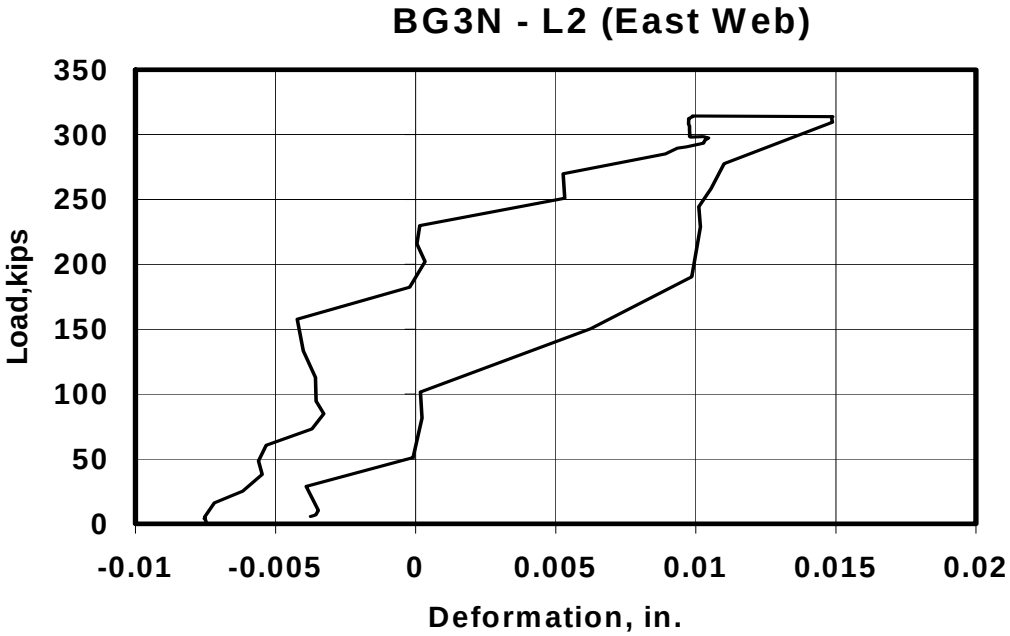
BG3N - L2 (East Web)
Load,kips
350
300
250
200
150
100
50
0
-0.01
-0.005
0
0.005
0.01
0.015
0.02
Deformation, in.

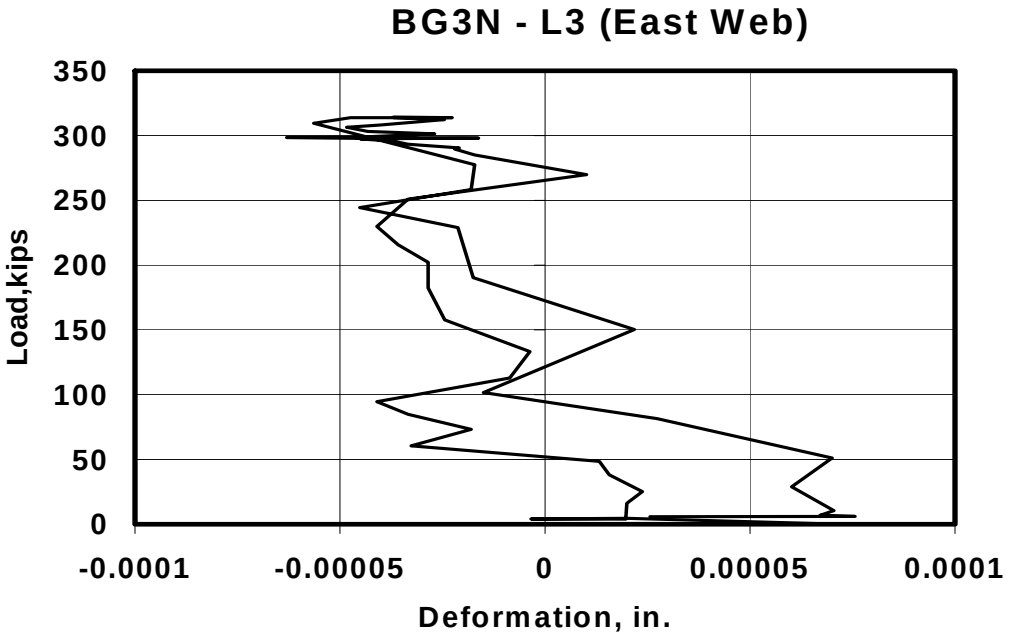
BG3N - L3 (East Web)
Load,kips
350
300
250
200
150
100
50
0
-0.0001
-0.00005
0
0.00005
0.0001
Deformation, in.

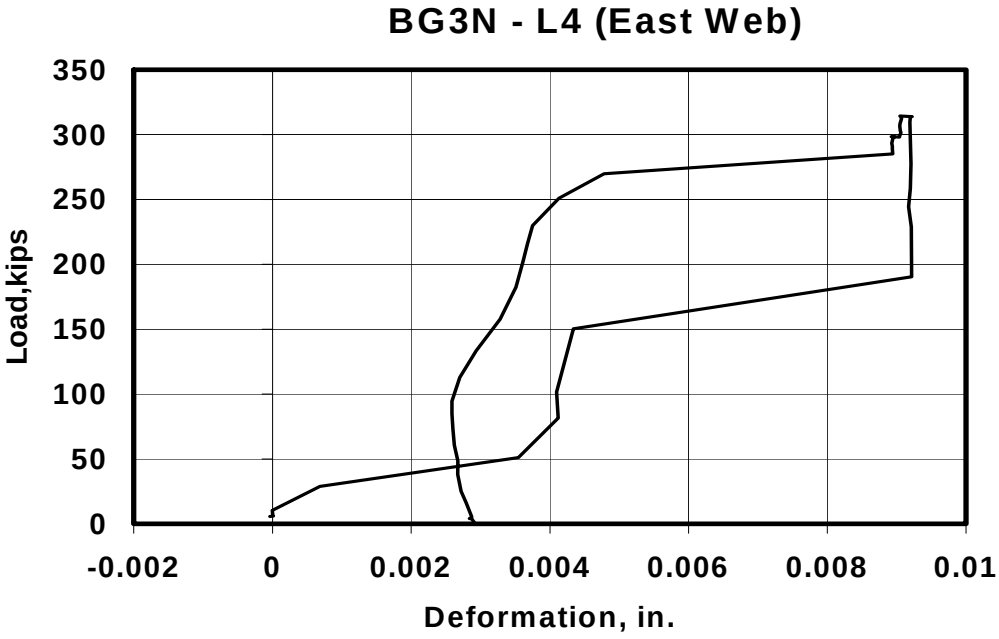
BG3N - L4 (East Web)
Load,kips
350
300
250
200
150
100
50
0
-0.002
0
0.002
0.004
0.006
0.008
0.01
Deformation, in.

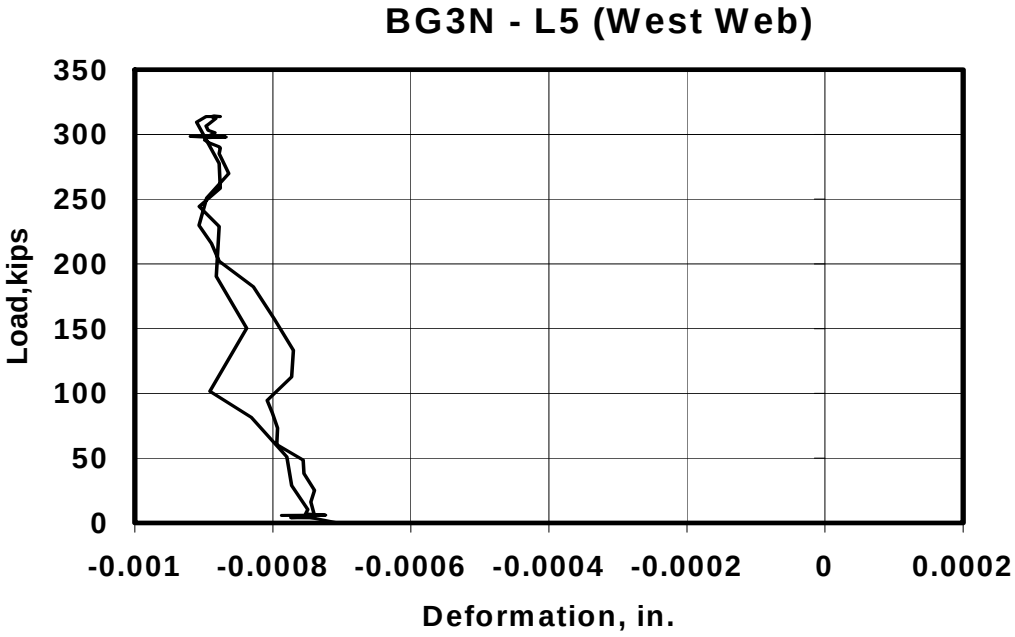
BG3N - L5 (West Web)
Load,kips
350
300
250
200
150
100
50
0
-0.001
-0.0008
-0.0006
-0.0004
-0.0002
0
0.0002
Deformation, in.

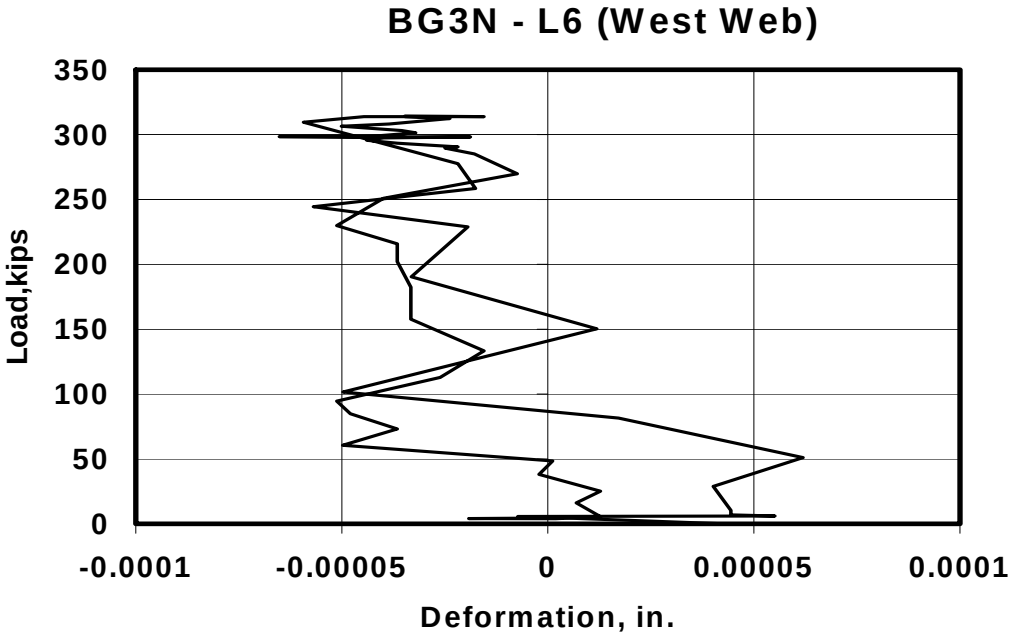
BG3N - L6 (West Web)
Load,kips
350
300
250
200
150
100
50
0
-0.0001
-0.00005
0
0.00005
0.0001
Deformation, in.

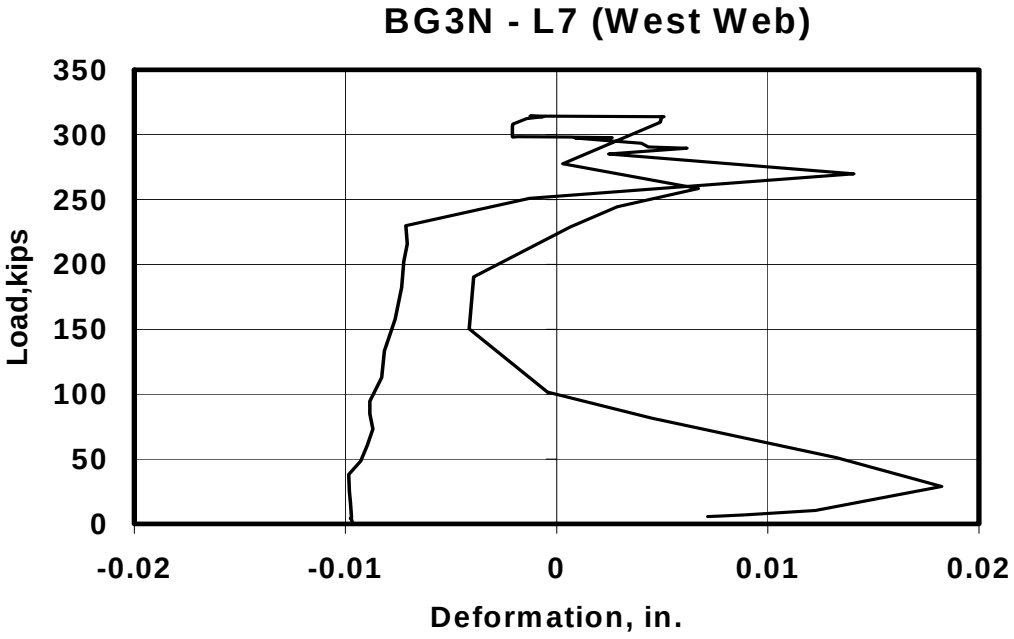
BG3N - L7 (West Web)
Load,kips
350
300
250
200
150
100
50
0
-0.02
-0.01
0
0.01
0.02
Deformation, in.

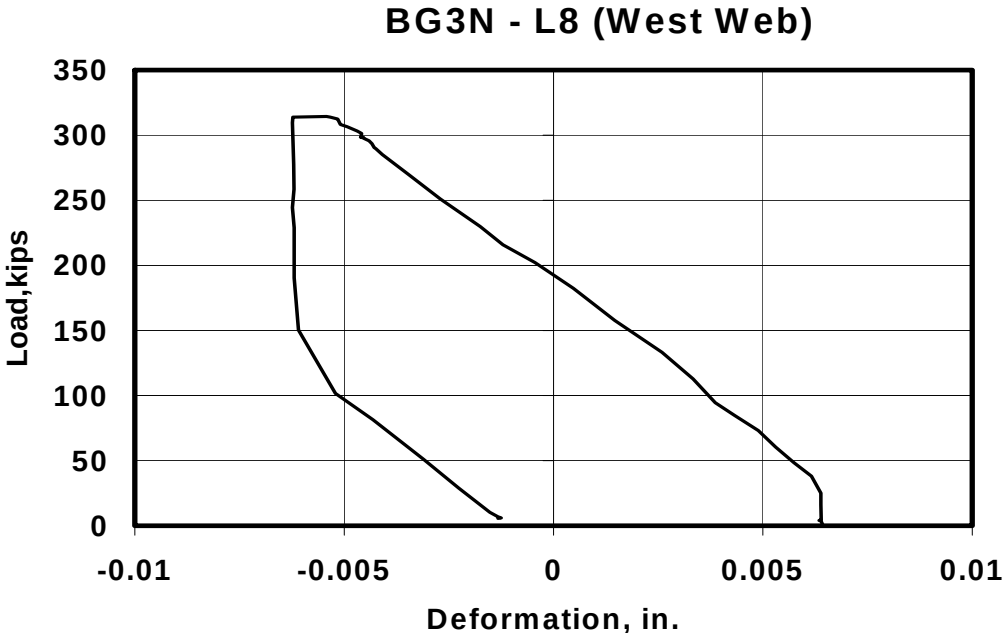
BG3N - L8 (West Web)
Load,kips
350
300
250
200
150
100
50
0
-0.01
-0.005
0
0.005
0.01
Deformation, in.

C.1.3 1000 Load Cycles

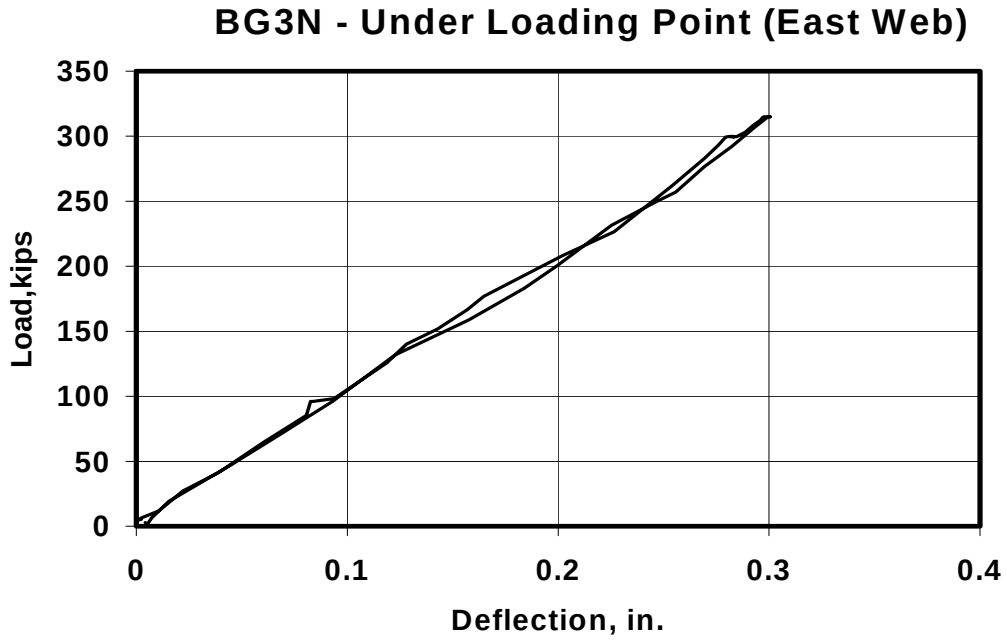

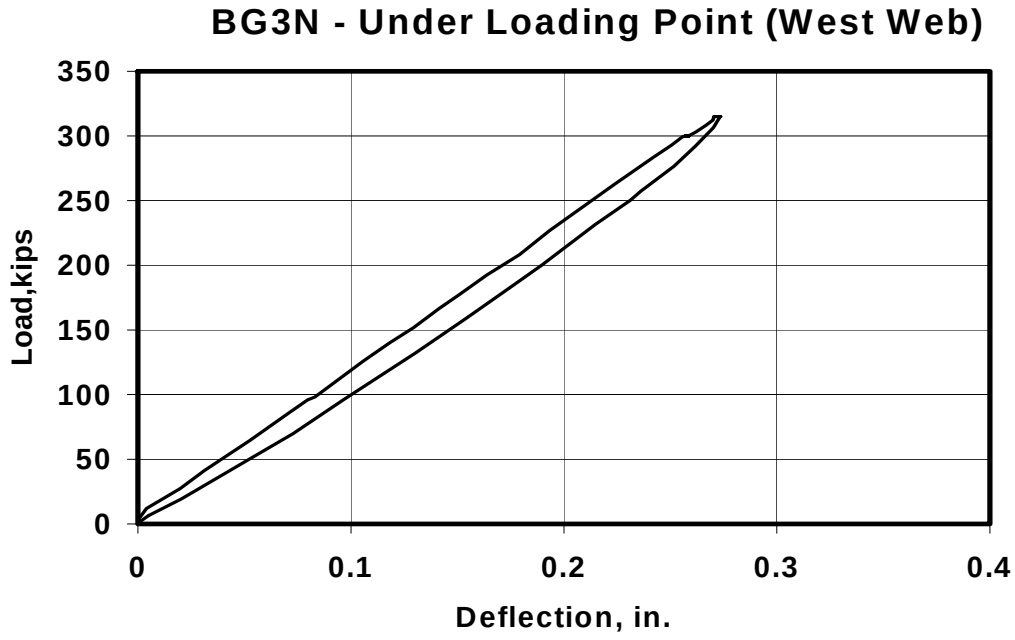

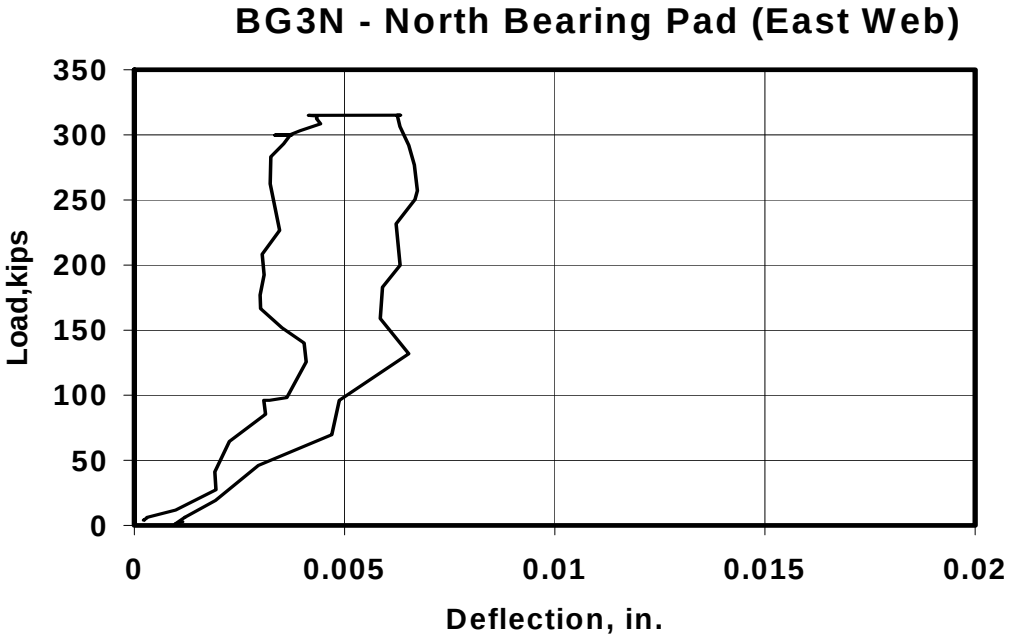
BG3N - North Bearing Pad (East Web)
Load,kips
350
300
250
200
150
100
50
0
0
0.005
0.01
0.015
0.02
Deflection, in.

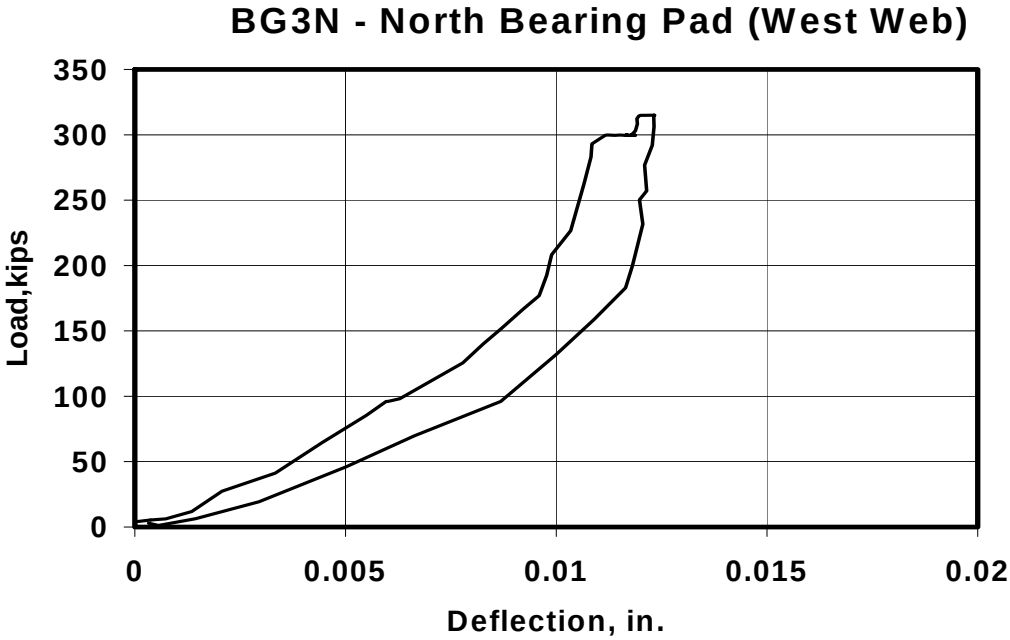
BG3N - North Bearing Pad (West Web)
Load,kips
350
300
250
200
150
100
50
0
0
0.005
0.01
0.015
0.02
Deflection, in.

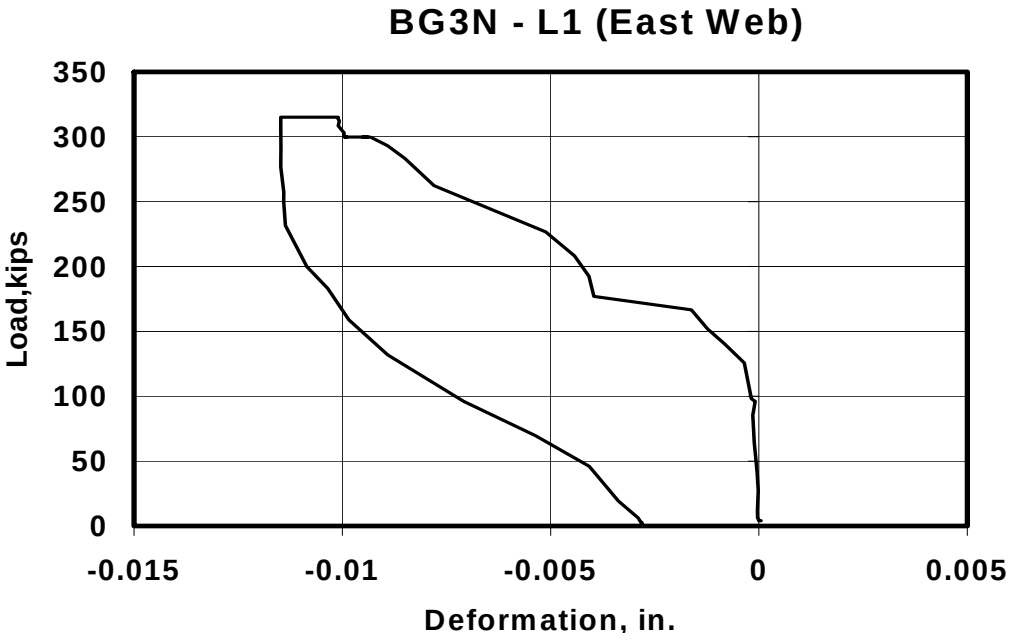
BG3N - L1 (East Web)
Load,kips
350
300
250
200
150
100
50
0
-0.015
-0.01
-0.005
0
0.005
Deformation, in.

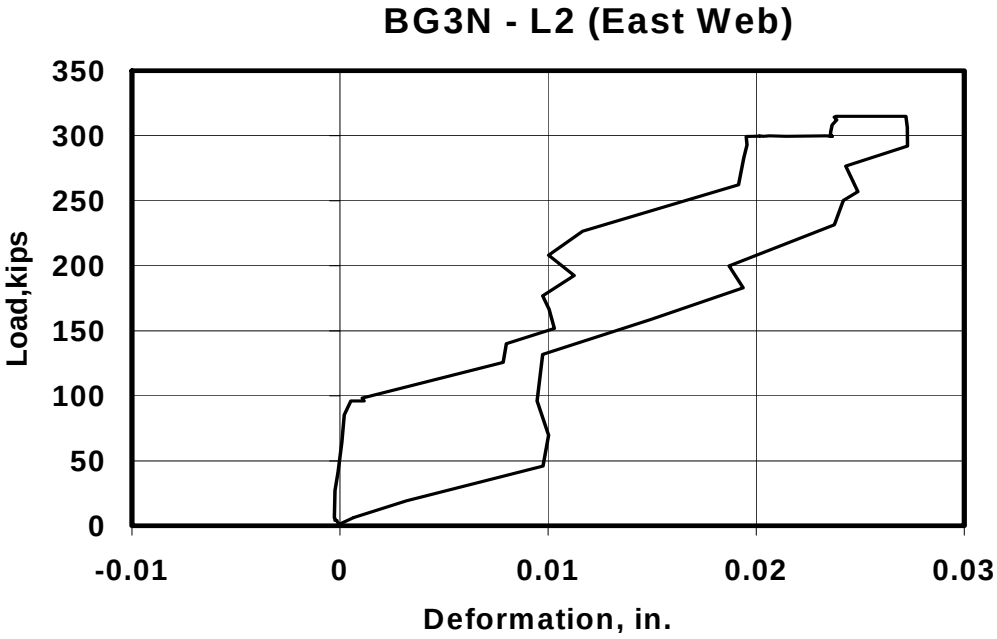
BG3N - L2 (East Web)
Load,kips
350
300
250
200
150
100
50
0
-0.01
0
0.01
0.02
0.03
Deformation, in.

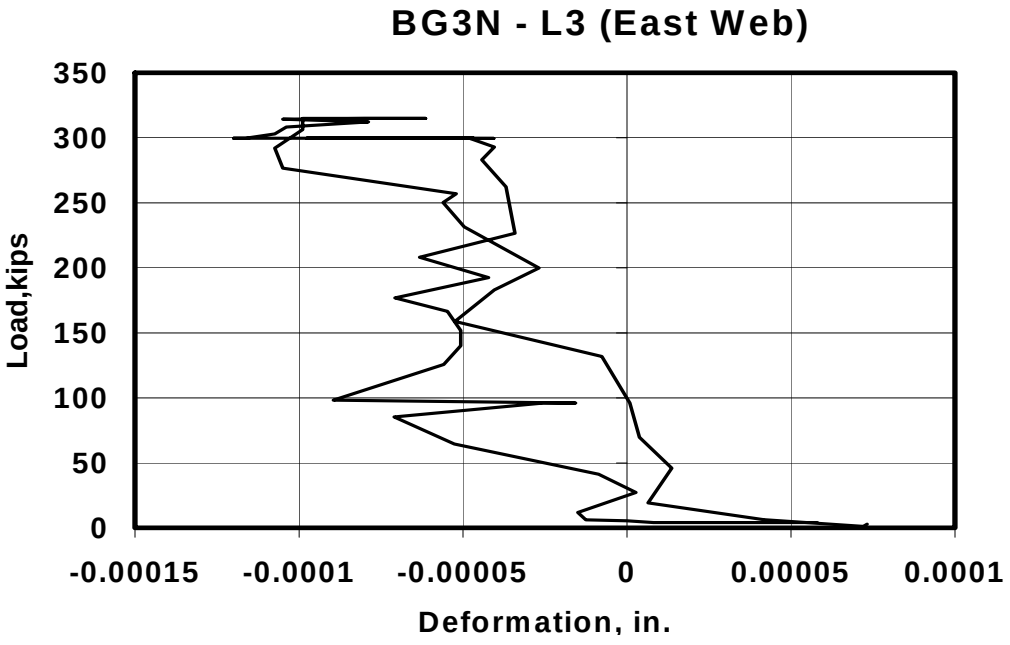
BG3N - L3 (East Web)
Load,kips
350
300
250
200
150
100
50
0
-0.00015
-0.0001
-0.00005
0
0.00005
0.0001
Deformation, in.

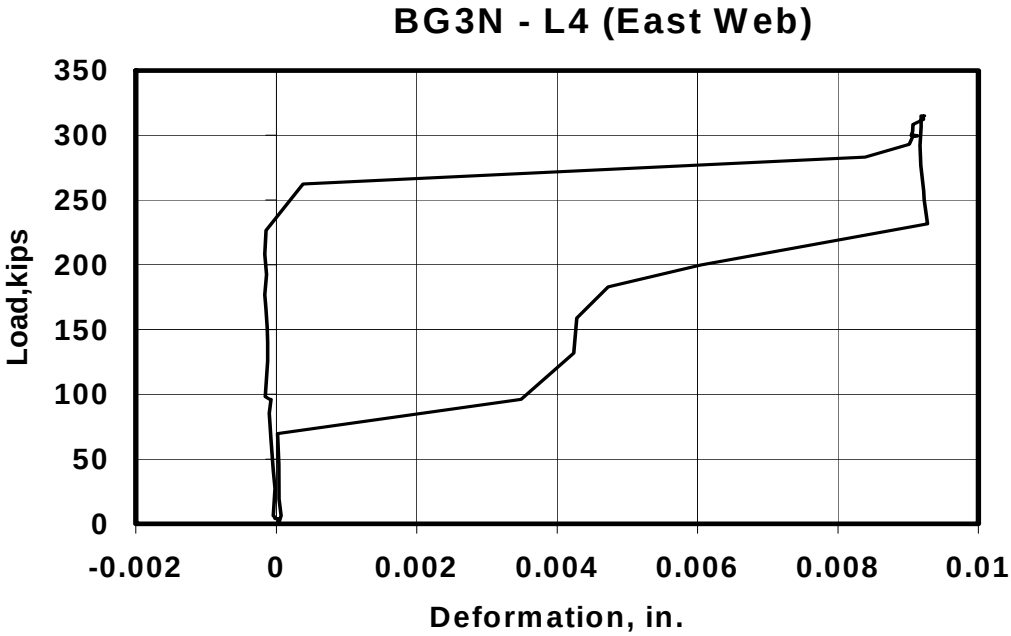
BG3N - L4 (East Web)
Load,kips
350
300
250
200
150
100
50
0
-0.002
0
0.002
0.004
0.006
0.008
0.01
Deformation, in.

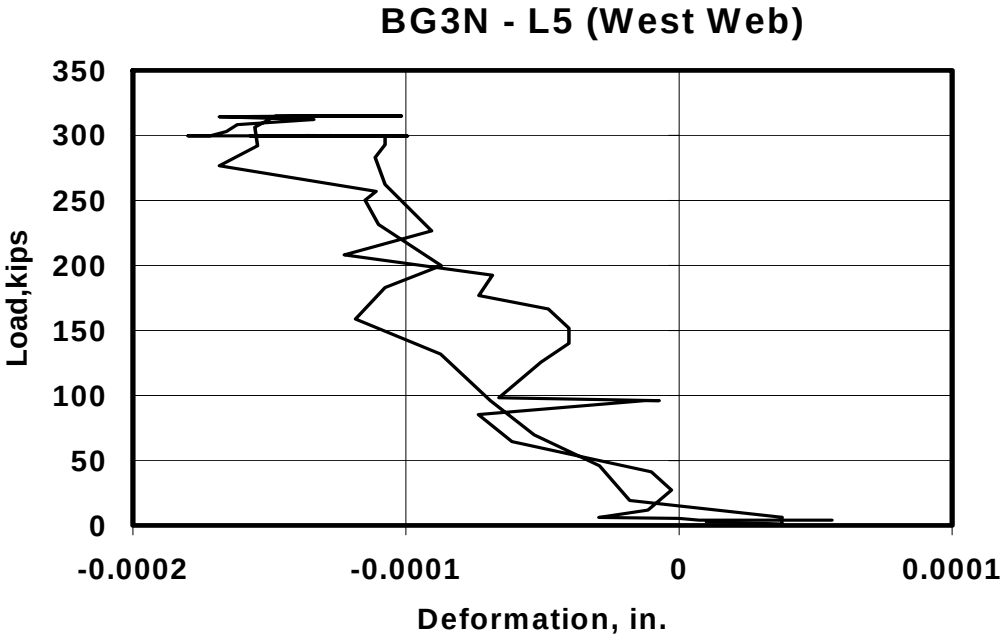
BG3N - L5 (West Web)
Load,kips
350
300
250
200
150
100
50
0
-0.0002
-0.0001
0
0.0001
Deformation, in.

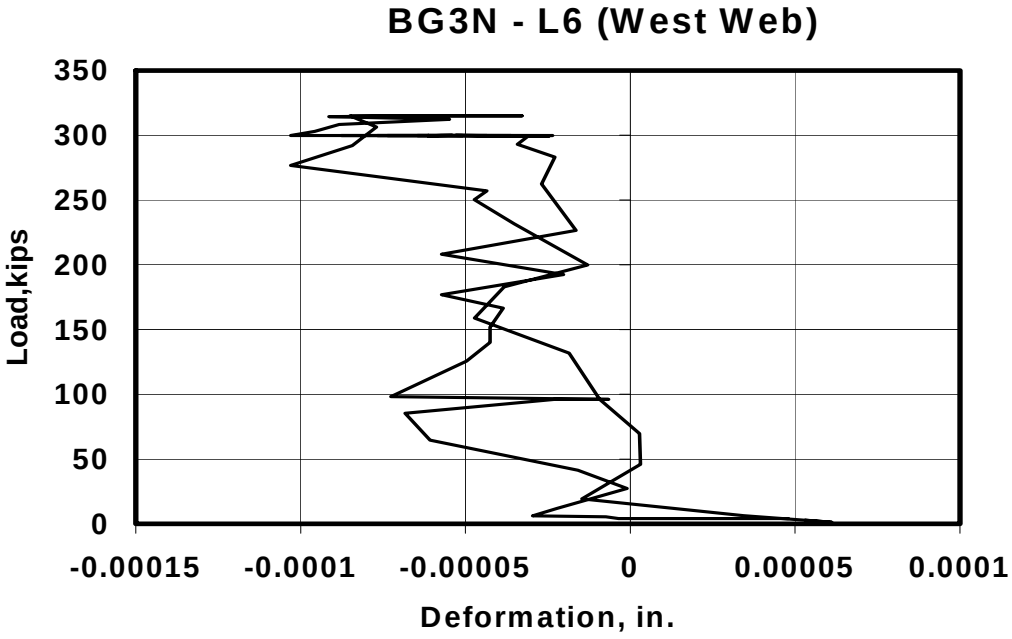
BG3N - L6 (West Web)
Load,kips
350
300
250
200
150
100
50
0
-0.00015
-0.0001
-0.00005
0
0.00005
0.0001
Deformation, in.

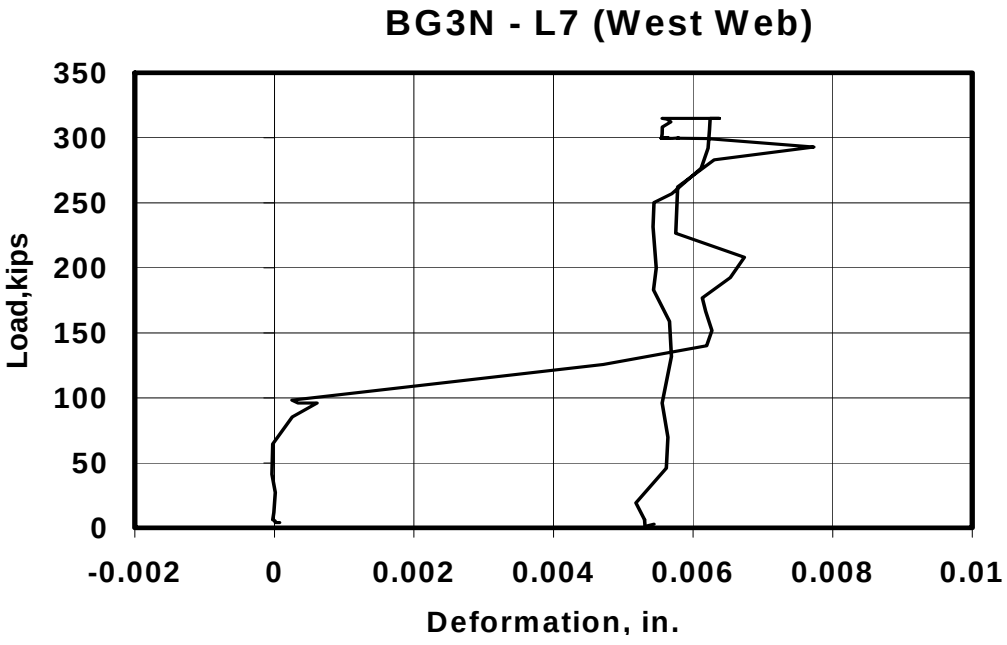
BG3N - L7 (West Web)
Load,kips
350
300
250
200
150
100
50
0
-0.002
0
0.002
0.004
0.006
0.008
0.01
Deformation, in.

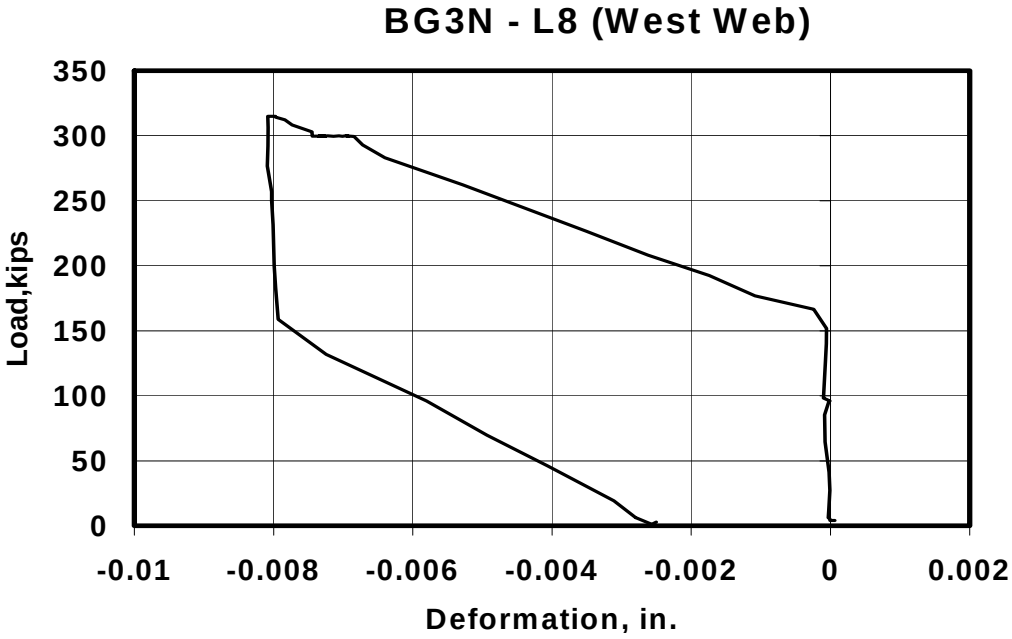
BG3N - L8 (West Web)
Load,kips
350
300
250
200
150
100
50
0
-0.01
-0.008
-0.006
-0.004
-0.002
0
0.002
Deformation, in.

C.1.4 10,000 Load Cycles

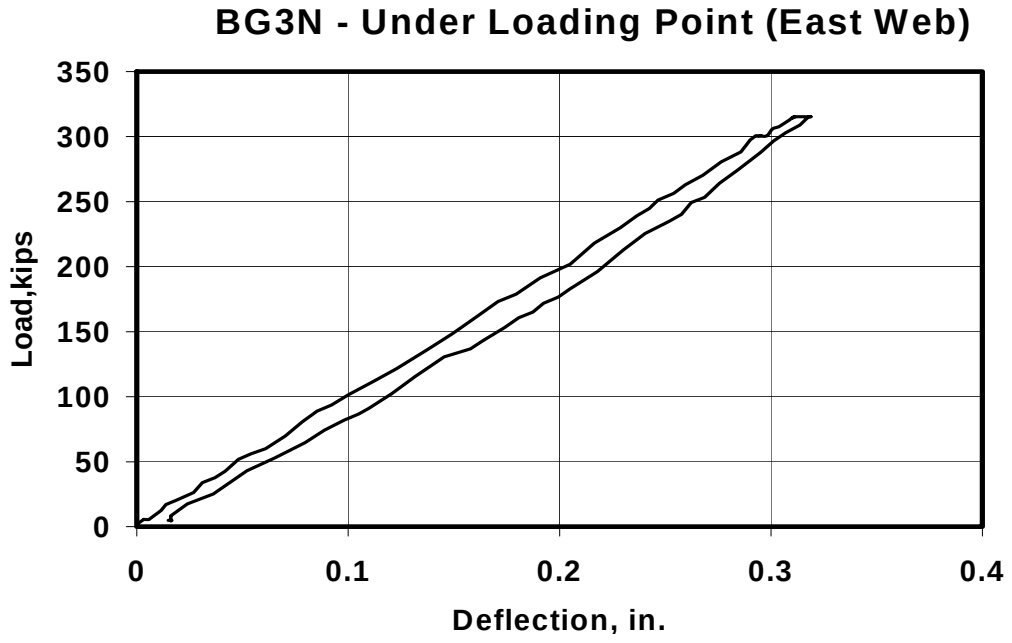

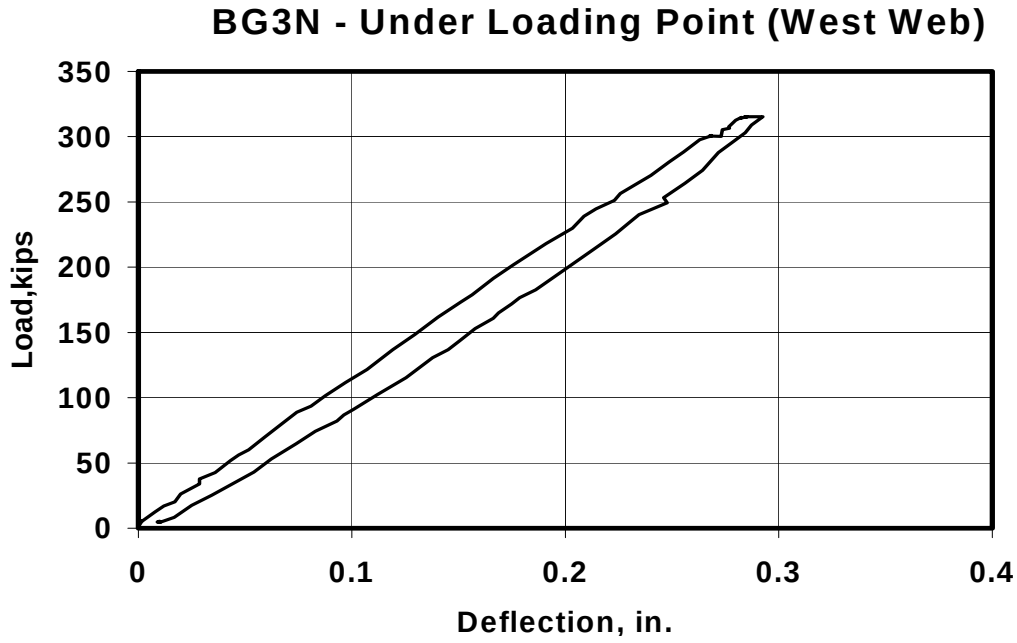

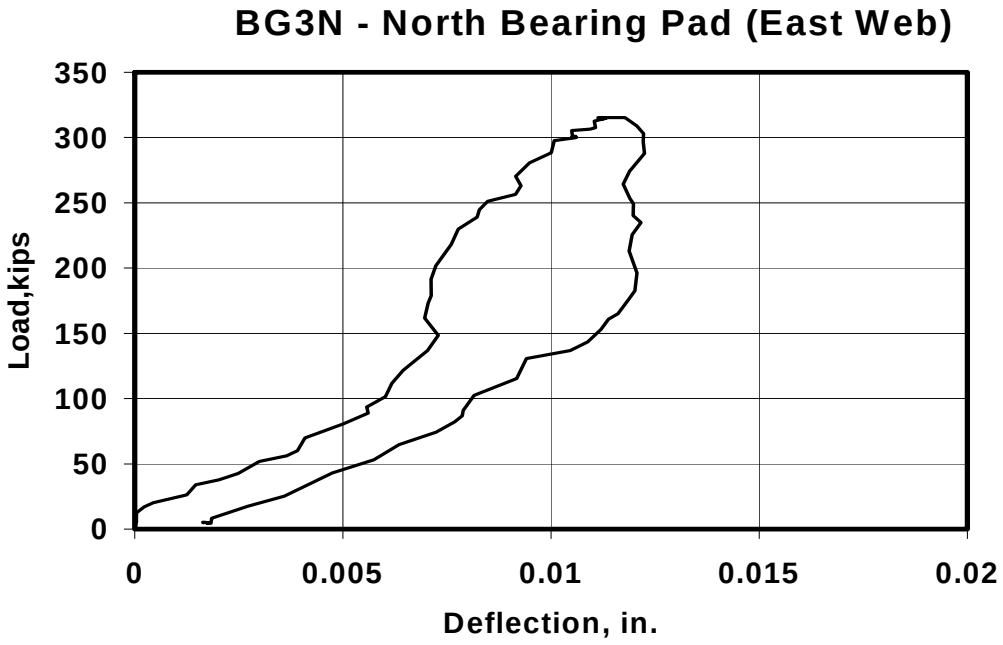
BG3N - North Bearing Pad (East Web)
Load,kips
350
300
250
200
150
100
50
0
0
0.005
0.01
0.015
0.02
Deflection, in.

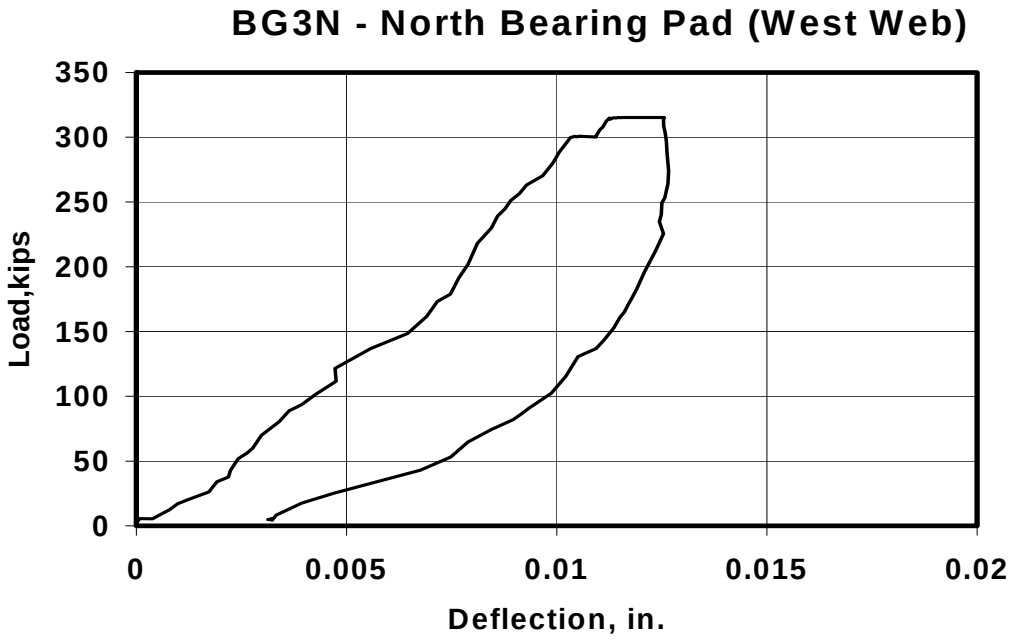
BG3N - North Bearing Pad (West Web)
Load,kips
350
300
250
200
150
100
50
0
0
0.005
0.01
0.015
0.02
Deflection, in.

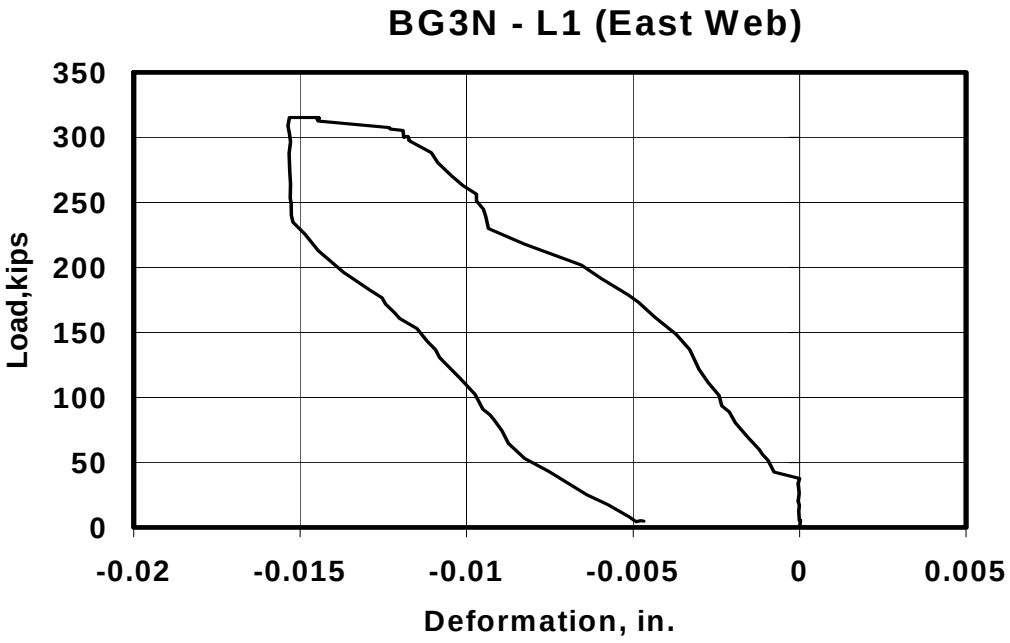
BG3N - L1 (East Web)
Load,kips
350
300
250
200
150
100
50
0
-0.02
-0.015
-0.01
-0.005
0
0.005
Deformation, in.

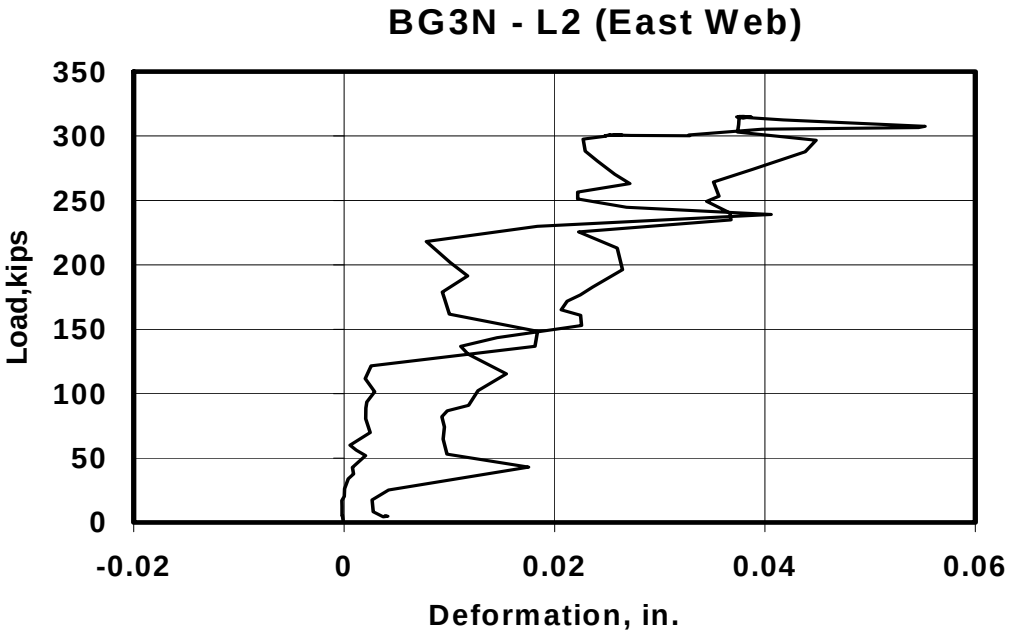
BG3N - L2 (East Web)
Load,kips
350
300
250
200
150
100
50
0
-0.02
0
0.02
0.04
0.06
Deformation, in.

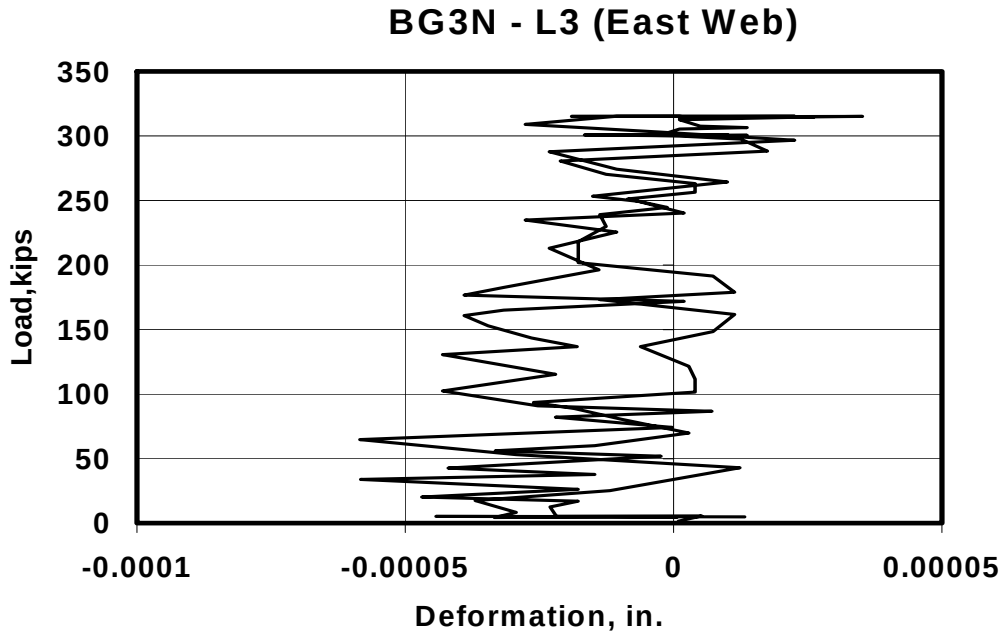
BG3N - L3 (East Web)
350
300
250
200
150
100
50
0
Load,kips
-0.0001
-0.00005
0
0.00005
Deformation, in.

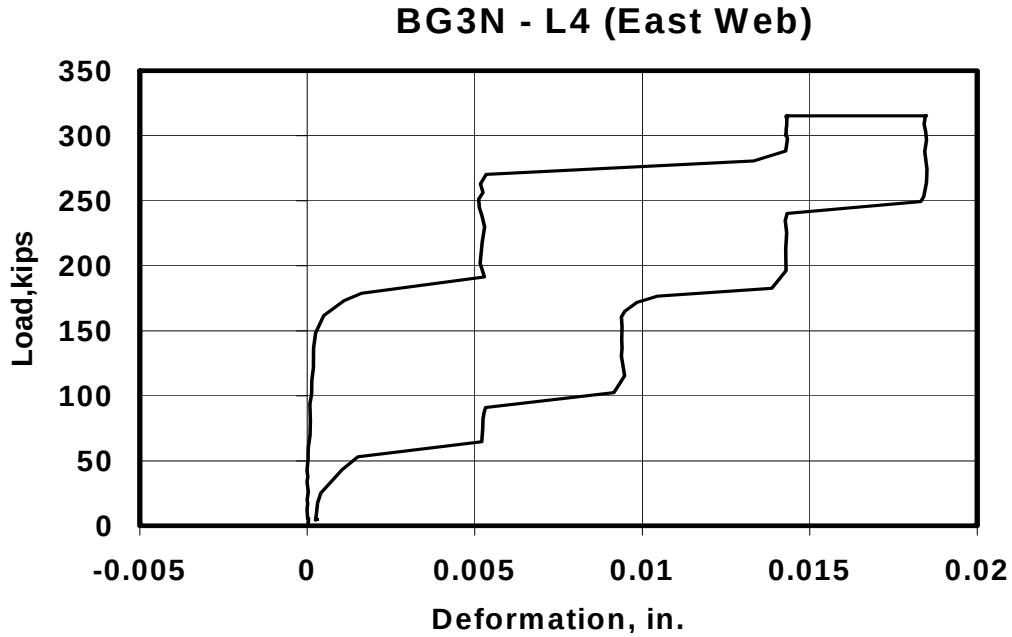
BG3N - L4 (East Web)
350
300
250
200
150
100
50
0
Load,kips
-0.005
0
0.005
0.01
0.015
0.02
Deformation, in.

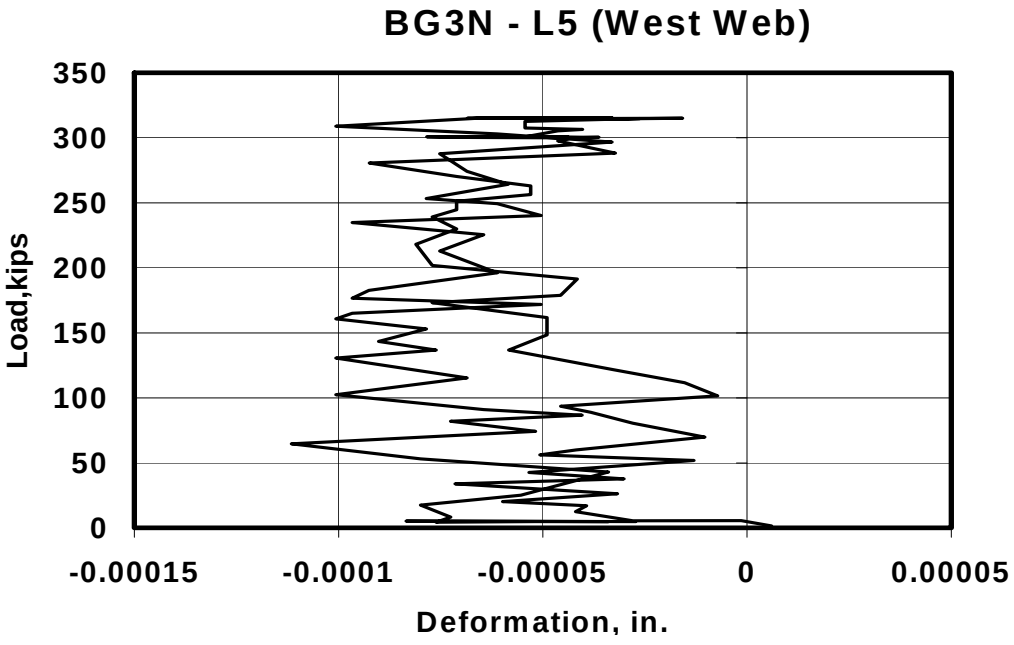
BG3N - L5 (West Web)
Load,kips
350
300
250
200
150
100
50
0
-0.00015
-0.0001
-0.00005
0
0.00005
Deformation, in.

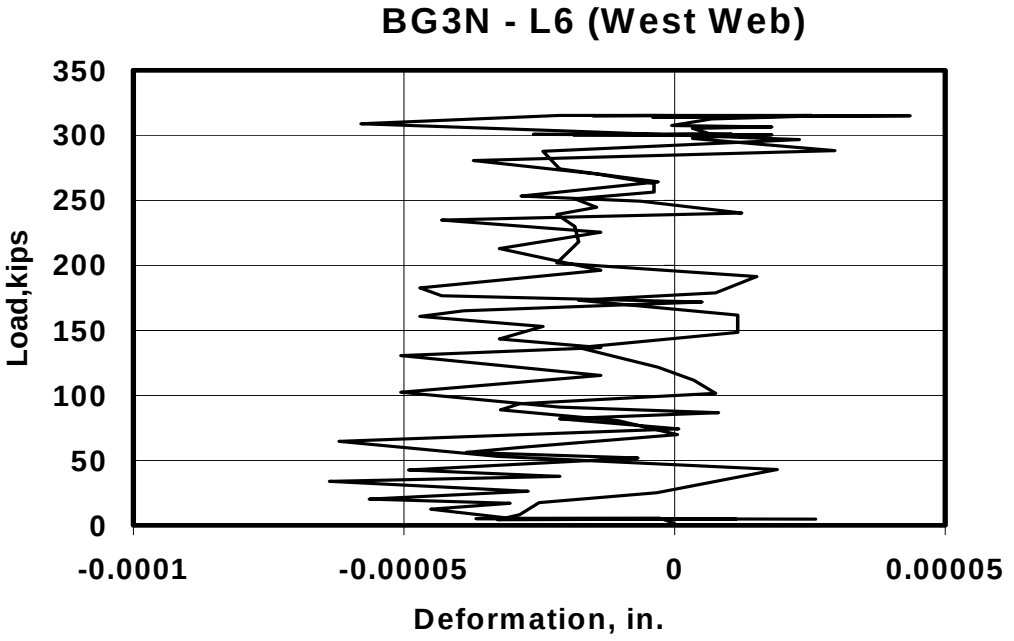
BG3N - L6 (West Web)
Load,kips
350
300
250
200
150
100
50
0
-0.0001
-0.00005
0
0.00005
Deformation, in.

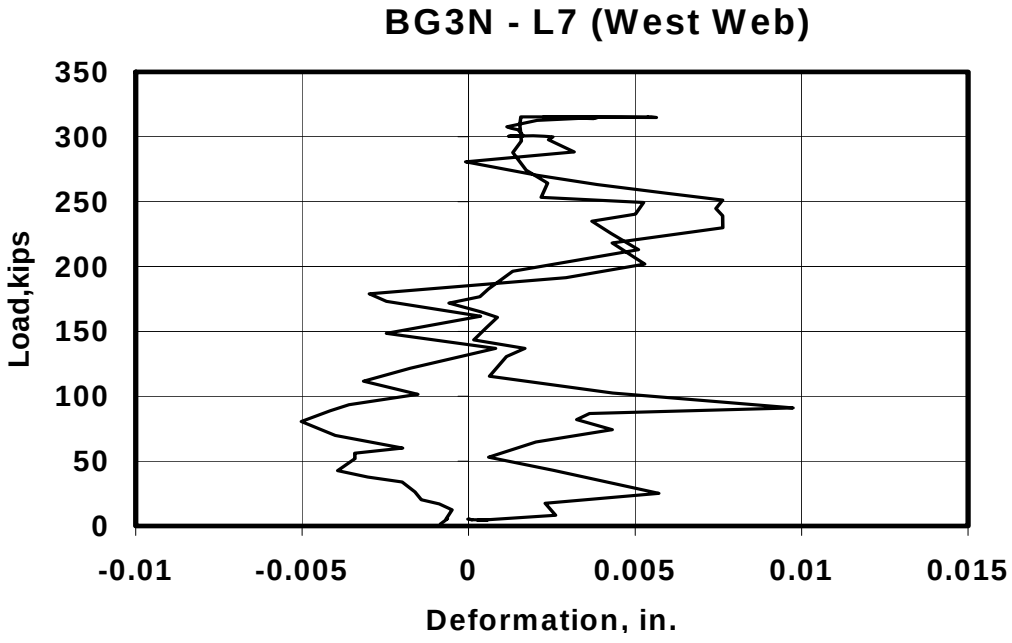
BG3N - L7 (West Web)
Load,kips
350
300
250
200
150
100
50
0
-0.01
-0.005
0
0.005
0.01
0.015
Deformation, in.

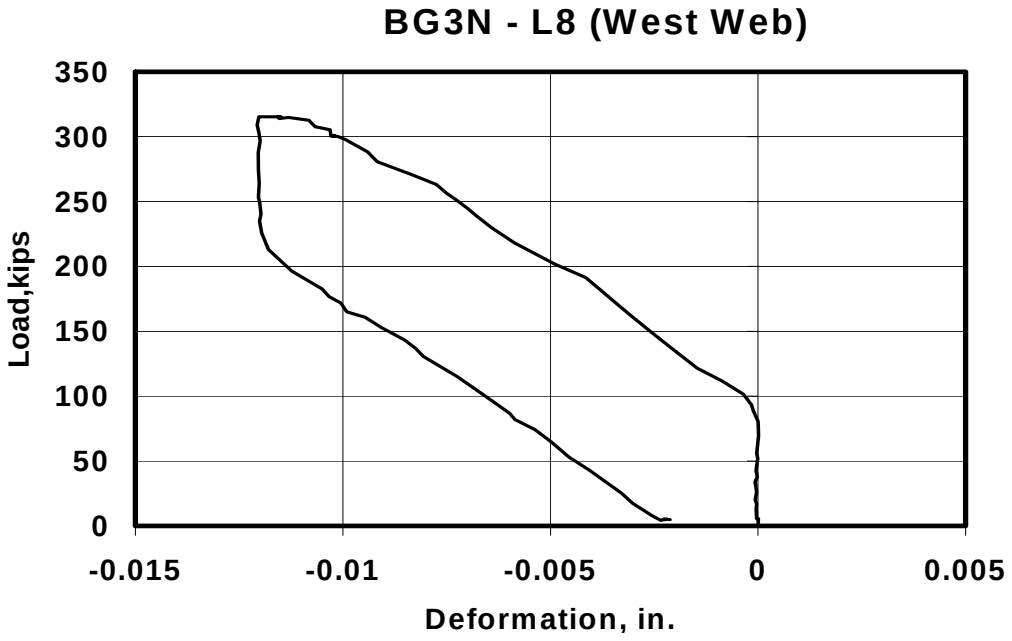
BG3N - L8 (West Web)
Load,kips
350
300
250
200
150
100
50
0
-0.015
-0.01
-0.005
0
0.005
Deformation, in.

C.2 BG3S

C.2.1 10,000 Load Cycles

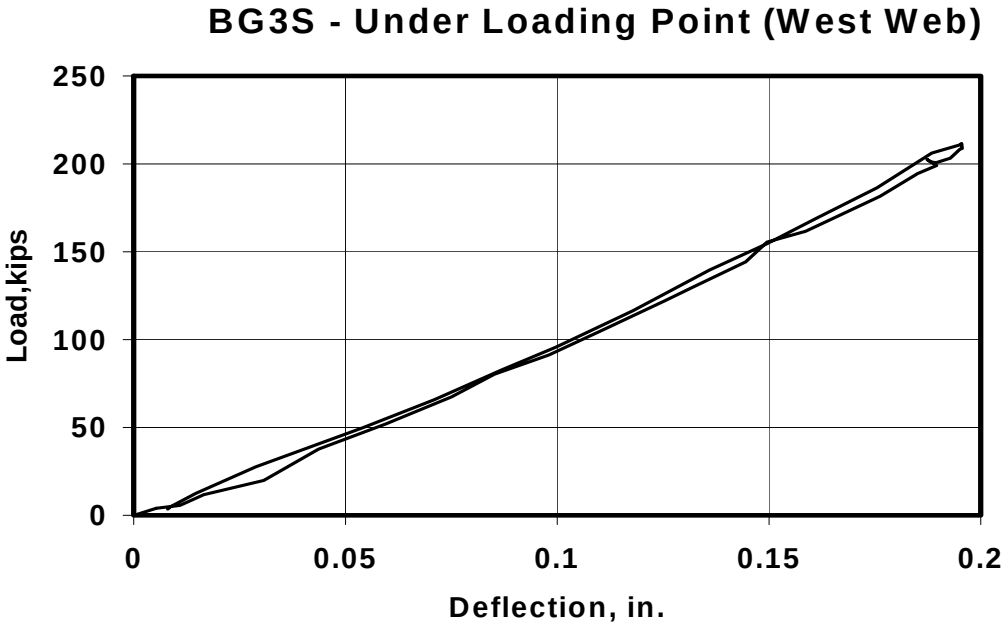

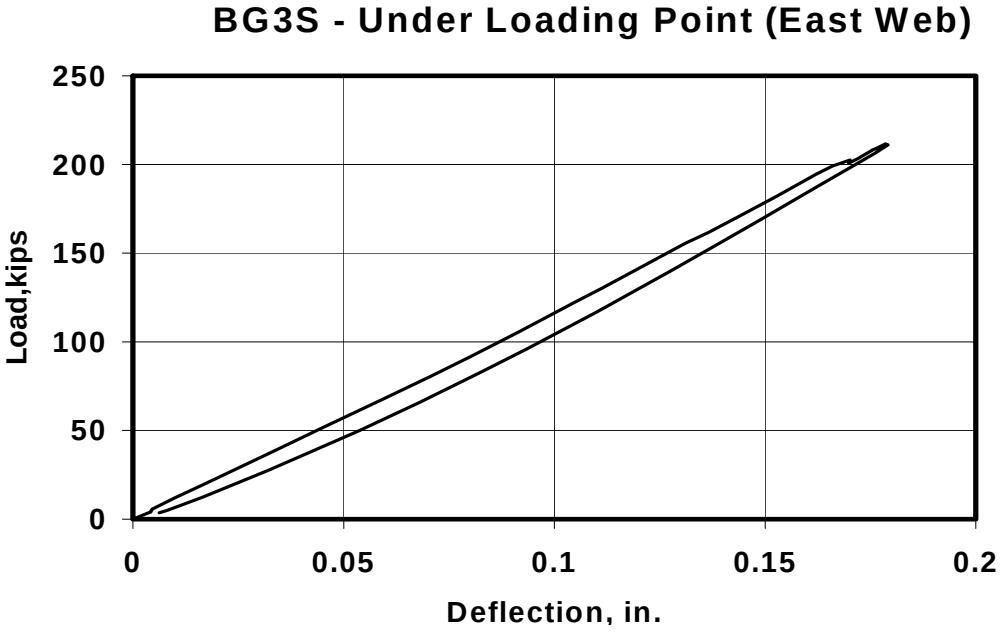

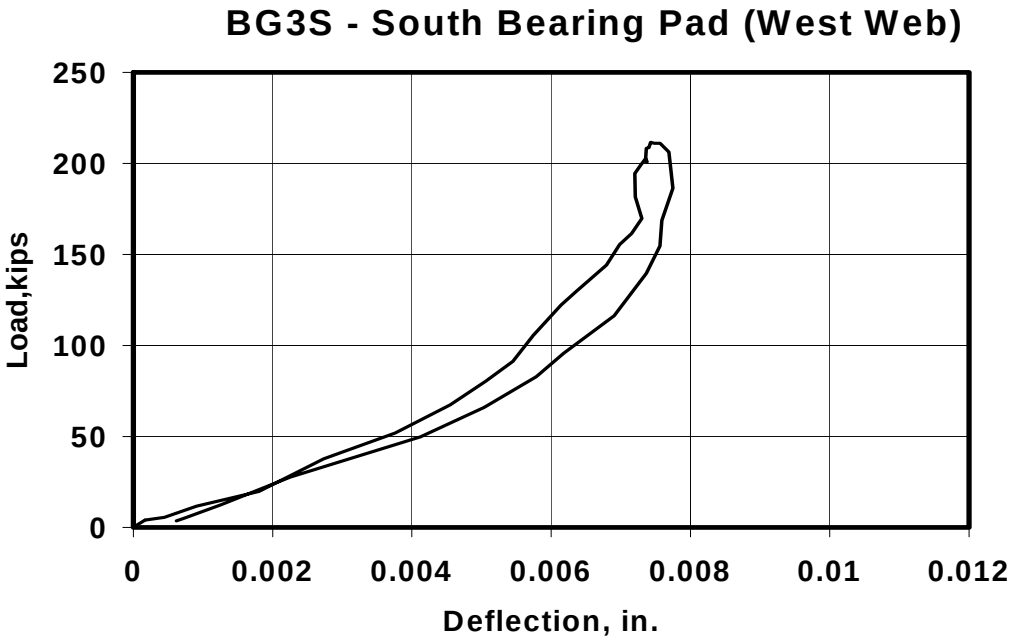
BG3S - South Bearing Pad (West Web)
Load,kips
250
200
150
100
50
0
0
0.002
0.004
0.006
0.008
0.01
0.012
Deflection, in.

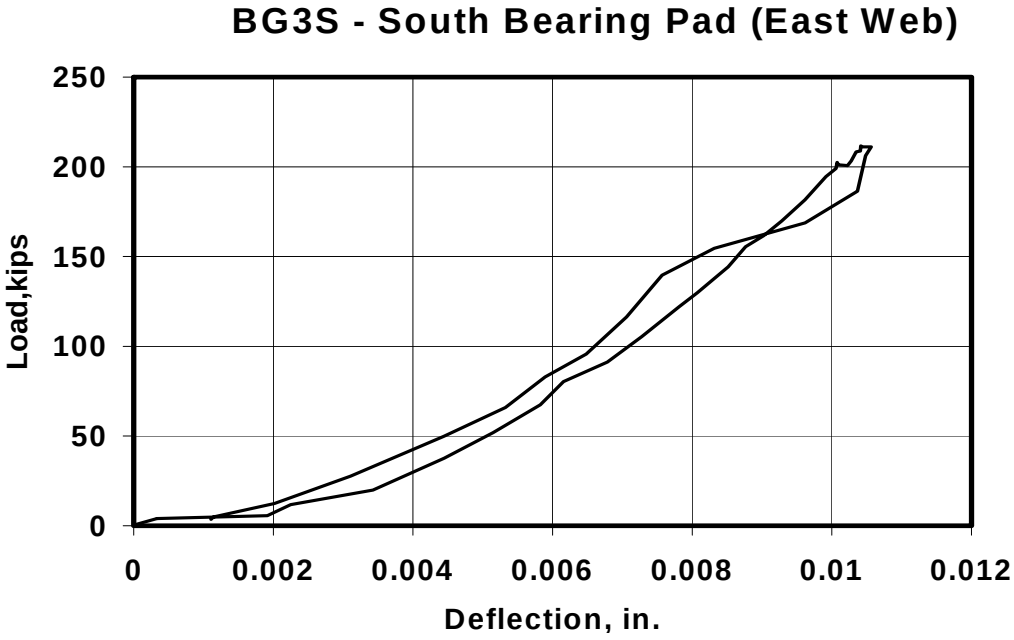
BG3S - South Bearing Pad (East Web)
Load,kips
250
200
150
100
50
0
0
0.002
0.004
0.006
0.008
0.01
0.012
Deflection, in.

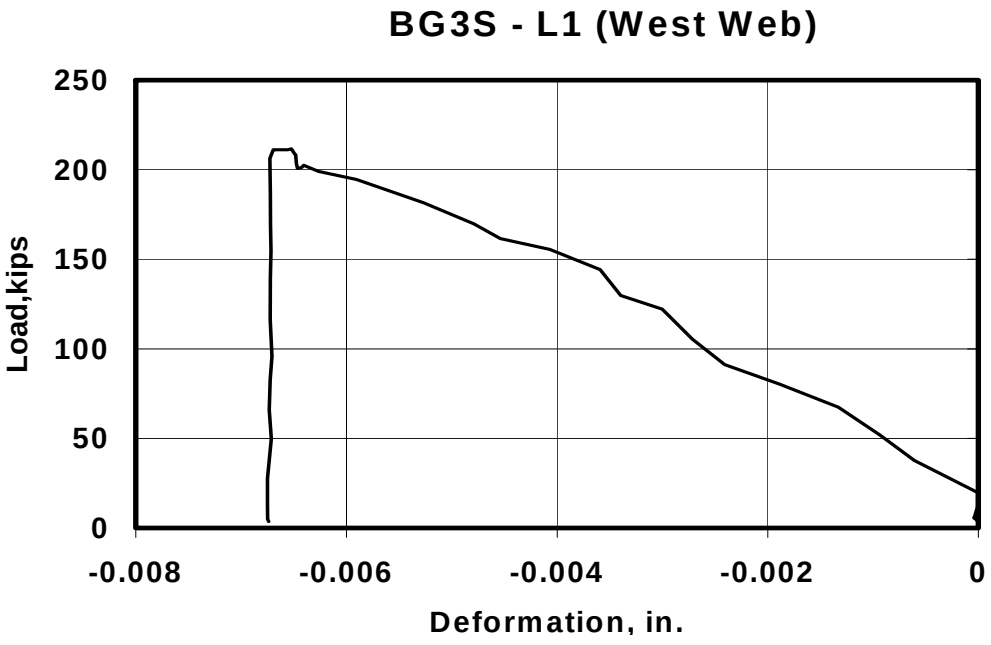
BG3S - L1 (West Web)
250
200
150
100
50
0
Load,kips
-0.008
-0.006
-0.004
-0.002
0
Deformation, in.

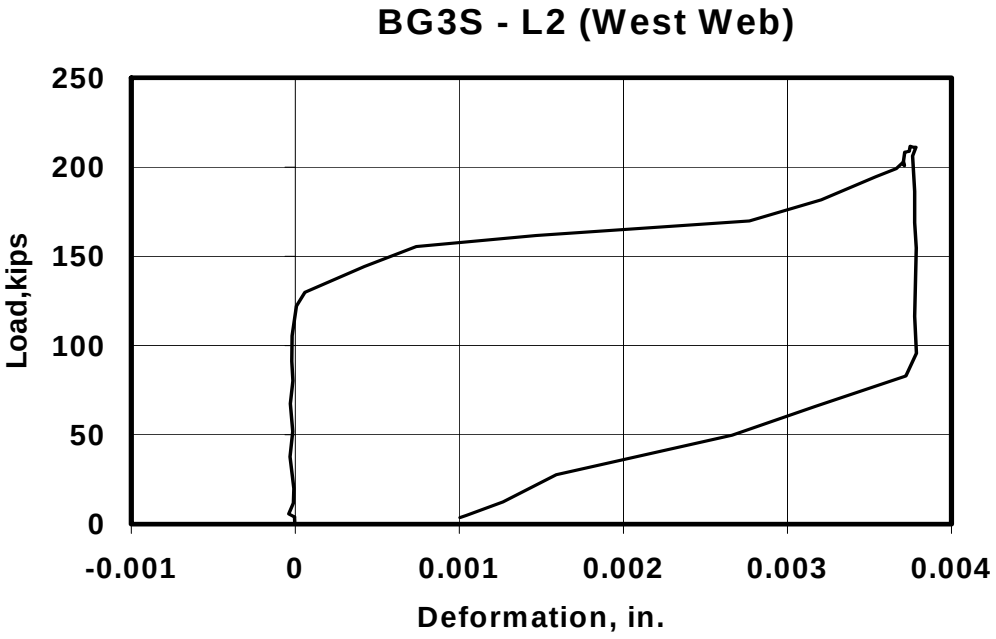
BG3S - L2 (West Web)
250
200
150
100
50
0
Load,kips
-0.001
0
0.001
0.002
0.003
0.004
Deformation, in.

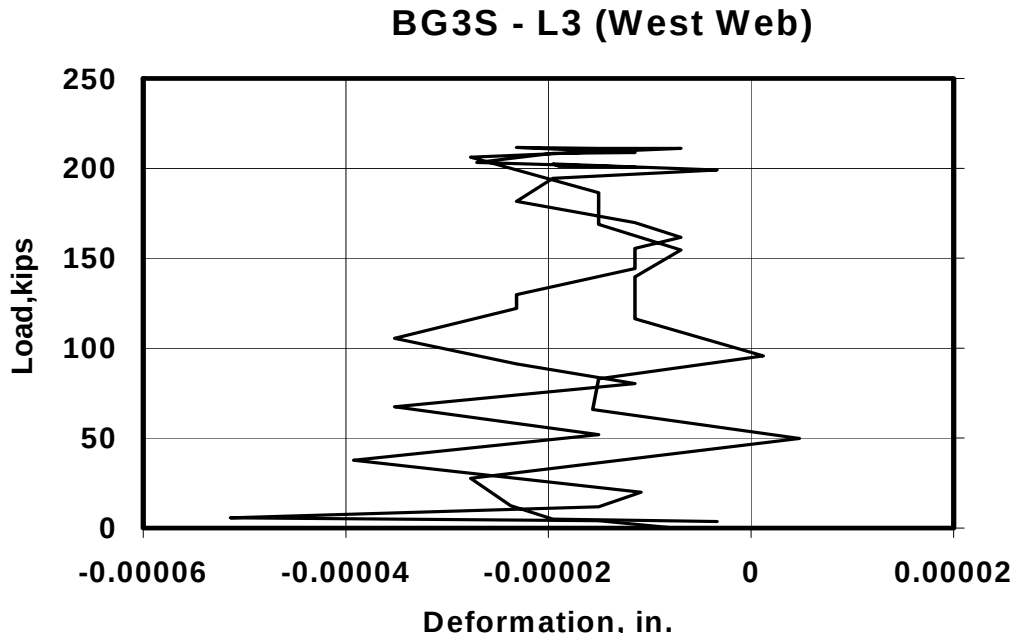
BG3S - L3 (West Web)
250
200
150
100
50
0
Load,kips
-0.00006
-0.00004
-0.00002
0
0.00002
Deformation. in.

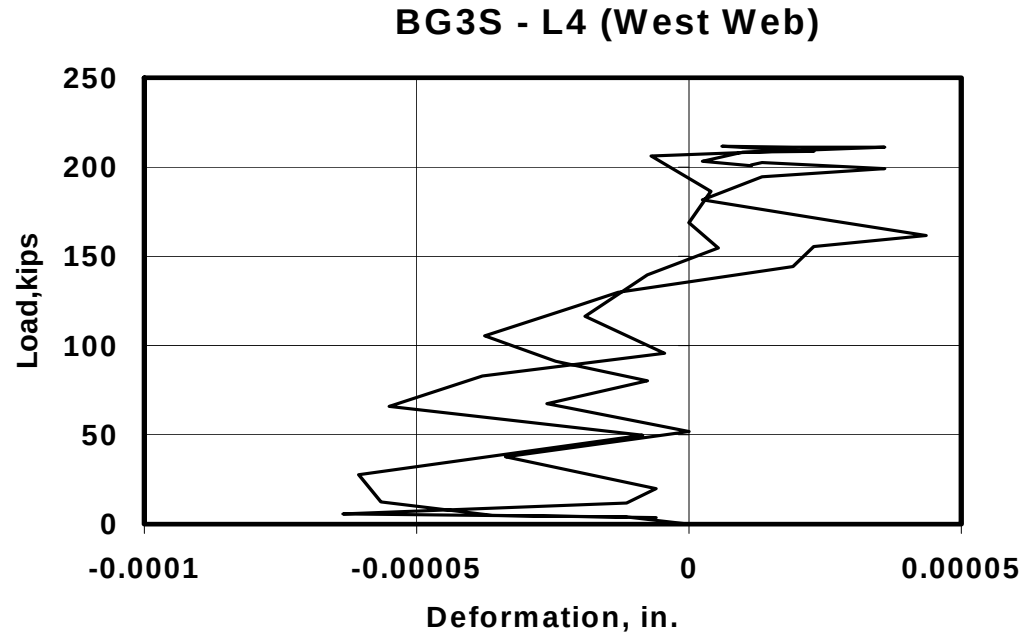
BG3S - L4 (West Web)
250
200
150
100
50
0
Load,kips
-0.0001
-0.00005
0
0.00005
Deformation, in.

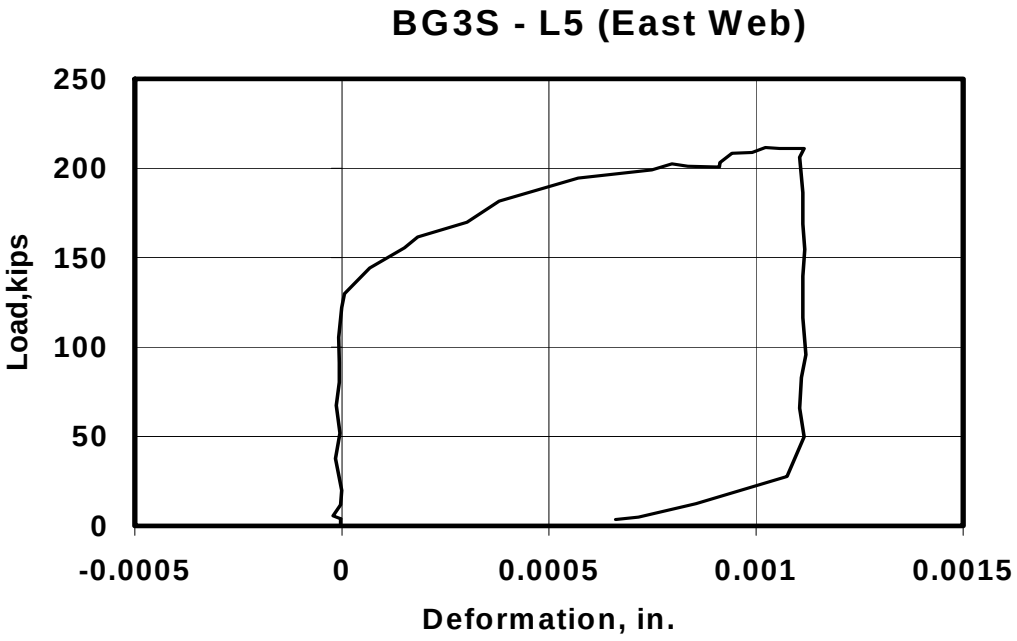
BG3S - L5 (East Web)
250
200
150
100
50
0
Load,kips
-0.0005
0
0.0005
0.001
0.0015
Deformation, in.

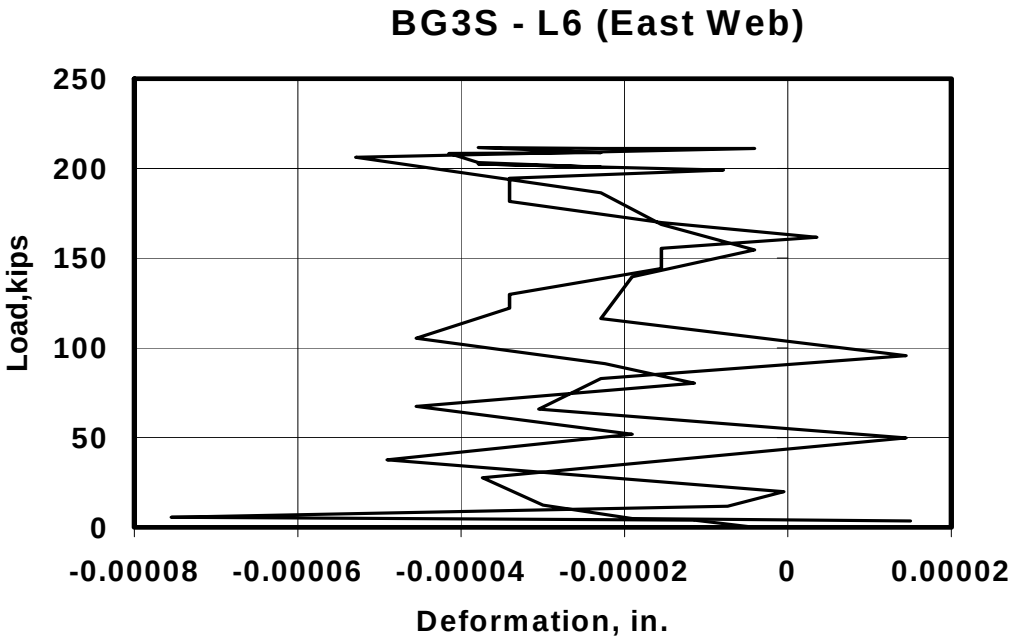
BG3S - L6 (East Web)
250
200
150
100
50
0
Load,kips
-0.00008
-0.00006
-0.00004
-0.00002
0
0.00002
Deformation, in.

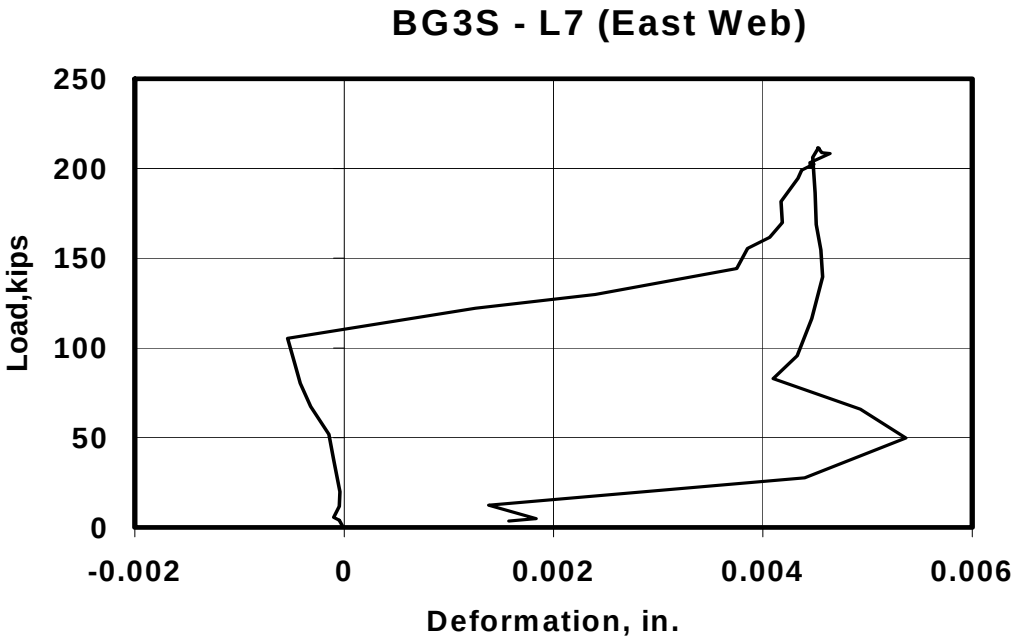
BG3S - L7 (East Web)
250
200
150
100
50
0
Load,kips
-0.002
0
0.002
0.004
0.006
Deformation, in.

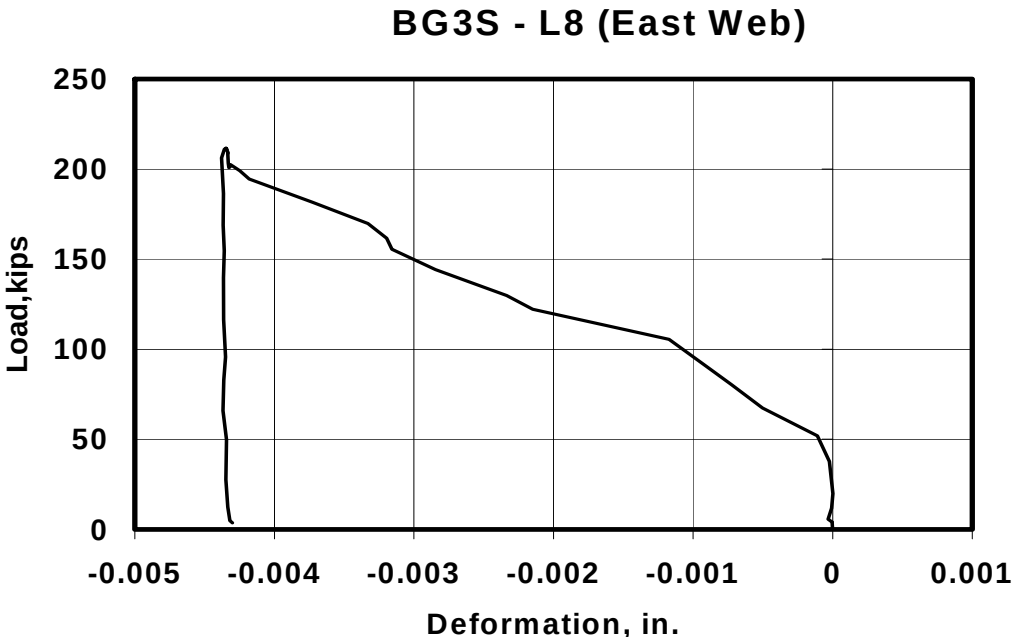
BG3S - L8 (East Web)
250
200
150
100
50
0
Load,kips
-0.005
-0.004
-0.003
-0.002
-0.001
0
0.001
Deformation, in.

C.2.2 3,328,600 Load Cycles (Quasi-static Test to Failure)

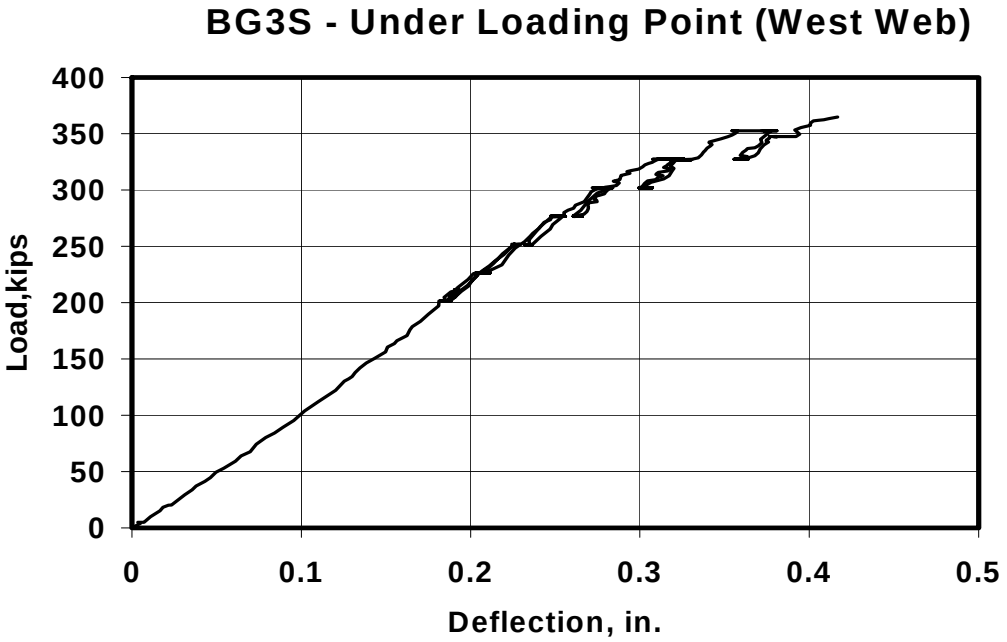

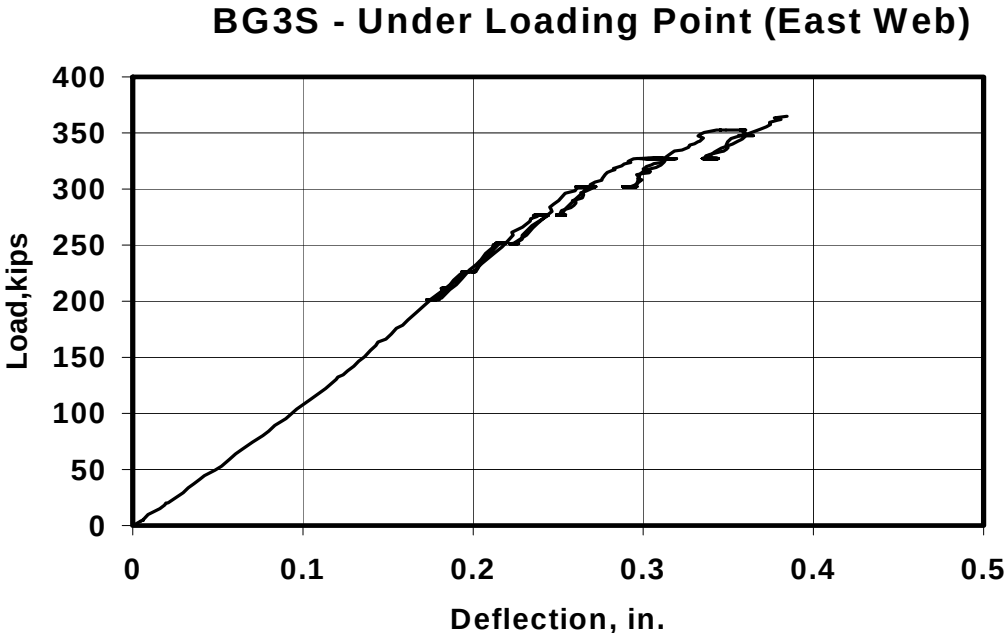

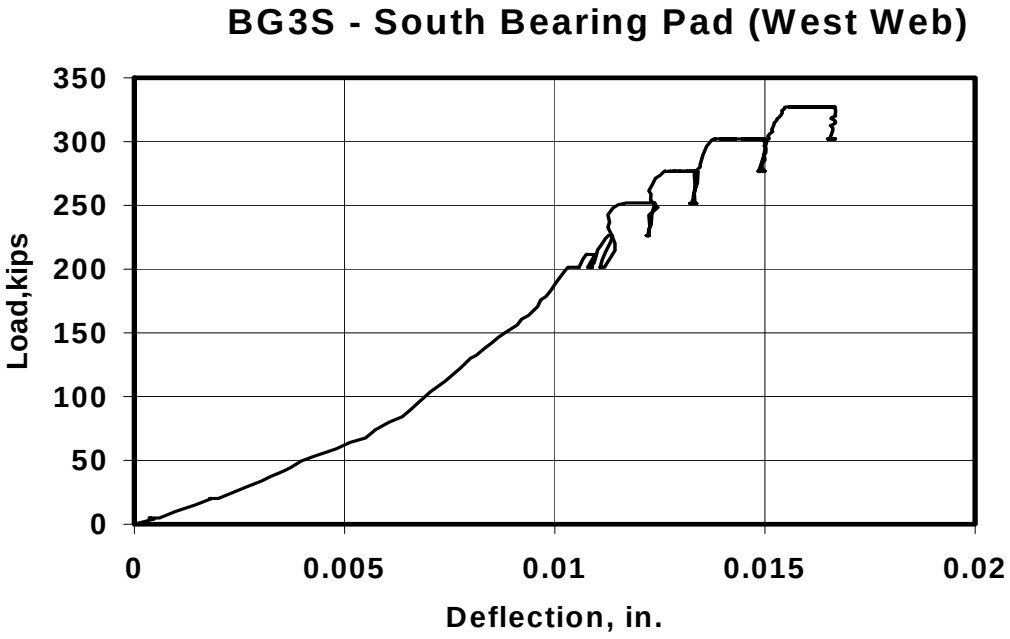
BG3S - South Bearing Pad (West Web)
Load,kips
350
300
250
200
150
100
50
0
0
0.005
0.01
0.015
0.02
Deflection, in.

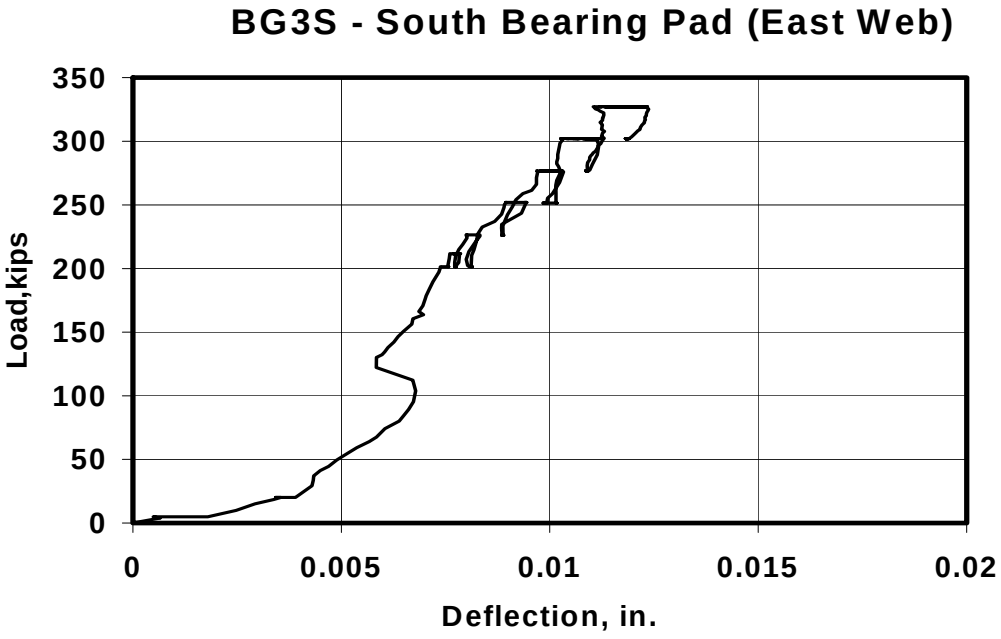
BG3S - South Bearing Pad (East Web)
Load,kips
350
300
250
200
150
100
50
0
0
0.005
0.01
0.015
0.02
Deflection, in.

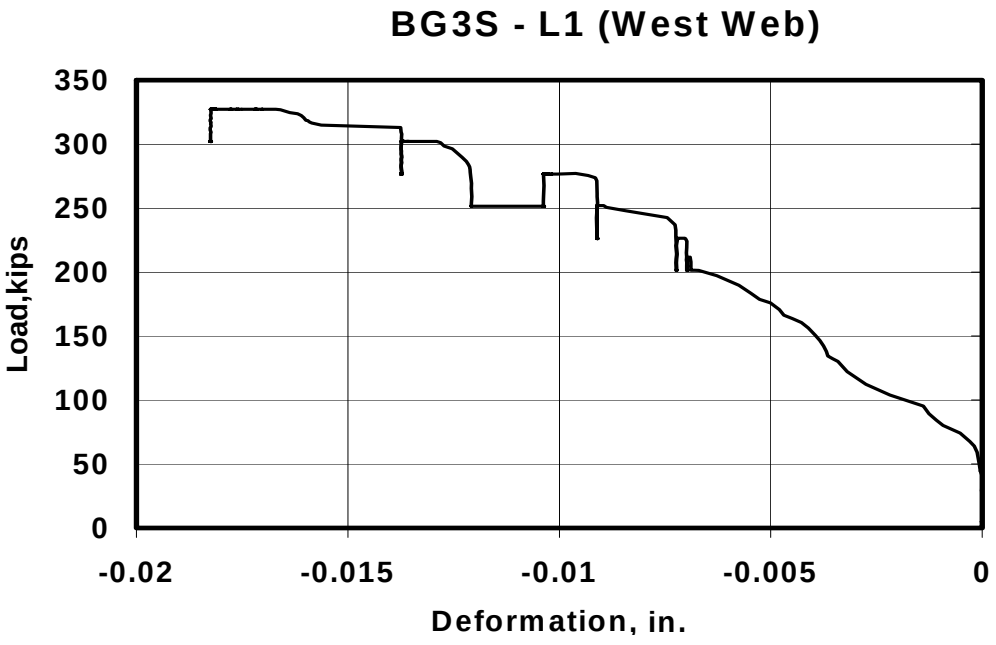
BG3S - L1 (West Web)
Load,kips
350
300
250
200
150
100
50
0
-0.02
-0.015
-0.01
-0.005
0
Deformation, in.

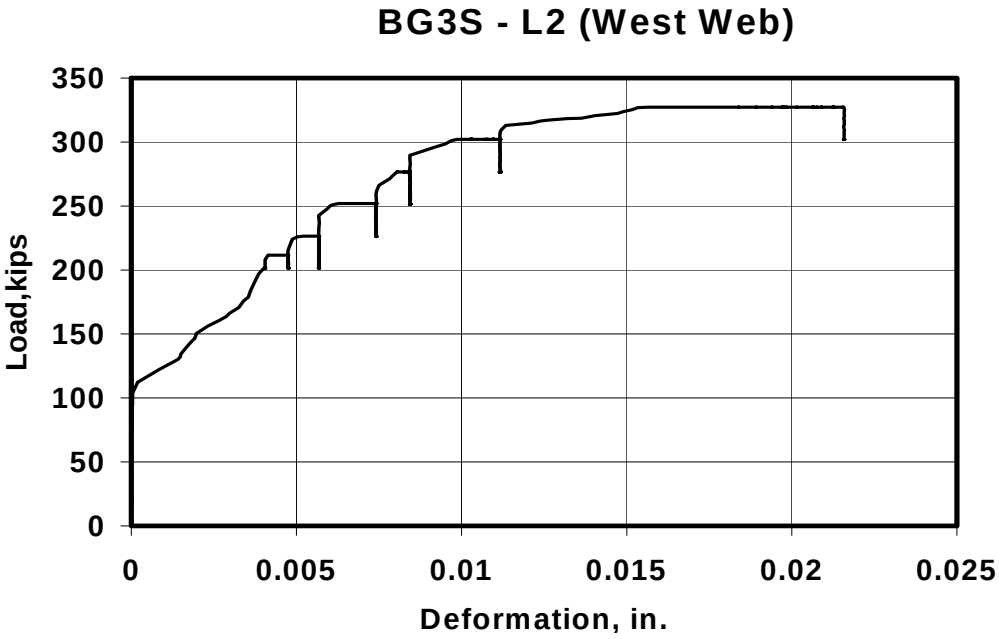
BG3S - L2 (West Web)
Load,kips
350
300
250
200
150
100
50
0
0
0.005
0.01
0.015
0.02
0.025
Deformation, in.

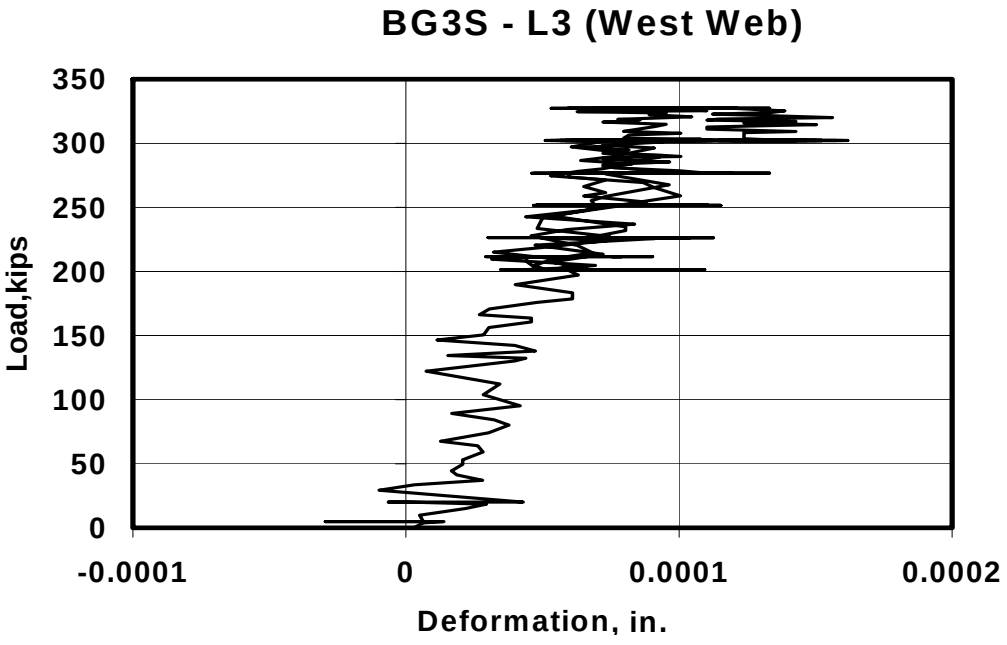
BG3S - L3 (West Web)
Load,kips
350
300
250
200
150
100
50
0
-0.0001
0
0.0001
0.0002
Deformation, in.

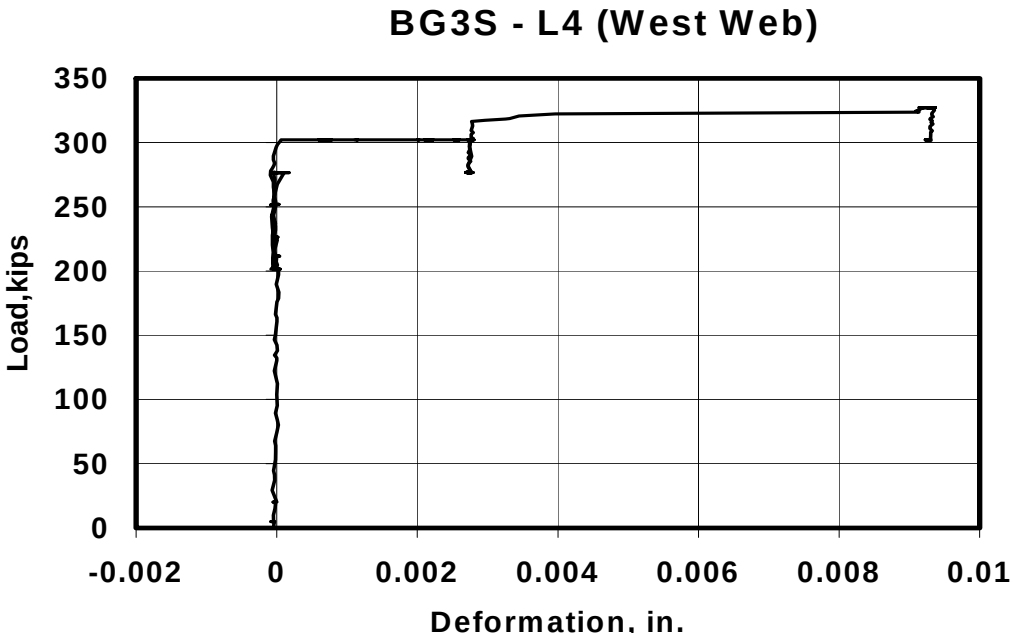
BG3S - L4 (West Web)
Load,kips
350
300
250
200
150
100
50
0
-0.002
0
0.002
0.004
0.006
0.008
0.01
Deformation, in.

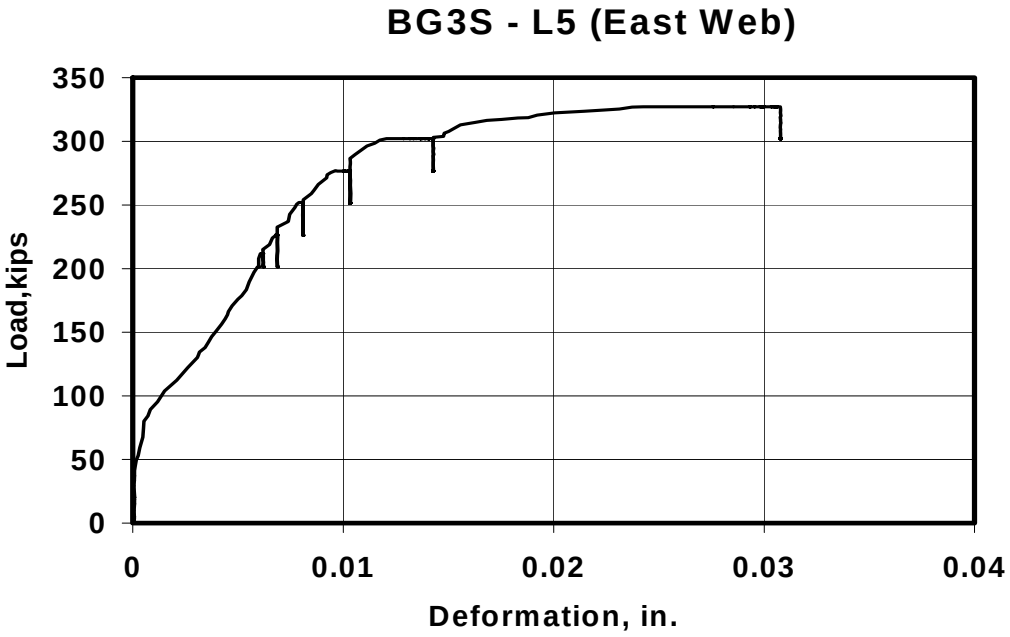
BG3S - L5 (East Web)
Load,kips
350
300
250
200
150
100
50
0
0
0.01
0.02
0.03
0.04
Deformation, in.

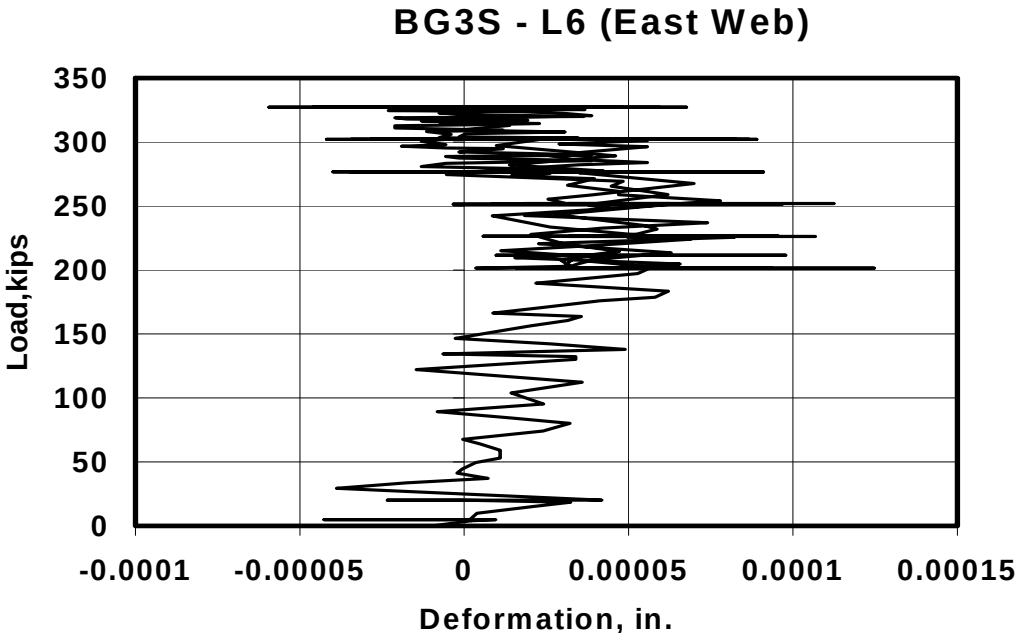
BG3S - L6 (East Web)
Load,kips
350
300
250
200
150
100
50
0
-0.0001
-0.00005
0
0.00005
0.0001
0.00015
Deformation, in.

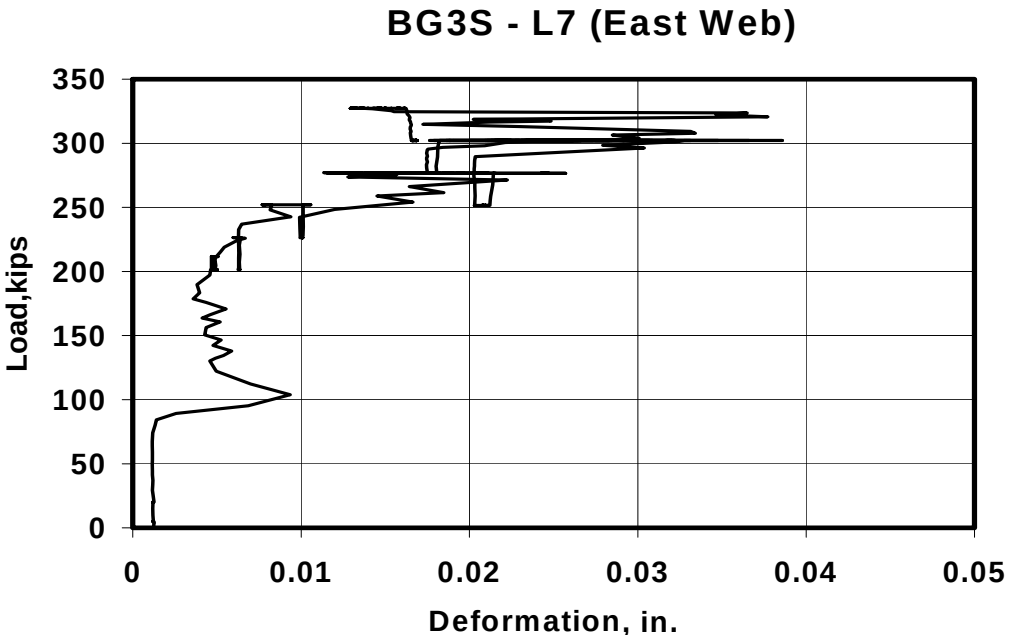
BG3S - L7 (East Web)
Load,kips
350
300
250
200
150
100
50
0
0
0.01
0.02
0.03
0.04
0.05
Deformation, in.

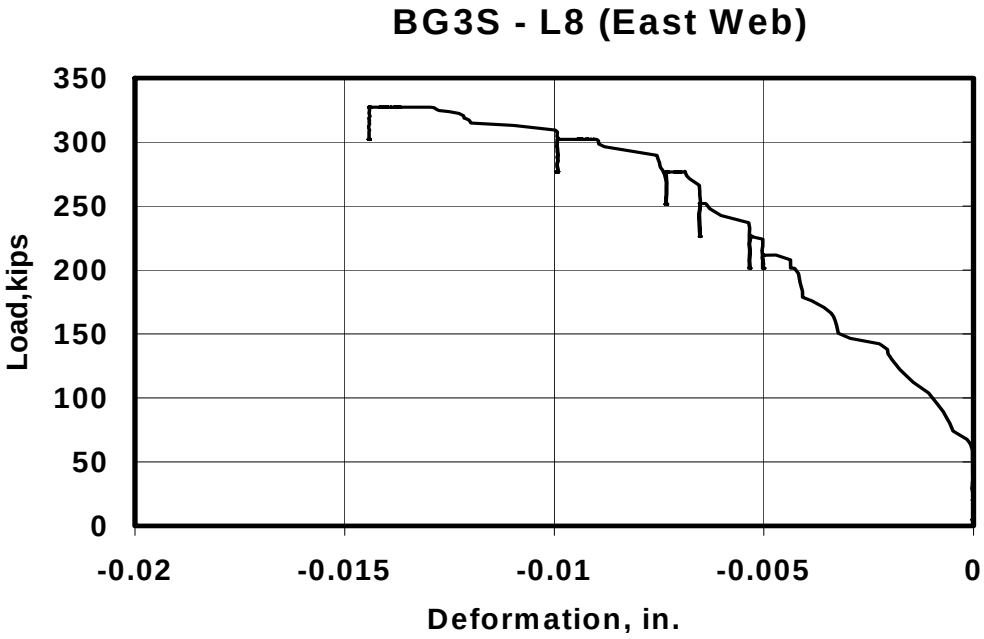
BG3S - L8 (East Web)
Load,kips
350
300
250
200
150
100
50
0
-0.02
-0.015
-0.01
-0.005
0
Deformation, in.

References

AASHTO (1996). *Standard Specifications for Highway Bridges*. 16th ed., American Association of State Highway and Transportation Officials, Inc., Washington, D.C.

ACI Committee 215 (1999). "Considerations for Design of Concrete Structures Subjected to Fatigue Loading," (ACI 215R-74), *ACI Manual of Concrete Practice, Part 1*, Farmington Hills, Michigan.

ACI Committee 221.1 (1998). "Guide for Use of Normal Weight Aggregates in Concrete," (ACI 221R-96), *ACI Manual of Concrete Practice, Part 1*, Farmington Hills, Michigan.

ACI Committee 318 (1999). *Building Code Requirements for Structural Concrete* (ACI 318-99) *and* Commentary (ACI 318R-99) Farmington Hills, Michigan.

Bachman, P. M., Kreger, M. E. and Breen, J. E. (1987). "An Exploratory Investigation of Shear Fatigue Behavior of Prestressed Concrete Girders," *Research Report 465-1*, Center for Transportation Research, The University of Texas at Austin, Austin, Texas.

Boenig, A. (2000). "Bridges with Premature Concrete Deterioration: Field Observations and Large Scale Testing," *Master's Thesis prepared for The Graduate School of the University of Texas at Austin*, Austin, Texas.

Collepardi, M. (1999). "Damage by Delayed Ettringite Formation," *Concrete International*, V. 21, No 1, January 1999, pp.69-74.

Fúnez, Luz Marina (1999). "Field Observation of Bridges with Premature Concrete Deterioration: Structural Implications," *MS Report*.

Graddy, J. C., Burns, N. H. and Klingner, R. E. (1995). "Factors Affecting the Design Thickness of Bridge Slabs," *Research Report 1305-3F*, Center for Transportation Research, The University of Texas at Austin, Austin, Texas.

Hime, W. C. (1996). "Delayed Ettringite Formation—A Concern for Precast Concrete?" *PCI Journal*, July-August 1996, pp. 26-30.

Kesner, K. E. (1997). "Detection and Quantification of Distributed Damage in Concrete Using Transient Stress Waves," *Master's Thesis prepared for Cornell University of Civil & Environmental Engineering.*

Klingner, R. E., Fowler, T. J. and Kreger, M. E. (2000). "Mitigation Techniques for In-Service Structures with Premature Concrete Deterioration," *Proposal prepared for Texas Department of Transportation.*

Klingner, R. E. and Fowler, T. J. (1998). "Structural Assessment of In-Service Bridges with Premature Concrete Deterioration," *Proposal prepared for Texas Department of Transportation.*

Lawrence, B. L., Moody, E. D., Guillemette, R. N. and Carrasquillo, R. L. (1997). "Evaluation and Mitigating Measures for Premature Concrete Deterioration in Texas Department of Transportation Concrete Elements."

MacGregor, J. G. (1997). *Reinforced Concrete Mechanics and Design*, 3rd ed., Prentice-Hall, Inc., Upper Saddle River, New Jersey, pp. 79 and 753-819.

Mielenz, R. C., Marusin, S. L., Hime, W. G. and Jugovic, Z. T. (1995). "Investigation of Prestressed Concrete Railway Tie Distress," *Concrete International*, V. 17, No. 12, December 1995, pp. 62-68.

Matsumoto, N. (1985). "A Fatigue Study of Deformed Reinforcing Bars," *Master's Thesis prepared for The Graduate School of the University of Texas at Austin*, Austin, Texas.

Tinkey, B. V. (2000). "Nondestructive Testing of Prestressed Bridge Girders with Distributed Damage," *Master's Thesis prepared for The Graduate School of the University of Texas at Austin*, Austin, Texas.